Université de Montréal

Development and studies of electrochromic and electrofluorochromic organic materials

Par

Chengzhang Yao

Département de Chimie, Université de Montréal

Faculté des Arts et des Sciences

Mémoire présenté à la Faculté des Arts et des Sciences

en vue de l'obtention du grade de Maitre en Chimie

Avril, 2020

Résumé:

Les matériaux électrochromiques organiques ont été un domaine de recherche novateur au cours des dernières décennies. Ces composés qui répondent à un potentiel appliqué par un changement de couleur sont dits électrochromes. Leur intérêt est principalement dû à leur synthèse facile, à haut rendement et à leur aspect écologique par rapport à leurs homologues inorganiques. En règle générale, ces composés ne changent de couleur qu'avec un potentiel appliqué. Développer des composés qui changent à la fois leur couleur et leur fluorescence avec un potentiel appliqué pour une utilisation dans des dispositifs électrofluorescents reste un défi majeur.

Dans cette étude, une série de composés contenant de la triphénylamine (TPA) et du benzothiadiazole (BZT) ont été évalués. Ils ont été couplés à différents groupes terminaux pour moduler les propriétés photophysiques et électrochimiques. Ces composés ont été entièrement caractérisés par spectroscopie d'absorption, spectroscopie de fluorescence, voltammétrie cyclique, spectroélectrochimie et diffraction des rayons X. Cela nous a permis d'examiner l'influence de leur structure sur les propriétés. Cela nous a également permis d'identifier les composés d'intérêt idéaux pour une utilisation dans des appareils fonctionnels.

Les dispositifs contenant du TPA et du BZT sont idéalement employée pour la fabrication de « fenêtre intelligente ». Cela est dû à l'activité électrochimique du TPA ainsi qu'à la fluorescence à l'état solide du noyau BZT. Pour améliorer encore les propriétés des dispositifs, un système passif était le but ultime. Cela contraste avec les dispositifs actifs où un potentiel doit être appliqué en continu pour que la couleur induite soit cohérente.

Dans ce but, des couches cathodiques ont été préparées et étudiées dans un dispositif et leur utilisation comme réservoir d'ions dans un dispositif électrochromique / électrofluorescent passif a été testée. Les résultats préliminaires ont montré que les dérivés d'anthraquinone avaient des propriétés idéales pour les couches cathodiques.

Mots clés: électrochromisme, triphénylamine, benzothiadiazole, anthraquinone, fenêtre intelligente.

Abstract:

Organic electrochromic materials have been a hot area of research during the past decades. These compounds that respond to an applied potential with a color change are said to be electrochromic. Their interest is mainly because of the easy synthesis, convenient mass production, and eco-friendly preparation compared to their inorganic counterparts. Typically, these compounds change only their color with an applied potential. To develop compounds that change both their color and their fluorescence with a potential applied for use in electrofluorescent devices remains a major challenge.

In this study, a series of compounds containing triphenylamine (TPA) and benzothiadiazole (BZT) were evaluated. They were coupled with different end groups to tune the photophysical and electrochemical properties. These compounds were fully characterized by absorption spectroscopy, fluorescence spectroscopy, cyclic voltammetry, spectroelectrochemistry, and X-ray diffraction along with other techniques. This allowed us to examine the influence of their structure on the properties. It also allowed us to identify the ideal compounds of interest for use in functioning devices.

The devices containing TPA and BZT are ideally ‘smart window’ applications. This is due to the electrochemical activity by TPA as well as the solid state fluorescence of the BZT core. To further improve the properties of devices, a passive device was the ultimate goal. This is in contrast to active devices where a potential must be applied continuously for the induced color to be consistent.

Towards this goal, cathodic layers were prepared and investigated in a device and their use as an ion reservoir in a passive electrochromic / electrofluorescent device was tested. Preliminary results, showed that anthraquinone derivatives had ideal properties for the cathodic layers.

Key words: electrochromism, triphenylamine, benzothiadiazole, anthraquinone, smart window.

Table des matières

Liste des figures

Liste des tableux

Remerciements

This thesis is impossible to finish without the people below whom I sincerely thank for their encouragement and support during my master studies at the Universite de Montreal. I am sorry that I cannot include everyone in the chapter but all your kindness are deeply remembered and I will never forget them.

First and foremost, I would like to thank Professor William Skene for all his help he provided during my master time. From the training program back in summer, 2017, I had the chance to work in Prof. Skene's lab where I first learned how to do chemistry experiments as a real researcher. Thanks for his patience and encouragement as well as the dedication for chemistry, which promoted my enthusiasm in the field of chemistry. It is also a great honor to be one of Prof. Skene's master students. The essential materials used for experiments were readily achievable in the lab, along with his guidance, patience, and comprehension. The numerous versions of manuscripts for both publications and my memoire.

I will not forget all the support from Michael Lerond, who helped me a lot in both labs and in daily life. Thanks for his thoughtful plan for taking care of the labs we used every day. I learned a lot of details for carrying out experiments from him. He is one of the most important friends during my master life.

Great thanks to those who also helped me throughout master study, Yohan Gautier, Alex Malinge, Al Ahmad Abdel, Olivier Schott, Dr. Lei Hu, Dr. Hu Zhang, Dr. Daniel Chartrand and Dr. Maris Thierry. Also thanks to our trainees, Raj Shekhar, Nacer Belkessa and Jasper Pantratz who joined us during the summer time in 2019.

Thanks to my friends for the company during two yeas in Canada. Yang Li, Arunprabaharan Subramanian who helped me get out from the depressed emotions when I faced difficulties.

Various scholarships supported my master study, most importantly, MITACS scholarships, which supported me all the way from training time to master study. Thanks to the department for the multiple funding. A special thanks to Marguerite-Jacques-Lemay for your kind scholarship that supported my hard time living in Canada.

Last, I would like to thank all my family members in China for being my strong supporting team. Without them, I cannot complete this study.

1. Introduction

During the last few decades, many conductive organic electronics have been invented to provide human beings with a better life, for example, Organic Light-Emitting Diode (OLED), Organic Photovoltaics (OPVs), Organic field-effect transistors (OFETs) and so on. These materials can undergo a redox process with external applied stimulus and they show different applications in our daily life.[1]

1.1 Electrochromic materials

Electrochromic materials, known as chromophores, affect the optical color or opacity of a surface when a voltage is applied.[2] First appeared in the inorganic field, WO_3, is the most performaning electrochromic material. It has octahedral structures of oxygen that surround a central metal atom and they are joined together at the corners. This arrangement results in a three-dimensional nanoporous structure with "tunnels" between individual octahedral segments. It can change color from dark blue to nearly transparent with an applied external voltage as shown in the equation below:

$$WO_3 + n(H^+ + e^-) \rightarrow H_nWO_3.$$

The inorganic electronics such as WO_3 shown above can be easily single crystalline, fast processed by heating and very stable, but these materials usually have low flexibility which reduce the applications of these materials into biochemistry or ‘smart’ devices. However, the organic materials can mantain low temperature and have higher flexibility at the same time. Although organic electronics face the problem of less stability and lower carrier mobility, they are still competiable with inorganic electronics.[3] Typical organic electrochromic materials can be classified as small chromophores, polymer chromophores and metal complexes chromophores. The most studied molecules are outlined below.

1.1.1. **Prussian Blue**

Prussian blue is a dark blue pigment produced by the oxidation of ferrous ferrocyanide salts. It has the chemical formula $Fe^{III}_4[Fe^{II}(CN)_6]^3$.[4] It was used by European artists as painting pigment. Chemists used it as a chromophore in electrochromic devices due to its reversible electrochemistry:

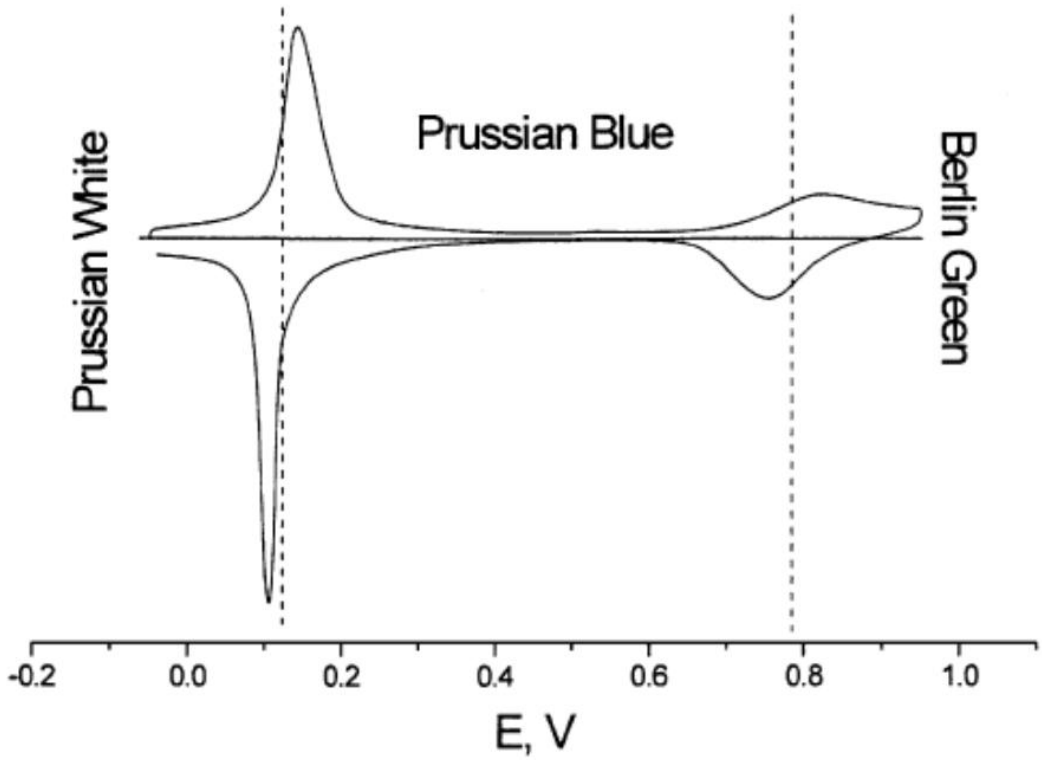

Figure 1.1: Cyclic voltammogram of Prussian Blue. Reprinted with permission from [5]. Copyright (2001) WILEY-VCH.

From the cyclic voltammogram above, we can clearly see that Prussian Blue can change from Prussian White to Berlin Green reversibly. The transfer of electrons is compensated by the entrapment of cations in the film. According to the equation below, reversible Prussian Blue to Prussian White redox process according to:

$Fe^{III}_4[Fe^{II}(CN)_6]^3 + 4e^- + 4\ K^+ \leftrightarrow K_4Fe^{II}_4[Fe^{II}(CN)_6]^3$

At high anodic potentials, Prussian Blue converts to its fully-oxidized form as is clearly seen in cyclic voltammograms due to the presence of the corresponding set of peaks (**Figure 1.1**). The fully-oxidized redox state is denoted as Berlin Green, or in some cases, as Prussian Yellow, as per the equation showed blow:

$Fe^{III}_4[Fe^{II}(CN)_6]^3 - 3e^- + 3A^+ \leftrightarrow K_4Fe^{III}_4[Fe^{III}(CN)_6A]^3$

Prussian Blue based chromophores, have been used in biosensors and bioanalytical devices involving hydrogen peroxide producing oxidases.[6, 7]

1.1.2.PEDOT: Poly(3,4-ethylenedioxythiophene)

Poly(3,4-ethylenedioxythiophene) as known as PEDOT, has the advantages of optical transparency in its conducting state, high stability, moderate band gaps and low redox potential. It is used for fabricating transparent electrodes because of these properties. For commercial purposes, the polymerization is done in the presence of polystyrene sulfonate (PSS) to increase its solubility. The resulting polymer is known as PEDOT:PSS. This material is of important in the organic electronics area, being used in over 10,000 papers.[8] This polymer was initially developed to give a soluble conducting polymer that lacked undesired α,β- and β,β-couplings within the polymer backbone. These undesired couplings were major problems with the first generation semiconductor: P3HT, prepared via direct arylation polymerization(DArP).[9, 10] While the PEDOT is not water soluble, it can be dispersed in water as the PEDOT:PSS copolymer. The water-soluble polyelectrolyte system has good film-forming properties, high conductivity, high visible light transmissivity, and excellent stability.[11] The neutral state of PEDOT exhibits an electronic bandgap, defined as the on-set of the π-π* absorption, of 1.6-1.7 eV and a λ_{max} of 610 nm, making it deep blue in color. It can reversibly change from deep blue to pale blue with a low applied voltage. More interestingly, the color of neutral state of PEDOT can be tuned by controlling the band-gap. To demonstrate bandgap control, a few of the examples reported include spacers of vinylene (Eg = 1.4 eV), 2,5-dialkoxyphenylene (Eg = 1.75 to 2.0 eV), biphenyl (Eg =2.3 eV), dialkylfluorene (Eg = 2.3 eV), and carbazole (Eg =2.5 eV).[12] In general, the electronic band-gap of a conjugated chain is controlled by varying the degree of π-overlap along the backbone via steric interactions, and by controlling the electronic character of the electron-donating or accepting substituents. This provides the means to modulate the color with a wide range of colors being accessible (**Figure 1.3**). The applications of PEDOT and its derivatives can be expanded into antistatic agentrs, electrode materials, electrochromic windows and so on.

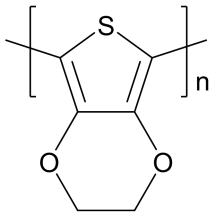

Figure 1.2: Structure of PEDOT.

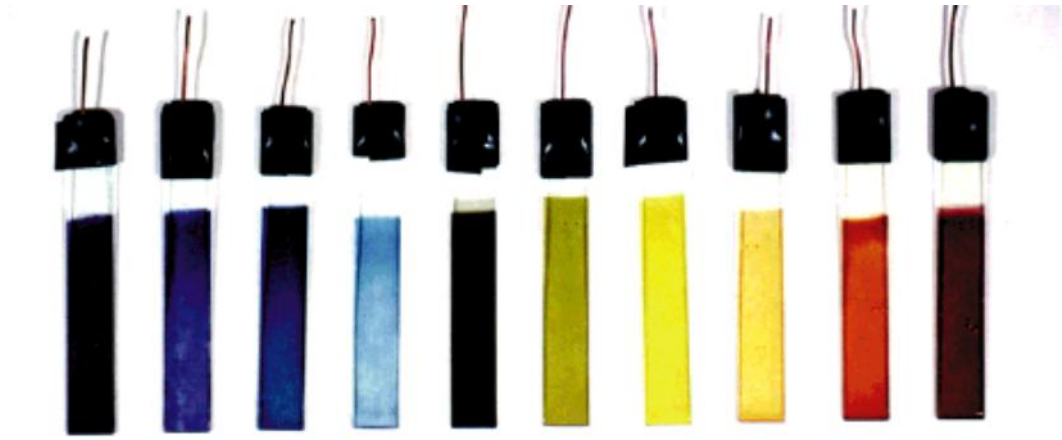

Figure 1.3: Photos of EDOT-based polymers with different bandgaps. Reprinted with permission from [8]. Copyright (2000) WILEY-VCH.

1.1.3. Viologen

Viologens are organic compounds with the formula of $(C_5H_4NR)_2^{n+}$. The most common viologen is when the R group is a methyl, and it is widely used as herbicide.

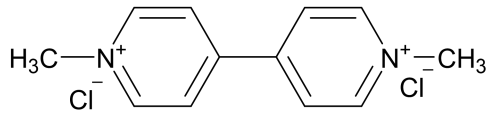

Figure 1.4: Structure of methyl viologen.

Viologens, in their dicationic form, typically undergo two one-electron reductions. The first reduction affords the deeply colored radical cation:

$[V]^{2+} + e^- \leftrightarrow [V]^+$

This is followed by a second reduction. The radical cations of 4,4'-viologens are blue and those of 2,2'-derivatives are green. The second reduction yields a yellow quinoid compound with the overall reversibly electron transfer represented below and in **Figure 1.5**:

$[V]^+ + e^- \leftrightarrow [V]^0$

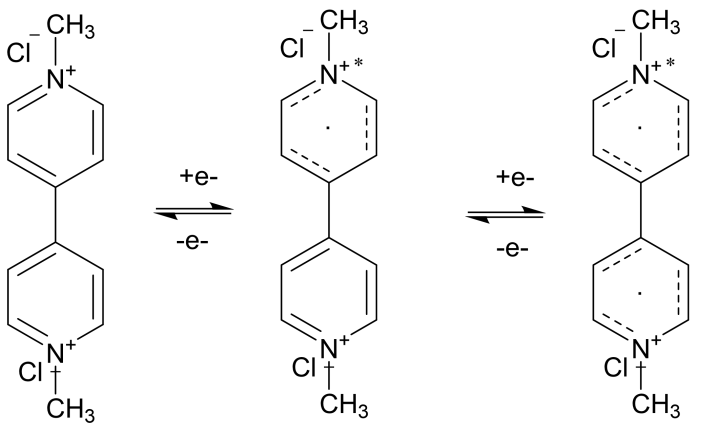

Figure 1.5: Viologen species accessible by reversible electrochemical reduction.[13]

To further development the family of viologens, their backbones can be extended leading to higher conductivities as well as stronger reducing properties.

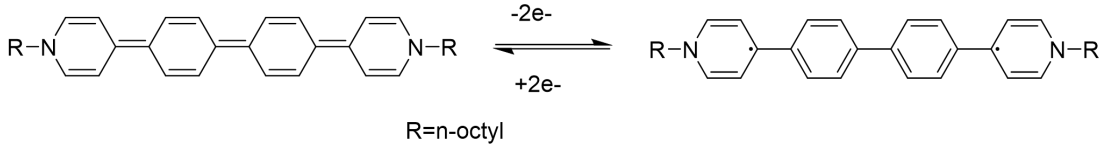

Figure 1.6: Isomeric structures of extended viologen derivatives.[14]

1.1.4. **Triphenylamine based chromophores**

The triphenylamine (TPA) has become a promising optoelectronic molecule for emergent electronic applications owing to its good thermal and morphological stability for electrochromic materials. It has been studied for over a decade and it still has great potential. It undergoes a reversible redox process with applied the positive voltage, leading to a color change from white to blue.

In 2014, the Audebert group prepared a series of TPA derivatives by changing the substituents with a strong donating group -OCH_3, or a weak withdrawing group, -CHO. These compounds were synthesized by cross-coupling reactions and then studied by cyclic voltammetry, UV/Vis spectroscopy, and fluorescence spectroscopy. By applying different potentials, four unique colored states (colorless, yellow, green, and blue) and three different emissions (non emissive, purple, and green fluorescent) were shown.[15]

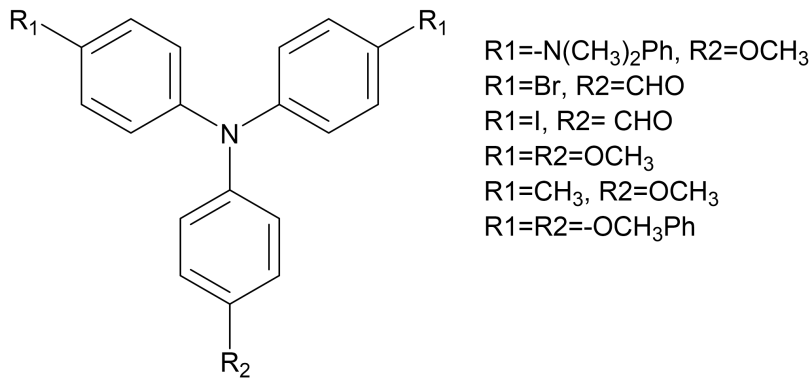

Figure 1.7: Structure of TPA based small molecules investigate by Audebert's group.

The TPA structure can also be modified by coupling the TPA core with various functional groups. In 2017, anthraquinone was coupled to the TPA block for use as super capacitors owing to two reversible reduction processes.[16] Surprisingly, the emission of the TPA-antraquinone derivatives were highly sensitive to solvents. As such, its emission could be tuned with large red-shifts up to 138 and 192 nm in non-polar or less polar solvents, respectively. Overall, it emitted rich colors. This study showed multifunctional chromophores could both emit with emissions in the visible region. Anthraquinone derivatives will be further developed in chapter 4.

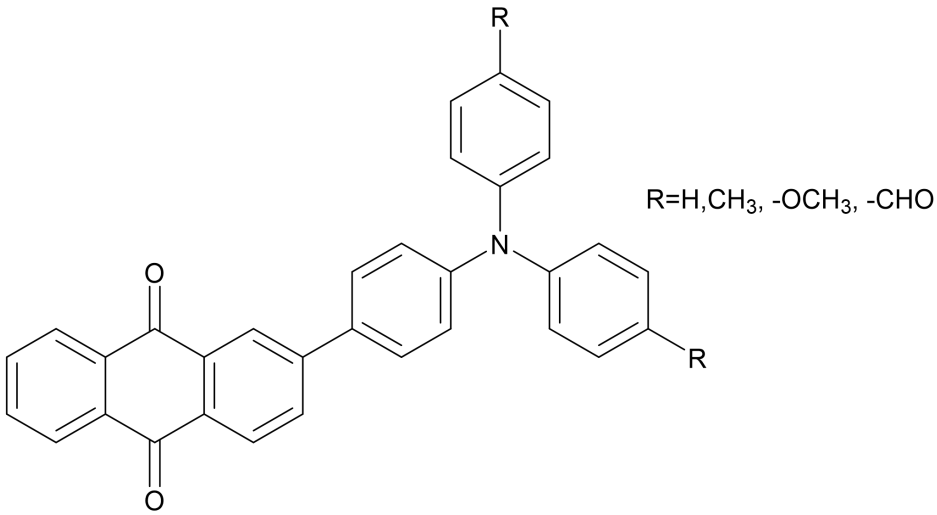

Figure 1.8: TPA-Anthraquinone derivatives explained by Li's group.

TPA was also coupled to chalcones via an Aldol reaction.[17] Six novel electrochromic compounds containing TPA and chalcone units were synthesized and they showed fast spectroelectrochemical response (change in absorption spectrum with applied potential) and high durability. They could switch between yellow and blue colors. By this token, chalcone-containing TPA moiety is an alternative approach for tuning the electrochromic behaviors.

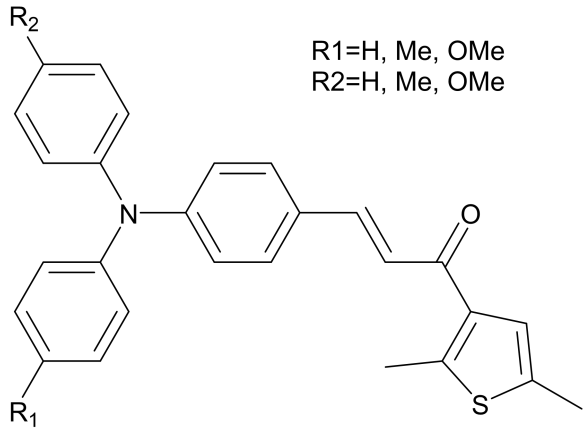

Figure 1.9: TPA-chalcone structures.

1.1.5. **Polymer chromophores containing TPA**

The triphenylamine (TPA) core can be incorporated into polymers and maintain its reversible one-electron oxidation. TPA based polymers for electrochromic use have been studied over the last decade, mostly as polyimides, polyamides as well as poly(hydrazide)s and poly(oxadiazole)s. TPA-polyimides were first reported by Liou's group,[18] by coupling diamine with various tetracarboxylic dianhydrides(**Figure 1.10**). The polyimides were moderately soluble in several organic solvents, and they could be cast into flexible, tough, and transparent films. The thermally stable polyimides films exhibited two well-defined oxidation redox couples (at 0.78 and 1.14 V versus Ag/AgCl) with distinct color changes from pale yellowish to green and then blue during oxidative scanning. Afterwards, Liou and Hsiao continuously reported a large variety of TPA-polyimides. Most of the polyimides were organo-processable, thermally stable, had excellent adhesion to indium tin oxide (ITO)-coated glass electrodes, and had good electrochemical stability. For adhesion process, spin coating or spray coating was chosen. The adhesion process has great influence on the device performance due to the layers' morphology. By attaching the two layers of different materials, the diffusion between the phases will lead to the change of performance via the electron doping processs for example. The TPA-polyimides also revealed electrochromic properties when applying positive potentials. They are considered as ideal anodic electrochromic materials due to their reversible oxidation potentials, electrochemical stability, and thin film formation. Representative examples of TPA-polyimides are shown in **Figure 1.11**, namely *N*-phenylcarbazole[19], adamantylphenoxy[20], viologen [21].

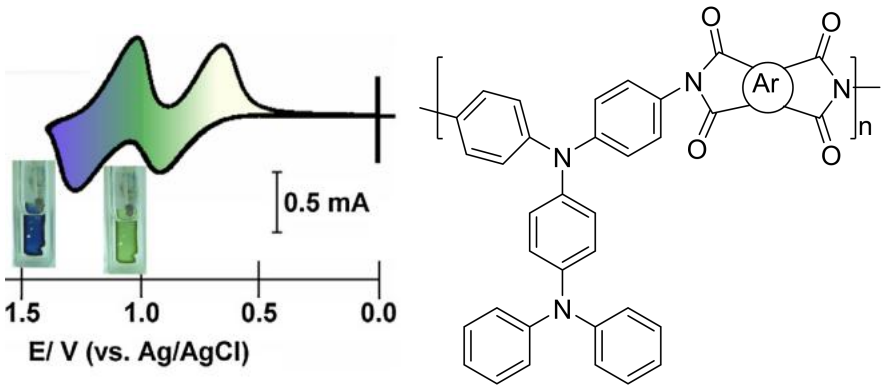

Figure 1.10: First report of TPA-polyimides. Reprinted with permission from [18]. Copyright (2005) American Chemical Society.

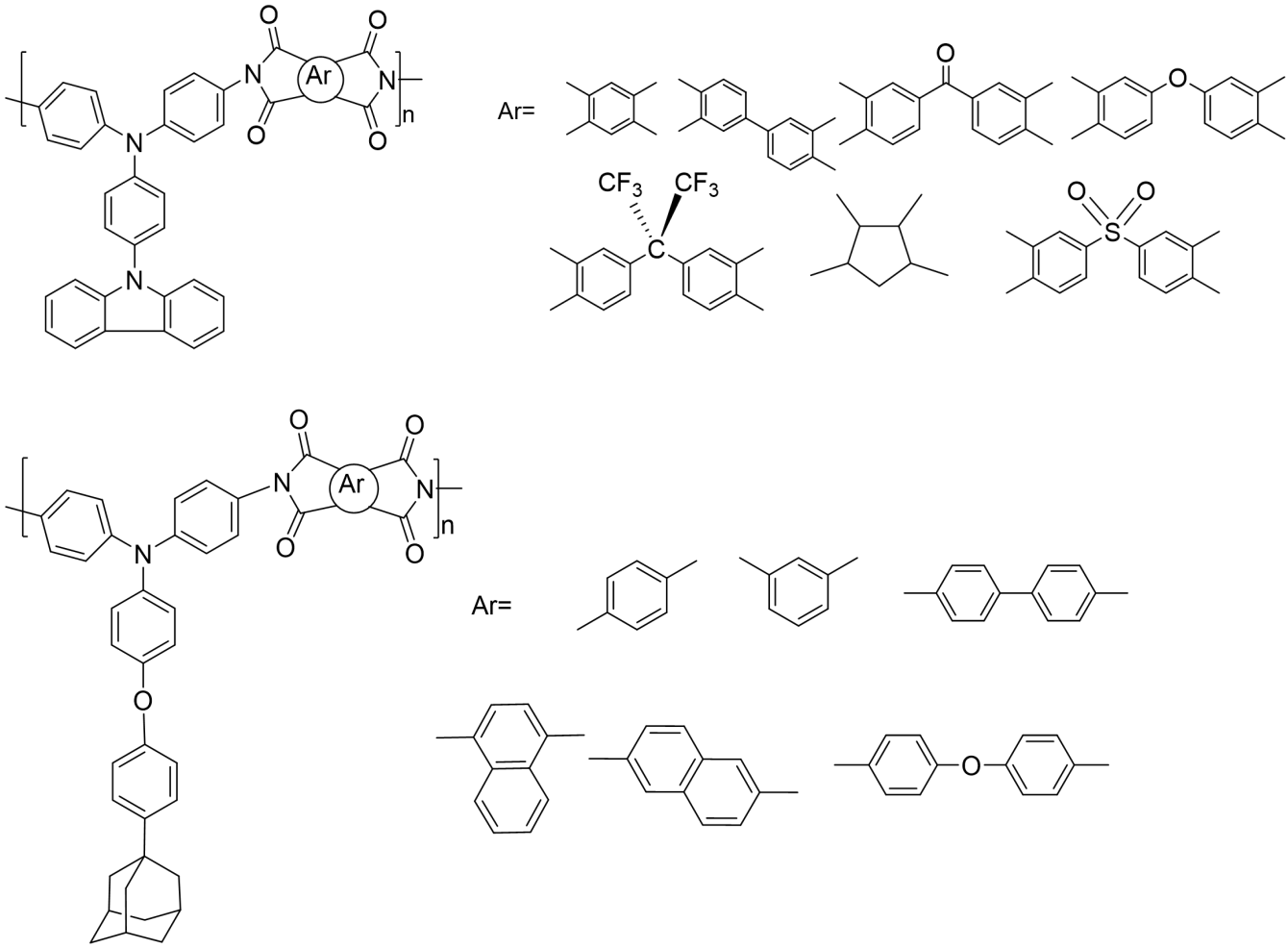

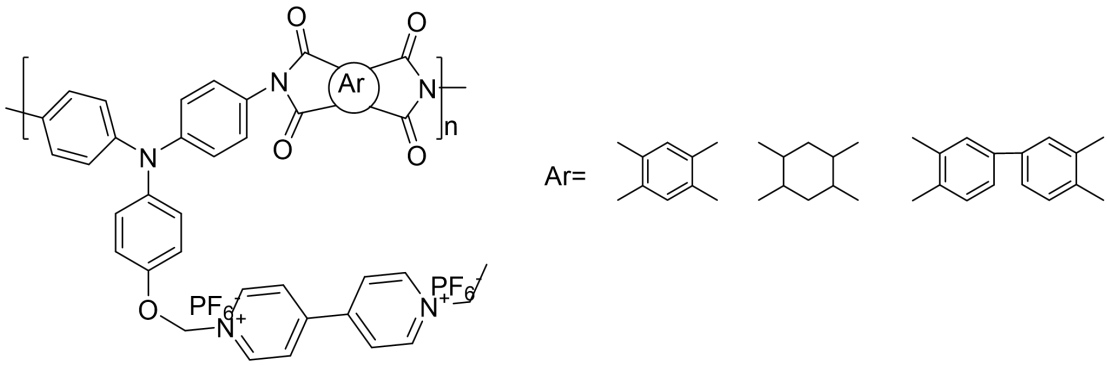

Figure 1.11: TPA-polyimides examples.[18-20]

Similarly, polyamides showed high levels of thermal stability and high glass-transition temperatures as well as high char yields. Some of the TPA-polyamides thin films revealed reversible electrochemistry with electrochromic high contrast ratio in the visible range or NIR region, high coloration efficiency, low switching time, and high stability for long-term electrochromic operation. A polyamide example from Hsiao's group exhibited excellent reversible electrochromic stability with good green coloration efficiency and high contrast of optical transmittance change up to 85%. Even after over 1000 cyclic switches, the polymer films exhibited excellent reversibility of electrochromic characteristics due to the *para*-substituted methoxy groups shown in **Figure 1.12**.[22]

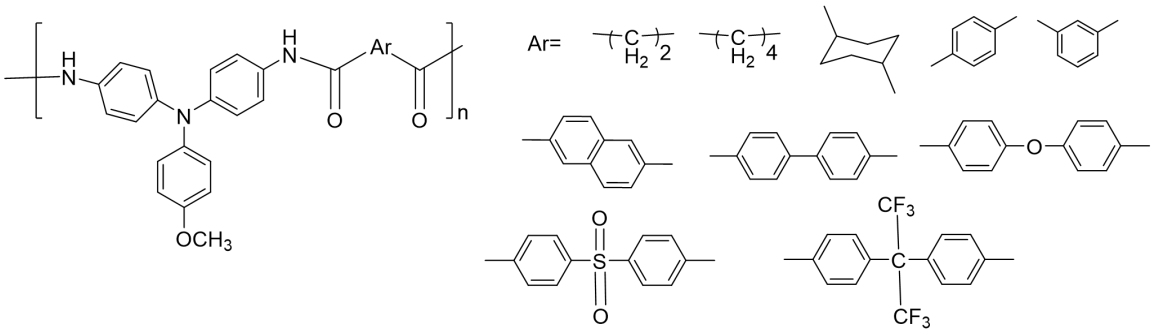

Figure 1.12: Example of TPA-polyamides, electrochromism properties and stability.[22]

Poly(oxadiazole)s are a well-known class of chemically and thermally stable heterocyclic polymers. However, there are infusible and are insoluble, as well as they have the tendency to be brittle. Also, polyoxadiazoles with an aromatic segments have limited processability. To overcome the process limitation of polyhydrazides, the precursors of polyoxadiazoles can be modified. Liou and Hsiao groups put significant effort into synthesizing soluble aromatic polyhydrazides and polyoxadiazoles containing TPA units in the main chain.[23, 24] The primary reason for their use was for high photoluminescence (PL) quantum yield as well as visible electrochromism, combined with the advantage of simple processability for obtaining flexible and mechanically robust films or thin film layers.[25, 26] This polymer exhibited pale to green

visible electrochromism as well as a considerably high PL quantum yield.[27] (Figure 1.13.)

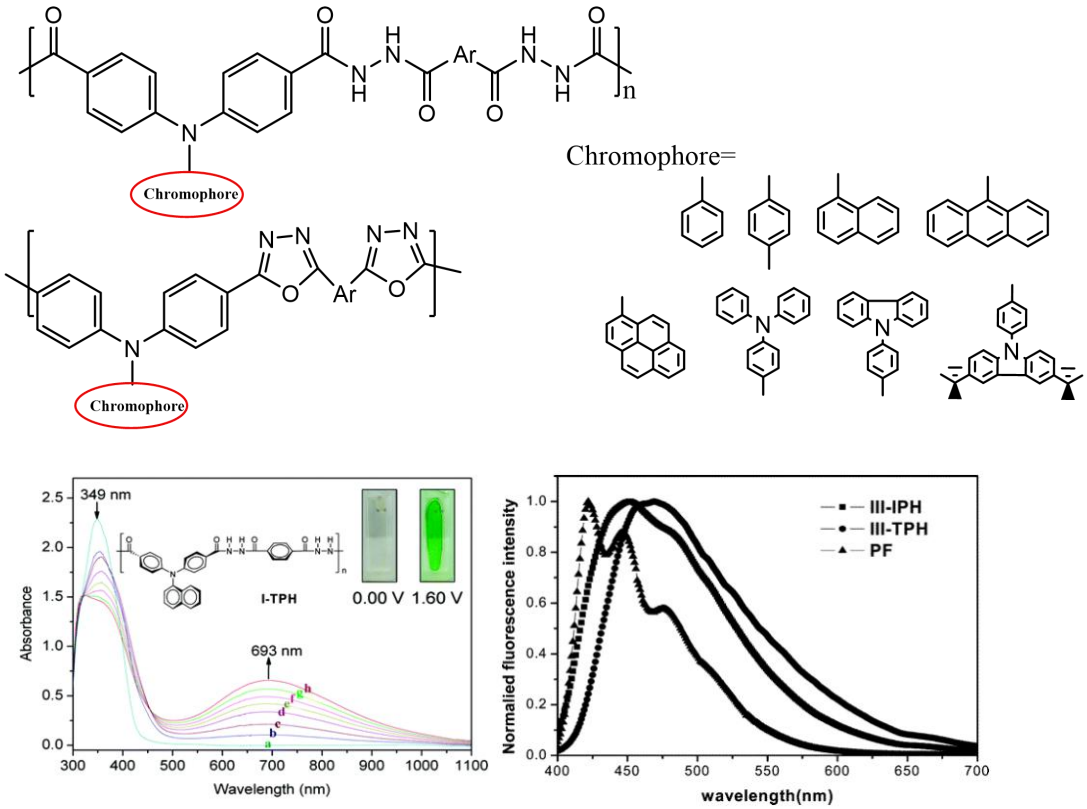

Figure 1.13: Poly(amine−1,3,4-oxadiazole)s structure and electrochromic properties. Reprinted with permission from [23]. Copyright (2006) American Chemical Society.

Despite numerous efforts for preparing non-conjugated polymers, they have problems including precursor insolubility, are difficult to print, and so on. Their extended electroluminochromic study being the sustainability of emission switching with applied potential has not been reported. Their stability in devices remains a problem. The challenge with polymers is their preparation along with their corresponding monomers that are time-consuming to prepare from thermal, photochemical, or electrochemical means.

1.2 Surface immobilization: from small molecules to devices

In working organic device, the first and foremost step is the immobilization of the materials on the electrode substrate. This is required to prevent their migration to the opposite electrode during device operation. The electrochrome mobility reduces the transmission % difference overtime, resulting in reduced coloration efficiency. The latter is a key performance metric of electrochromic devices. The electrochrome immobilization is therefore need to maintain device performance, and in turn, eliminate undesired memory effects. In the solid state, small molecules

are easily dissolved. When the layer is deposited on top, the challenge is how to resist their delamination with subsequent layer deposition, especially the required electrolytic gel. A straightforward option is to polymerize small molecules directly on the surface either via co-polymerization or functionalization of end groups.

1.2.1 Direct arylation polymerization

Traditional direct arylation polymerization (DArP) utilizes the successive coupling of conjugated monomers, whereby the activation of a C−H bond of one monomer reacts with a typically electrophilic functionality, such as an aryl halide, on another monomer. This is commonly used to prepare 'P3HT'. The first problem to solve was polythiophene's regioselectivity. Lemair et al. tried to address this by polymerizing 2-iodo-3-alkylthiophenes using a Heck-type reaction with $Pd(OAc)_2/NBu_4Br$ as catalyst. This led to the expected functionalized oligomers in good yields, but with low polymer molecular weight and regioregularities.[9] The regioregularity was shown to be solvent dependent, suggesting that the solubility of the polymer and the solvent polarity might influence the reaction pathways, where side reactions such as homo-coupling can occur (**Figure 1.14**) Then, Ozawa's group improved the polymerization with Pd ligands and Cs_2CO_3 as a base in refluxing THF. They obtained regioregular head-to-tail poly(3-hexylthiophene) (HT-P3HT) with high molecular weights (M_n = 30 600 g/mol, M_w/M_n = 1.60), and high regioregularity (98%) in almost quantitative yield (99%) by using Ligand **5** with o-Me_2N substituents as catalyst precursors (**Figure 1.15**).[10] To further simplify the reaction conditions and use more environmentally 'green' tools, carboxylic acid could be used as a proton shuttle to increase the reactivity.[28] Rudenko demonstrated the effect of acid pKa, steric bulk, and backbone cyclization on the reactivity of the DArP catalytic system. The pKa did not correlate with the DArP reactivity in the pKa range of 4.76−5.05. Increasing the acid size in the classes of linear, secondary, and tertiary acids led to a continuous increase in both the reaction yield and polymer molecular weight, However, for the case of cyclic secondary acids, the trend was reversed and a decrease of acid size led to an increase in the polymer yield and the molecular weight in an alternating fashion, depending on whether the acid contained an even or odd number of carbons. In the end, they reached an extremely high PDI value (10.7) in the case of bicyclic acids(**Figure 1.16**).

R=H, CH_3, $(CH_2)_2CH(CH_3)(C_2H_5)$, C_6H_{17}

Figure 1.14: P3HT polymerization by Lemair et al.[9]

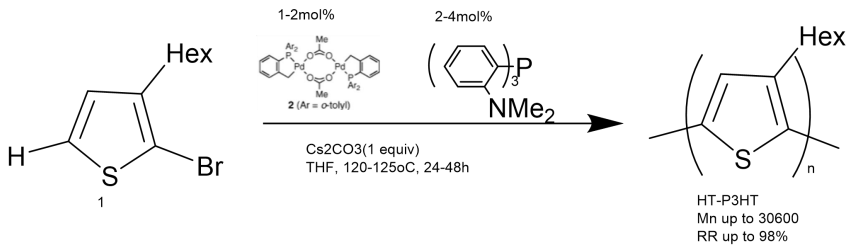

Figure 1.15: Ozawa's synthetic route of P3HT. [10]

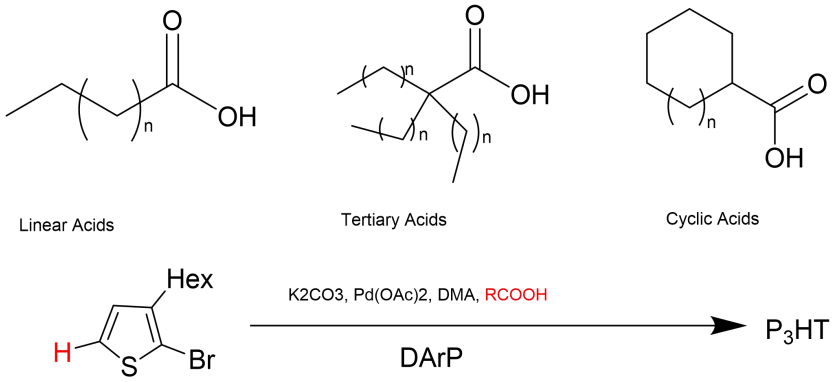

Figure 1.16: Rudenko et al. synthesis of P3HT with different types of carboxylic acids.[28]

1.2.2 Electropolymerization

As mentioned above, DArP is a promising way for making conjugated polymers, oxidative DArP can also be used for preparing donor−acceptor type materials, which are important for use in organic electronic applications. In short, this approach is environmentally friendly and it is an economic method for replacing traditional polymerizations methods such as Stille and Suzuki couplings.

To accelerate the immobilization process, Liou and Hsiao introduced electron-donating species as protecting groups to triarylamine moieties. These efficiently prevented the tail-to-tail coupling. The coupling reaction could be done with electropolymerizable monomers by attaching two or more unsubstituted TPA or carbazole units onto an electron-withdrawing core. In addition, the TPA core could also be fused to thiophenes, ethylenedioxythiophenes (EDOT), dithienylpyrroles, and chalcogenophenes (Se, Te) derivatives via an electrochemical process. Wang's group[29] reported a series of 2,5-dithienylpyrrole(DTP) derivatives with different triarylamines that underwent excellent transmittance change with applied potentials (**Figure 1.17**). Of interest, P(DTP-PNA) and P(DTP-PTA-DTP), which underwent more than two mediated colors from bright yellow to violet. Deng's group also reported a conducting polymer film based on dithiafulvenyl-triphenylamine-di(N-carbazole).[30]

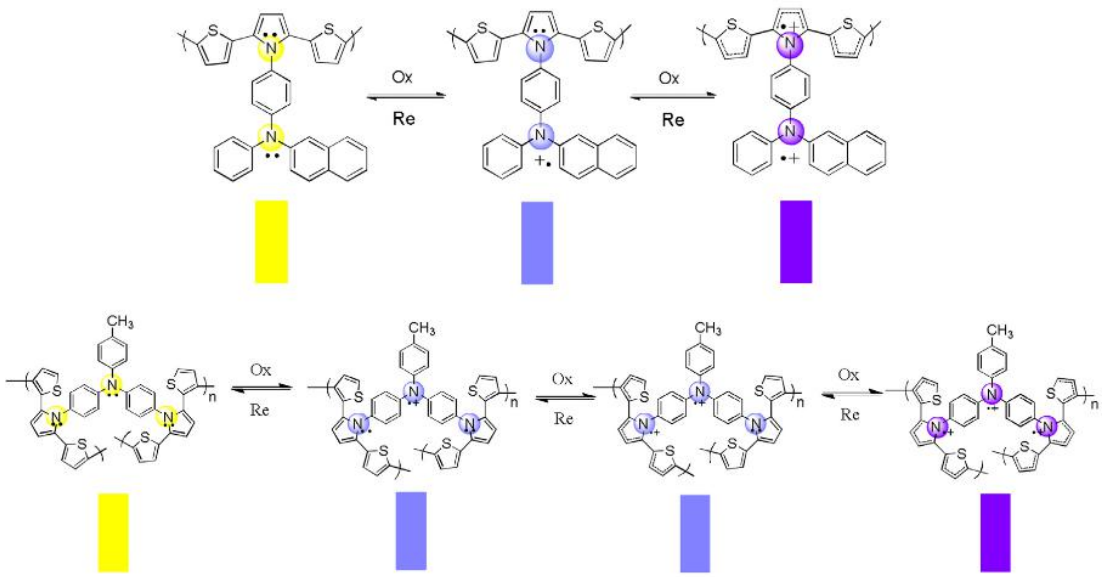

Figure 1.17: Electrochromism mechanism of P(DTP-PNA) and P(DTP-PTA-DTP). Reproduced with permission from [29]. Copyright (2017), Elsevier.

As shown in **Figure 1.18**, the TPA substituted with a strong dithiafulvenyl (DTF) acceptor was introduced at *N*-position of carbazole (CBZ), leading to a DTF-TPA-CBZ monomer. The polymer had three different color states with applied potential of -0.4 V, 1.2 V and 1.8 V, being light yellow, green and blue grey, respectively. Unfortunately, the coloration efficiency (see Section **2.5**) of this polymer was low, less than 30 $cm^2\ C^{-1}$. This was because of the polymer's electrochemical instability.[30]

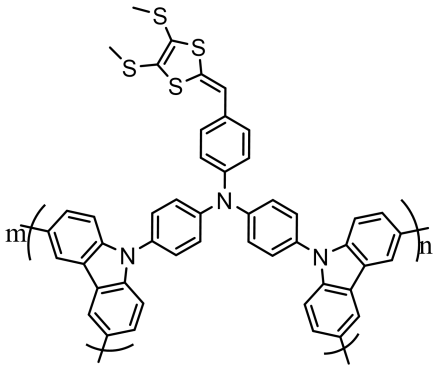

Voltage (V)	L *	a *	b *	Color
−0.4	73.86	0.47	17.57	Light yellow
1.2	64.53	−3.34	11.86	Green
1.8	57.72	−0.7	9.56	Blue grey

Figure 1.18: Structure of P(DTF-TPA-CBZ) and electrochromic color of its three states. Reproduced with permission from[30]. Copyright (2017), Elsevier.

Wu and Chung improved the coloration efficiency and stability of the electrochromic polymers by copolymerizing TPA and DTP monomers.[31] The resulting P(TTPA-co-DIT) and P(TTPA-co-BDTA) films had distinct electrochromic behaviors, from neutral state (yellow) to the oxidized state (blue), upon applying various potentials. In addition, the stabilities for the

color-bleached switching of the electrochromic device at the 100th cycle were higher than those of the copolymer films in an ionic liquid solution. The ΔT and coloration efficiency of P(TTPA-co-BDTA) and PProDOT-Et_2 in an electrochromic device with an applied potential of -1.0 V was 48.1% and 649.4 cm^2C^{-1} at 588 nm, respectively. These values are consisted with commercialized electrochromic compounds in **Figure 1.19**.

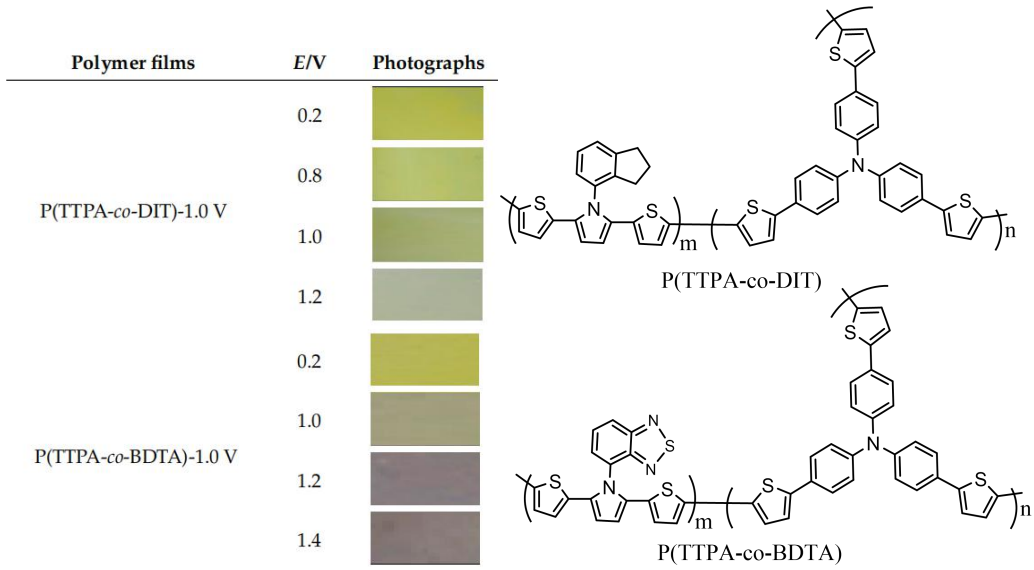

Figure 1.19: Structure of P(TTPA-co-DIT) and P(TTPA-co-BDTA) and their corresponding colors at different potentials.[31] copyrights (open access).

Despite the relative convenience of electrochemical polymerization of conducting polymers, both the cost and scalability limitations of this method cannot be ignored. Typically, only small scales of polymers can be prepared by this route. Moreover, the cost of using a large area platinum mesh electrode is high.

1.2.3 Photochemical cross-linking polymerization

A straightforward method for immobilization on surfaces is by the thermal polymerization monomers. However, this usually requires prolonged reaction times and high temperatures. To overcome these disadvantages, photochemical cross-linking polymerization can be done. The key advantage is that the polymerization can be patterned with a mask on the monomer surface. After irradiation and polymerization, the unreacted monomers can be rinsed from the surface. Usually a photoacid generator (PAG) is required.

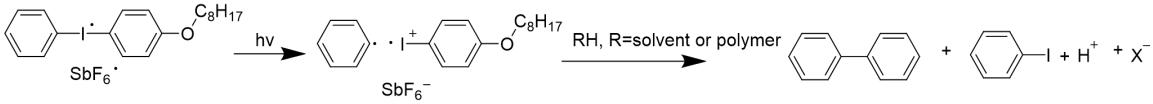

Figure 1.20. Photochemically mediated mechanism of photoacid generation.

Multiple strategies have been used for photo-polymerization, The most common ones will be introduced herein. Meerholz et al.[32] developed oxetane-functionalized organic semiconductors, for fabricatin multilayer OLEDs/PLEDs photo-lithographyically. In this approach, insoluble polymers are formed from the cationic ring opening polymerization (CROP) of oxetanes that is initiated by a photoacid generator, according to **Figure 1.20**. Using this approach. a full-color polymer organic light-emitting diode (OLED) display was fabricated by a direct photolithography process, that is, a process that allows direct structuring of the electroluminescent layer of the OLED by exposure to UV light. They attached oxetane side groups to the backbone of red-, green-, and blue-light emitting polymers and irradiated with a UV lamp for a short time and then spin-rising to remove the unreacted monomers. This allowed the use of photolithography to selectively cross-link thin films of these polymers. Temperatures around 60 ℃ gave the best resolution. The fabricated display was 200 × 600 μm^2 in size, and it exhibited good efficiency and color saturation.

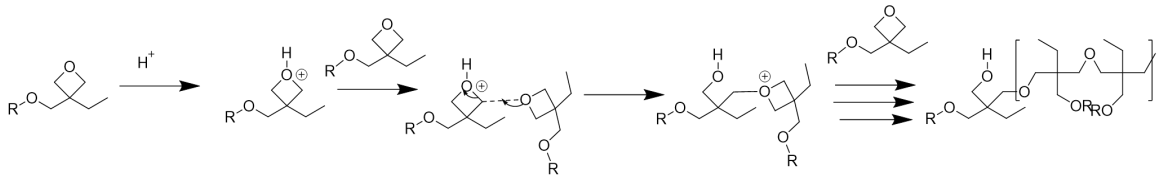

Figure 1.21. Mechanism of acid mediated oxetane ring opening polymerization.

However, there still remains a problem, even when using 25 wt % of PAG. Only 84% of the polymer film was cross-linked. The large amount of PAG used was problematic as it can potentially lead to increased amounts of unreactive cations. Another approach is to use oxiranes as cross-linkers. These are similar to oxetanes, but they have the advantages of shorter curing time and less harsh conditions. McDowell et al.[33] presented a protocol for photopatterning derivatives of poly(3,6-dimethoxy- 9,9-dialkylsilafluorenes) with resolutions exceeding 10 μm. The oxirane undergoes CROP by a simple photoacid and patterns were achieved by using photomasks with only 1 s of UV exposure. Curing at 90 ℃, and subsequent submersion in toluene for 30 s to remove non-cross-linked material gave good resolutions. The resulting cross-linked material possess blue photoluminescence with high solid state quantum yields (>80%) in **Figure 1.21**.

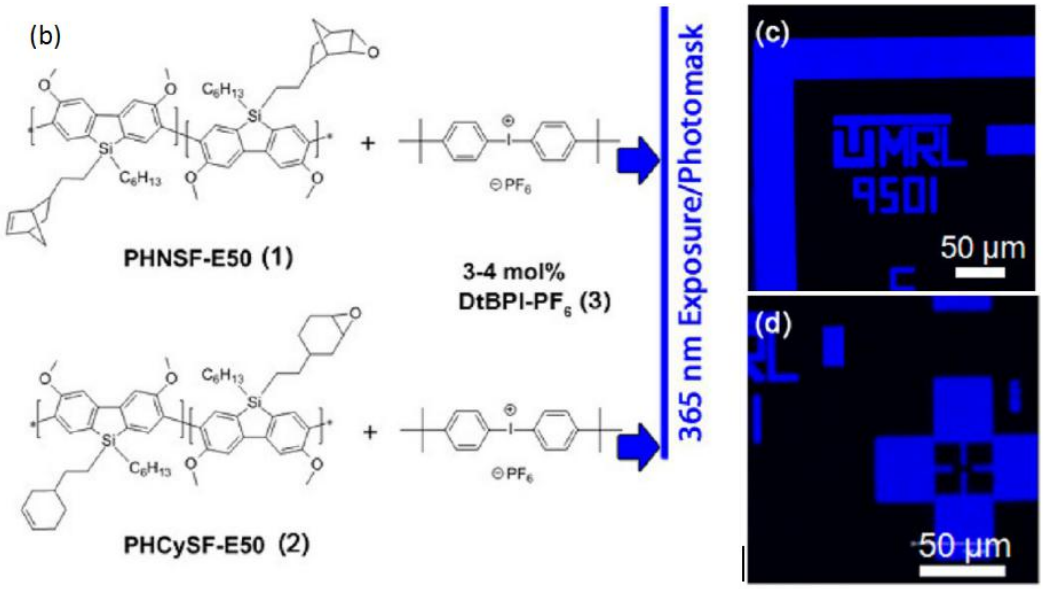

Figure 1.22. Oxiranes used by Mcdowell(left) and the blue photoluminescence pattern (right). Adapted with permission from[33]. Copyright (2014) American Chemical Society.

An alternate route is the pre-fuctionalization of conjugated polymers in organic semiconductors by diazides. These liberate singlet nitrenes and extrude nitrogen upon photolysis. Cho and co-workers[34] pursued this approach and they used bis(perfluorephenyl)-azide (bis-PFPA) as a cross-linker to form a robust solvent-resistant film. This prevented solvent-induced erosion during subsequent solution based device processing. These n-doping (N-NMBI) of semiconducting polymers improved the power conversion efficiency (PCE) of solar cells from 0.69% to 3.42%. The resulting devices showed good air stability, along with another important step towards efficient solution processed OPVs.

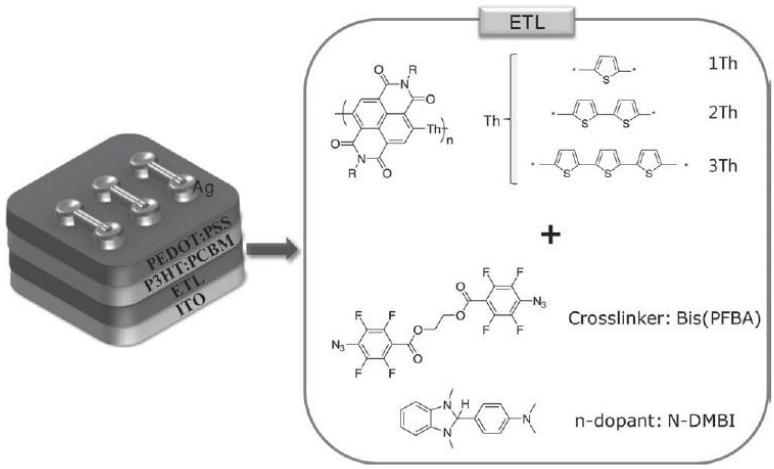

Figure 1.23. The structure of inverted solar cells and the materials used for in situ cross-linking and doping of electron transporting materials. Reprinted with permission from [34]. Copyright

(2011) WILEY-VCH.

Introducing cross-linking diazidesto alkylated polymer has its advantages. Mostly, the products can be synthesized without additional functional cross-linkable groups or reagents. The process is fast and it is compatible with any alkyl-substituted host. By optimizing the crosslinker structure, undesired side-reactions such as aromatic C-H-insertions can be suppressed. The polymers' core can also be photo-activated, for example with an anthraquinone core. Although this core undergoes a reversible reduction process, it can self-polymerize by irradiating at 254 nm and 360 nm. The redox property was however destroyed during the photochemical process. And, most of the photoinitiators are expensive and they are environmentally deleterious. Much improvement of this method is required for it to become eco-friendly.

1.3 Electroluminochromic materials

Electroluminochromic materials, defined similarly to electrochromic materials, undergo reversible changes in photoluminenscence with an applied external charge. This property is of great importance in optoelectronics applications, like phones' screens. These changes can either be emission wavelength or emission intensity. Unlike electrochromic materials, their electroluminochromic counterparts and their applications such as smart windows, smart optoelectronic displays, military camouflage coatings and sensing probes are comparatively fewer in quantity and they are less established.[35] The emissions of these materials are bleached when they are either electrochemically oxidized or reduced. In some cases, their emission wavelength shifts, thus giving a new emission color that is ideal for signal applications. A material that can be both electrochromic and electroluminochromic in the visible region is of interest. However, sustained reversible florescence quenching remains a challenge with small molecules and they have poor durability. Polymers on the other hand, are advantageous because they are electrochemically more robust on the device surface. Comparing to small molecules, polymers are less likely to delamination, they have better film homogeneity. Via non-conjugated structural linkages or groups onto the fluorophore moieties, there is lesser electronic communication between them. However, their emission intensity is usually decreased due to their tangled structure and narrowing of their energy gap. One possible pathway is to design and synthesis of novel organic materials with multi-fluorochromic states by coupling different fluorophore moieties, i.e., switching between two or more different emission colors (instead of quenching) via control of the external electrical voltage applied. Or, another possible way is to improve the device fabrication process as to make more homogeneous layers for example by using vacuum evaporator.

1.3.1 Benzothiadiazole as core

Early in our group, we reported two *push-pull* *N,N*-dimethylamino-benzothiadiazole

fluorophores.[36] These compounds were found to exhibit solvochchromism, electrochromic and electrofluorochromic properties. For the cynao derivative, it changed from yellow to mauve in color by applying +1.3 V potential for 30s in an electrolyte solution. For the nitro derivative, it changed from yellow to pale violet and its fluorescence colour changed from grey-green to green, while undergoing the oxidation process. Tailoring the UV-visible color and emission wavelength are possible by modifying the electronic group of the BZT core. The application of *push-pull* chromophores will be explored in this master thesis.

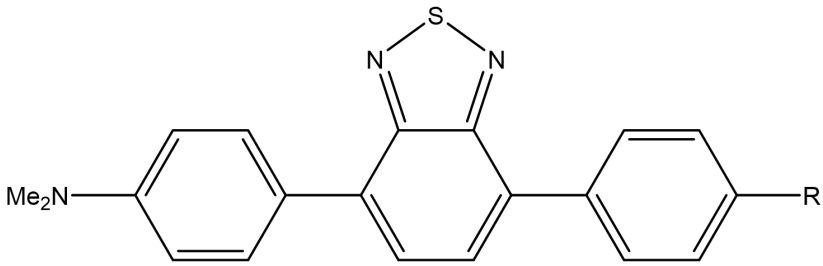

R= CN, NO_2

Figure 1.24. Structure of benzothiadiazole (BZT) derivatives.

1.3.2 Extension of TPA

An indolo[3,2-b]carbazole derivative bearing two diphenylamine termini has been synthesized by Liu's group in 2017. They extended the TPA group to a carbazole, leading to good electrochemical and photoluminescence properties.[37] By applying different potentials, a completely reversible conversion among three different colors (light-yellow, red, and blue) was possible. Moreover, a reversible turn-off and turn-on of its luminescence could also be tuned by electrochemical oxidation and reduction, respectively. This study extended the electroluminochromic materials into NIR region, as the oxidized species showed strong absorptions in the NIR region.

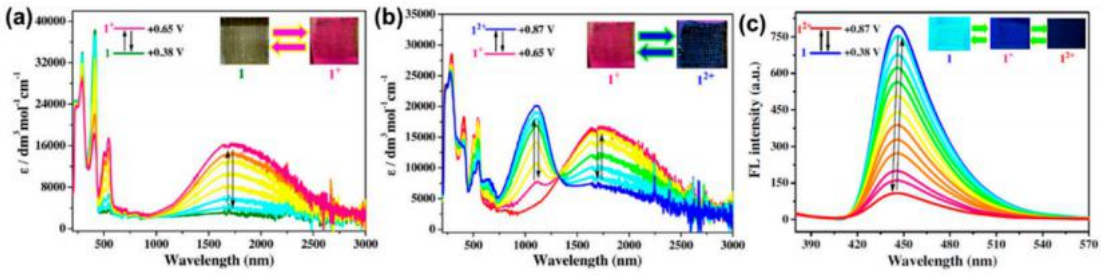

Figure 1.25. Color tuned properties by different potentials. Reproduced with permission from[37]. Copyright (2017), Elsevier.

In 2016, our group also reported an azomethine molecule whose emission can be quenched via two

azomethine bonds.[38] With electrochemical oxidation, the compound's absorbance changed from yellow to blue, while its photoluminescence intensity decreased sharply. Both molecules exhibited solvatochromism and they were also found to be aggregation induced emission (AIE, vide infra) active, which is of significance for its use in solid state devices.

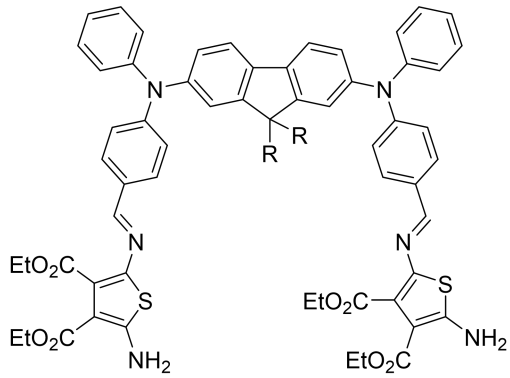

Figure 1.26. Structure of two azomethines.

From these two categories, it is evident that electro-active emitters are possible by combining the TPA core with conventional fluorophores. The remaining challenge is to maintain a high degree of emission in the solid state. This will be further demonstrated in chapter 2.

1.4 Aggregation induced emission effect

Typically, organic compounds that are aggregation induced emission (AIE) active have planar structures and they have higher photoemission efficiencies in solid state than in the solution. This is referred to as aggregation caused quenching. However, some fluorophores remain emissive when they are either aggregated or in the crystallized state.[39] The mechanism can be summarized along the following. According to fundamental physics, any movement, micro and macroscopic alike, consume energy. The intramolecular rotations of aromatics in AIE compounds that are active in solution serve as relaxation channels for its excitons to non-radiatively decay. In contrast in the aggregate state, the intramolecular rotations are restricted due to the physical constraint. The non-radiative pathways are blocked, leading to an increase in the solid state emission. This theory is referred to as restriction of intramolecular rotations (RIR).

The first AIE compound was reported by Tang et al (**Figure 1.27**).[40] The emission of the compound increased two orders of magnitude as the water fraction in the mixture solution increased.

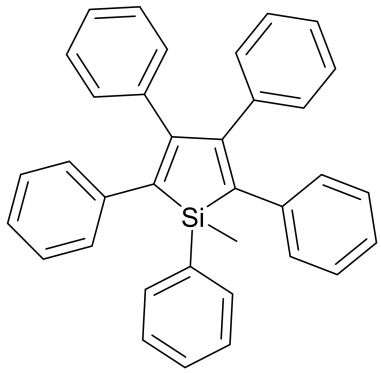

Figure 1.27. Structure of 1-methyl-1,2,3,4,5-pentaphenylsilole.

Since Tang's discovery, the area has become a hot field of interest because AIE could be used in various applications, including, biosensors,[41] organic perovskites,[42] OLEDs [43] and so on. Not surprisingly, the TPA group continues to play an important role in AIE based organic electronics. Liou's group took advantage of TPA and viologen groups to build a series of electrochromic materials.[44] These materials can undergo reversible oxidation, resulting in quenching of the original yellow emission. Fusing these two functional groups lowered the working potentials, shortened the switching response times, and increased the photoluminescence on/off contrast ratios.

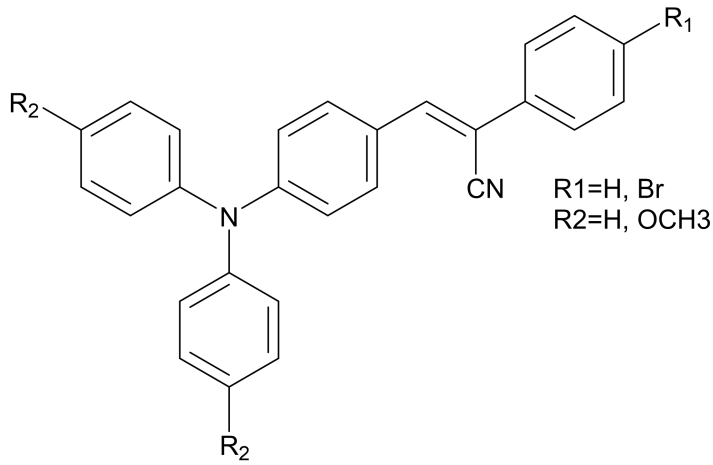

Figure 1.28. Structure of AIE TPA derivatives demonstrated by Liou.[44]

1.5 Jablonski diagram.

The Jablonski diagram is a diagram that illustrates the electronic states of a molecule and the transitions between them.[45] It shows both radiative and non-radiative transitions. From the diagram, it is clear that when a molecule absorbs a certain energy, it can be excited from the

ground state S_0 to excited singlet states S_1, S_2....S_n, and undergo intersystem crossing to the triplet excited state T_1, T_2...T_n. In a system with two spin -1/2 particles for example, the proton and electron in the ground state of hydrogen, measured on a given axis, each particle can be either spin up or spin down so the system has four basis states in all. For the triplet states, there are three states with a total spin angular momentum 1. While for singlet states, there is only one state with total spin angular momentum 0, which leads to 25 % of singlet states and 75% of triplet states. Taking S_2 as an example, the excited state can relax to the first excited state via internal conversion, followed by non-radiative process such as molecular vibration. From S_1 to S_0, the process can be radiative resulting in fluorescence. It is fast and often occurs within nanoseconds. If the energy gap between the S_1 and T_1 states is sufficiently small, intersystem crossing can occur. This leads to another form of radiative decay, which is phosphorescence. This process is usually longer than the fluorescence decay.

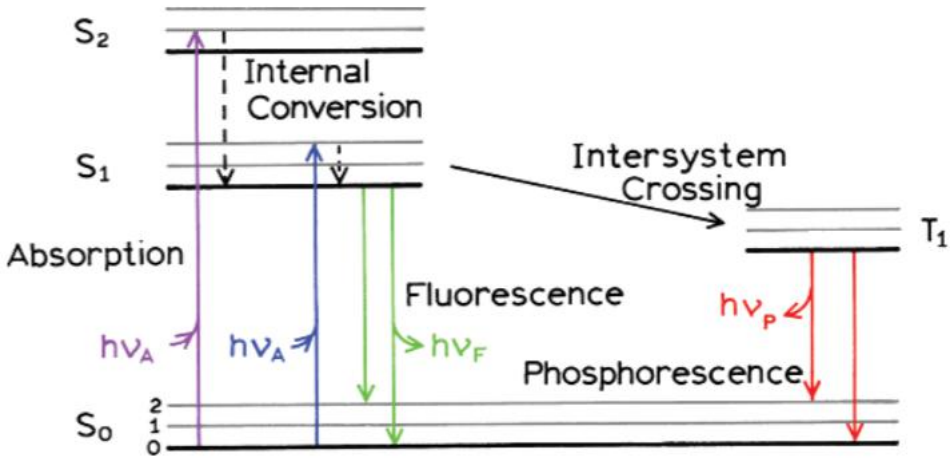

Figure 1.29. Energy states for a single molecule. Reprinted with permission from[46]. Copyright (2006), Springer.

1.6 Problems to be solved

From the literature survey described above, it is apparent that a win-win solution is possible with organic molecules in that they can be both electrochromic and electroluminochromic. This is addition to their many advantages compared to their inorganic counterparts such as an extensive palette of colors in visible and NIR region, better processability and compatible with flexible substrates. Unfortunately, organic materials lag in applications compared to the inorganic counterparts. For example, inorganic electrochromic materials have been commercially used in 'smart' windows, such as the Boeing 787 Dreamliner's window.[47] Organic molecules further

suffer from poor durability as the electrochromic layer can undergo self-bleaching in a short period time. However, for further eco-friendly requirements, the trend to replace inorganic materials with organic materials is inevitable. The challenge remains to design organic molecules that perform better than their inorganic counterparts such as color changes in the visible region, reversible fluorescence quenching, extend electrochemical durability and consistent emission color and wavelength with applied potentials. Nowadays, we can have organic electrochromic materials that change colors in the visible region or electrofluorochromic materials that change the emission color either by ‘on-off’ or by shfting the emission wavelength. However, to combine this two properties together, we have to design materials that remain high emission yield in solid state while still have the electrochromic abilities. Thus, AIE effect comes up to our mind that can design the compound with high emission yield in solid state. By attaching the electrochromic groups with the AIE core could solve this problem. Moreover, most of the studies have focused on the area of active layer in the operating device. The device has to be continously applying potential to maintain the colors. For energy saving aspect, it is better to make passive devices which means with once potential applied, it can remain the color for a longer time until a reversible potential applied to switch the color back. Thus, a complementary opposite layer in the operating device can be applied.

1.7 Objectives

To date, most materials are exclusively electrochromic. They therefore change colors in the visible spectrum with applied potential with limited fluorescence change. There are limited examples of materials capable of undertaking a dual chromic role; being electrochromic and electrofluorochromic.[48, 49] Towards this end, it is of interest to develop materials whose electrochemically mediated property changes include both reversible color changes and emission quenching in the visible region. To date, how to remain the emission yield in the solid state is a major problem for electrofluorochromic devices due to the self quenching. One possible way is to take advantages of AIE effect. Benzothiadiazole is one of the famous compound which can have great emission yield both in solution and solid state. To make the compound also electrochromic, TPA group can be introduced in to the design. This two process lead to the compound which has both electrochromic and electrofluorochromic potentials. By coupling with different end groups, electron-withdrawing or electron-donating. The compounds can be either *'push-pull'* or *'push-push'* to have different electron properties which can tune the spectrum range of absorption or emission. Towards these ends, benzothiadiazole fluorophores were investigated as potential dual-role materials. The effect of various electron withdrawing groups of a series of benzothiadiazole fluorophores on the key properties for their dual-role use in operating devices were evaluated. While people are putting great efforts on the active devices which a continuous potential has to be applied to keep the color switching, the new generation device-passive device can save a lot of energy due to the color memory effect. Anthraquinone derivatives were chosen due to the capacity of the core which can provide the memory effect. Further polymerize it on the surface can extend the stability and durability of this layer.

References

1. Klauk, H., *Organic electronics: materials, manufacturing, and applications*. John Wiley & Sons: 2006.
2. Granqvist, C. G., *Handbook of inorganic electrochromic materials*. Elsevier: 1995.
3. Akimoto, K., Semiconductor device including zinc oxide containing semiconductor film. Google Patents: 2012.
4. Dunbar, K. R.; Heintz, R. A., Chemistry of transition metal cyanide compounds: Modern perspectives. *Progress in Inorganic Chemistry* **1997,** *45*, 283-392.
5. Karyakin, A. A., Prussian blue and its analogues: electrochemistry and analytical applications. *Electroanalysis: An International Journal Devoted to Fundamental and Practical Aspects of Electroanalysis* **2001,** *13* (10), 813-819.
6. Zloczewska, A.; Celebanska, A.; Szot, K.; Tomaszewska, D.; Opallo, M.; Jönsson-Niedziolka, M., Self-powered biosensor for ascorbic acid with a Prussian blue electrochromic display. *Biosensors and Bioelectronics* **2014,** *54*, 455-461.
7. Itaya, K.; Shibayama, K.; Akahoshi, H.; Toshima, S., Prussian-blue-modified electrodes: An application for a stable electrochromic display device. *Journal of Applied Physics* **1982,** *53* (1), 804-805.
8. Groenendaal, L.; Jonas, F.; Freitag, D.; Pielartzik, H.; Reynolds, J. R., Poly (3, 4-ethylenedioxythiophene) and its derivatives: past, present, and future. *Advanced materials* **2000,** *12* (7), 481-494.
9. Se, M.; Papillon, J.; Schulz, E.; Lemaire, M., New synthetic method for the polymerization of alkylthiophenes. *Tetrahedron letters* **1999,** *40* (32), 5873-5876.
10. Wang, Q.; Takita, R.; Kikuzaki, Y.; Ozawa, F., Palladium-catalyzed dehydrohalogenative polycondensation of 2-bromo-3-hexylthiophene: an efficient approach to head-to-tail poly (3-hexylthiophene). *Journal of the American Chemical Society* **2010,** *132* (33), 11420-11421.
11. Jonas, F.; Krafft, W.; Muys, B. In *Poly (3, 4-ethylenedioxythiophene): Conductive coatings, technical applications and properties*, Macromolecular Symposia, Wiley Online Library: 1995; pp 169-173.
12. Dietrich, M.; Heinze, J.; Heywang, G.; Jonas, F., Electrochemical and spectroscopic characterization of polyalkylenedioxythiophenes. *Journal of Electroanalytical Chemistry* **1994,** *369* (1-2), 87-92.
13. Bockman, T.; Kochi, J., Isolation and oxidation-reduction of methylviologen cation radicals. Novel disproportionation in charge-transfer salts by X-ray crystallography. *The Journal of Organic Chemistry* **1990,** *55* (13), 4127-4135.
14. Porter, W. W.; Vaid, T. P.; Rheingold, A. L., Synthesis and Characterization of a Highly Reducing Neutral "Extended Viologen" and the Isostructural Hydrocarbon 4, 4 ""-Di-n-octyl-p-quaterphenyl. *Journal of the American Chemical Society* **2005,** *127* (47), 16559-16566.
15. Quinton, C.; Alain-Rizzo, V.; Dumas-Verdes, C.; Miomandre, F.; Clavier, G.; Audebert, P., Redox-and protonation-induced fluorescence switch in a new triphenylamine with six stable active or non-active forms. *Chemistry–A European Journal* **2015,** *21* (5), 2230-2240.

16. Li, Y.; Tan, T.; Wang, S.; Xiao, Y.; Li, X., Highly solvatochromic fluorescence of anthraquinone dyes based on triphenylamines. *Dyes and Pigments* **2017,** *144*, 262-270.
17. Jin, H.; Li, X.; Tan, T.; Wang, S.; Xiao, Y.; Tian, J., Electrochromic properties of novel chalcones containing triphenylamine moiety. *Dyes and Pigments* **2014,** *106*, 154-160.
18. Cheng, S.-H.; Hsiao, S.-H.; Su, T.-H.; Liou, G.-S., Novel aromatic poly (amine-imide) s bearing a pendent triphenylamine group: synthesis, thermal, photophysical, electrochemical, and electrochromic characteristics. *Macromolecules* **2005,** *38* (2), 307-316.
19. Liou, G.-S.; Hsiao, S.-H.; Chen, H.-W., Novel high-T g poly (amine-imide) s bearing pendent N-phenylcarbazole units: synthesis and photophysical, electrochemical and electrochromic properties. *Journal of Materials Chemistry* **2006,** *16* (19), 1831-1842.
20. Hsiao, S.-H.; Liou, G.-S.; Kung, Y.-C.; Pan, H.-Y.; Kuo, C.-H., Electroactive aromatic polyamides and polyimides with adamantylphenoxy-substituted triphenylamine units. *European polymer journal* **2009,** *45* (8), 2234-2248.
21. Yen, H. J.; Tsai, C. L.; Chen, S. H.; Liou, G. S., Electrochromism and Nonvolatile Memory Device Derived from Triphenylamine-Based Polyimides with Pendant Viologen Units. *Macromolecular rapid communications* **2017,** *38* (9), 1600715.
22. Chang, C.-W.; Liou, G.-S.; Hsiao, S.-H., Highly stable anodic green electrochromic aromatic polyamides: synthesis and electrochromic properties. *Journal of Materials Chemistry* **2007,** *17* (10), 1007-1015.
23. Liou, G.-S.; Hsiao, S.-H.; Chen, W.-C.; Yen, H.-J., A new class of high T g and organosoluble aromatic poly (amine− 1, 3, 4-oxadiazole) s containing donor and acceptor moieties for blue-light-emitting materials. *Macromolecules* **2006,** *39* (18), 6036-6045.
24. Yen, H. J.; Liou, G. S., Synthesis, photoluminescence, and electrochromism of novel aromatic poly (amine-1, 3, 4-oxadiazole) s bearing anthrylamine chromophores. *Journal of Polymer Science Part A: Polymer Chemistry* **2009,** *47* (6), 1584-1594.
25. Hsiao, S. H.; Wang, H. M.; Guo, W.; Sun, C. H., Enhancing Redox Stability and Electrochromic Performance of Polyhydrazides and Poly (1, 3, 4-oxadiazole) s with 3, 6-Di-tert-butylcarbazol-9-yltriphenylamine Units. *Macromolecular Chemistry and Physics* **2011,** *212* (8), 821-830.
26. Kung, Y. C.; Hsiao, S. H., Soluble, redox-active, and blue-emitting poly (amide-hydrazide) s and poly (amide-1, 3, 4-oxadiazole) s containing pyrenylamine units. *Journal of Polymer Science Part A: Polymer Chemistry* **2011,** *49* (22), 4830-4840.
27. Liou, G.-S.; Hsiao, S.-H.; Chen, W.-C.; Yen, H.-J. J. M., A new class of high T g and organosoluble aromatic poly (amine− 1, 3, 4-oxadiazole) s containing donor and acceptor moieties for blue-light-emitting materials. **2006,** *39* (18), 6036-6045.
28. Rudenko, A. E.; Thompson, B. C., Influence of the carboxylic acid additive structure on the properties of poly (3-hexylthiophene) prepared via direct arylation polymerization (DArP). *Macromolecules* **2015,** *48* (3), 569-575.
29. Cai, S.; Wen, H.; Wang, S.; Niu, H.; Wang, C.; Jiang, X.; Bai, X.; Wang, W., Electrochromic polymers electrochemically polymerized from 2, 5–dithienylpyrrole (DTP) with different

triarylamine units: Synthesis, characterization and optoelectrochemical properties. *Electrochimica Acta* **2017,** *228*, 332-342.

30. Zhou, P.; Wan, Z.; Liu, Y.; Jia, C.; Weng, X.; Xie, J.; Deng, L., Synthesis and electrochromic properties of a novel conducting polymer film based on dithiafulvenyl-triphenylamine-di (N-carbazole). *Electrochimica Acta* **2016,** *190*, 1015-1024.

31. Wu, T.-Y.; Chung, H.-H., Applications of tris (4-(thiophen-2-yl) phenyl) amine-and dithienylpyrrole-based conjugated copolymers in high-contrast electrochromic devices. *Polymers* **2016,** *8* (6), 206.

32. Gather, M. C.; Koehnen, A.; Falcou, A.; Becker, H.; Meerholz, K., Solution-processed full-color polymer organic light-emitting diode displays fabricated by direct photolithography. *Advanced Functional Materials* **2007,** *17* (2), 191-200.

33. McDowell, J. J.; Maier-Flaig, F.; Wolf, T. J.; Unterreiner, A.-N.; Lemmer, U.; Ozin, G., Synthesis and Application of Photolithographically Patternable Deep Blue Emitting Poly (3, 6-Dimethoxy-9, 9-dialkylsilafluorene) s. *ACS applied materials & interfaces* **2014,** *6* (1), 83-93.

34. Cho, N.; Yip, H. L.; Davies, J. A.; Kazarinoff, P. D.; Zeigler, D. F.; Durban, M. M.; Segawa, Y.; O'Malley, K. M.; Luscombe, C. K.; Jen, A. K. Y., In-situ Crosslinking and n-Doping of Semiconducting Polymers and Their Application as Efficient Electron-Transporting Materials in Inverted Polymer Solar Cells. *Advanced Energy Materials* **2011,** *1* (6), 1148-1153.

35. Chua, M. H.; Zhu, Q.; Shah, K. W.; Xu, J., Electroluminochromic materials: from molecules to polymers. *Polymers* **2019,** *11* (1), 98.

36. Wałęsa-Chorab, M.; Tremblay, M.-H.; Ettaoussi, M.; Skene, W. G., Photophysical, electrochemical, and spectroelectrochemical investigation of electronic push–pull benzothiadiazole fluorophores. *Pure and Applied Chemistry* **2015,** *87* (7), 649-661.

37. Zhang, J.; Chen, Z.; Wang, X.-Y.; Guo, S.-Z.; Dong, Y.-B.; Yu, G.-A.; Yin, J.; Liu, S.-H., Redox-modulated near-infrared electrochromism, electroluminochromism, and aggregation-induced fluorescence change in an indolo [3, 2-b] carbazole-bridged diamine system. *Sensors and Actuators B: Chemical* **2017,** *246*, 570-577.

38. Wałęsa-Chorab, M.; Tremblay, M. H.; Skene, W. G., Hydrogen-Bond and Supramolecular-Contact Mediated Fluorescence Enhancement of Electrochromic Azomethines. *Chemistry–A European Journal* **2016,** *22* (32), 11382-11393.

39. Hong, Y.; Lam, J. W.; Tang, B. Z., Aggregation-induced emission. *Chemical Society Reviews* **2011,** *40* (11), 5361-5388.

40. Luo, J.; Xie, Z.; Lam, J. W.; Cheng, L.; Chen, H.; Qiu, C.; Kwok, H. S.; Zhan, X.; Liu, Y.; Zhu, D., Aggregation-induced emission of 1-methyl-1, 2, 3, 4, 5-pentaphenylsilole. *Chemical communications* **2001,** (18), 1740-1741.

41. Huang, Z.; Chen, Y.; Wang, R.; Zhou, C.; Liu, X.; Mao, L.; Yuan, J.; Tao, L.; Wei, Y., An acrylate AIE-active dye with a two-photon fluorescent switch for fluorescent nanoparticles by RAFT polymerization: synthesis, molecular structure and application in cell imaging. *RSC Advances* **2020,** *10* (10), 5704-5711.

42. Lim, C. K.; Maldonado, M.; Zalesny, R.; Valiev, R.; Ågren, H.; Gomes, A. S.; Jiang, J.; Pachter, R.; Prasad, P. N., Interlayer-Sensitized Linear and Nonlinear Photoluminescence of Quasi-2D

Hybrid Perovskites Using Aggregation-Induced Enhanced Emission Active Organic Cation Layers. *Advanced Functional Materials* **2020,** *30* (16), 1909375.

43. Guo, X.; Yuan, P.; Qiao, X.; Yang, D.; Dai, Y.; Sun, Q.; Qin, A.; Tang, B. Z.; Ma, D., Mechanistic Study on High Efficiency Deep Blue AIE-Based Organic Light-Emitting Diodes by Magneto-Electroluminescence. *Advanced Functional Materials* **2020**, 1908704.

44. Chen, S.-Y.; Chiu, Y.-W.; Liou, G.-S., Substituent effects of AIE-active α-cyanostilbene-containing triphenylamine derivatives on electrofluorochromic behavior. *Nanoscale* **2019,** *11* (17), 8597-8603.

45. Frackowiak, D., The jablonski diagram. *Journal of Photochemistry and Photobiology B: Biology* **1988,** *2* (3), 399.

46. Lakowicz, J. R., *Principles of fluorescence spectroscopy*. Springer Science & Business Media: 2013.

47. Xu, J. W.; Toppare, L.; Li, Y.; Xu, C.; Kim, E.; Zhong, Y.-W.; Zhang, C.; Beneduci, A.; Ak, M.; Hsiaob, S.-H., *Electrochromic Smart Materials: Fabrication and Applications*. Royal Society of Chemistry: 2019.

48. Su, K.; Sun, N.; Yan, Z.; Jin, S.; Li, X.; Wang, D.; Zhou, H.; Yao, J.; Chen, C., Dual-Switching Electrochromism and Electrofluorochromism Derived from Diphenylamine-Based Polyamides with Spirobifluorene/Pyrene as Bridged Fluorescence Units. *ACS Applied Materials & Interfaces* **2020**.

49. Wu, J.; Han, Y.; Liu, J.; Shi, Y.; Zheng, J.; Xu, C., Electrofluorochromic and electrochromic bifunctional polymers with dual-state emission via introducing multiple c—h⋯ π bonds. *Organic Electronics* **2018,** *62*, 481-490.

2. Experimental Methods

2.1. Spectroscopy, electrochemistry, spectroelectrochemistry measurements

This section will be fully explained in Chapter 3 section experimental.

2.2 Device fabrication

Functioning electrochromic/electrofluorochromic devices were fabricated with a sandwich architecture. The electrolyte gel consisted of $LiClO_4$ (300 mg) and PMMA (120 kDa, 700 mg) that were added to acetonitrile (5 mL). The mixture was heated and stirred until a homogeneous solution was obtained. Next, propylene carbonate (2 g) was added to the mixture and it was stirred overnight to yield a highly viscous and transparent gel. Two ITO coated glass substrates were used to fabricate the device. First, the electrochromic material was spray coated on one substrate. Next, the conductive electrolyte gel was spread over the other ITO electrode. The two plates were sandwiched together and held in place with a metal clip. A commercial glass/metal glue was applied at the interface of the plates to seal the device. Caution was taken to ensure the glue did not contact either the gel or electrochromic materials and to ensure it did not diffuse into the device before it was cured. Copper tape was then applied to each substrate for connecting to the potentiostat with alligator clips. Then devices were operated by applying potentials differently to show the electrochromic properties.

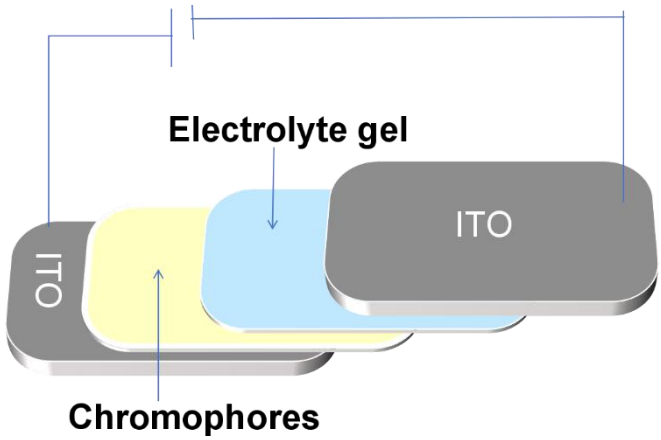

Figure 2.1. Sandwich structure for fabricating electrochromic device.

2.3 Other characterizations

Nuclear magnetic resonance (NMR)

^{1}H NMR and ^{13}C NMR of the targeted compounds were done with the Bruker Avance 400. The NMR data were further treated by MestReNova program.

Mass spectra

Accurate mass of each sample was done at the Centre régional de spectrométrie de masse with samples prepared (0.5 mg/mL) in a given solvent (3 mL) in the required mass sample vials.

X-ray diffraction

Single crystals were growth by the slow solvent evaporation. The given compound (1 mg) was dissolved in dichloromethane (1 mL). After careful evaporation at room temperature, single crystals were obtained. The structures were resolved with the collaboration of Drs. Michel Simard, Maris Thierry, and Daniel Chartrand.

Temperature dependent spectroscopy

Chromophores were dissolved in anhydrous 2-methyltetrahydrofuran and they were cooled to -160 ℃，-130 ℃，-100 ℃，-70 ℃，-40 ℃，-10 ℃ and 20 ℃ with liquid N_2. The experiment was carried out with the CoolSpek UV model USP-203-B, which contains a cryostat along with a temperature controller. The instrument was then connected to a FLSP-920 fluorometer. The excitation wavelength for the measurement was determined by the absorption maximum. At each given temperature, the sample was stabilized for 5 minutes in the cuvette before the emission scan was recorded.

AIE study

Different ratios of water/THF in 10, 20, 40, 60 ,80, 100 volume percent solutions were prepared. The same amount of chromophore was added to each solution. After degassing with N_2 for 30 minutes, an emission spectrum was scanned. The N_2 purged samples were also irradiated under a hand-UV-lamp in the dark environment to qualitative evaluate the AIE properties.

Deposit of chromophores on substrates

Spin coating was chosen to form a homogeneous thin film of chromophores on microscopic glass substrates at different spin speed and deposit times. The quantum yield was measured in triplic

and they were averaged for the solid state emission yield.

Spray coating was chosen to deposit the electrolyte gel in a small area when fabricating the devices. The air brush was carefully cleaned 3 times both at the beginning and the end using acetone.

Preparing ITO plates

The ITO plates were obtained from Delta technologies, Ltd, USA. The surface resistance has 8-12 Ω / cm^2. Before using, a careful cleaning process was done. Immersing the ITO plates in an ultrasonic bath with acetone, water and anhydrous ethanol for 15 minutes separately and then dried under N_2. The substrates were stored in glovebox until they were used.

2.4 Quantum yield

The fluorescence quantum yield (Φ_{fl}) is the amount of photon emission over amount of light absorbed.[1] Absolute values can be calculated from the following equation (**2.1**):

$$\phi_x = \phi_{ST}\left(\frac{Grad_x}{Grad_{ST}}\right)\left(\frac{\eta_x^{\,2}}{\eta_{ST}^{\,2}}\right)$$

Equation **2.1**： Fluorescence quantum yield.

The subscripts ST and X describe the reference and sample respectively, Φ is the fluorescence quantum yield, Grad is the area from the plot of fluorescence intensity vs absorbance, and η is the refractive index of the solvent.

In this study, we used the same solvent and glass substrate for both the references and samples. In this way, the difference in η can be ignored. The absolute quantum yield was directly calculated from the integrated areas of emission and excitation over the difference between the scattering of the reference and the sample at the wavelength.[2]

2.5 Coloration efficiency

The coloration efficiency η is a standard which is used for comparing the electrochromic materials. It is defined as the relationship between the injected/ejected charge as a function of electrode area (Q) and the change in optical density, ΔOD, at a specific wavelength λ, according to the following equation (**2.2**):

$$\eta = \frac{\Delta OD}{Q}, \text{ where } \Delta OD = \log\left[\frac{T_{ox}}{T_{red}}\right].$$

Equation **2.2: Coloration efficiency.**

The electrode area can be calculated from the working area of the 19-hole honeycomb electrode or the area of the ITO plates for devices.[3]

Better performing electrochromic materials, ideally have higher coloration efficiencies, meaning fast response and significant transmittance changes.

References

1. Lakowicz, J. R., *Principles of fluorescence spectroscopy*. Springer Science & Business Media: 2013.
2. Williams, A. T. R.; Winfield, S. A.; Miller, J. N., Relative fluorescence quantum yields using a computer-controlled luminescence spectrometer. *Analyst* **1983,** *108* (1290), 1067-1071.
3. Gaupp, C. L.; Welsh, D. M.; Rauh, R. D.; Reynolds, J. R., Composite coloration efficiency measurements of electrochromic polymers based on 3, 4-alkylenedioxythiophenes. *Chemistry of Materials* **2002,** *14* (9), 3964-3970.

3. Study of a red emissive fluorophore which has dual role in both electrochromic and electrofluorochromic

In this chapter, a molecule was synthesized by Suzuki-Miyaura coupling of triphenylamine (TPA) and benzothiadiazole (BZT), followed by coupling with *N*,*N*-dimethylamine. This molecule was designed to take advantages of the electrochemical properties of TPA as well as BZT's strong emission. The intense solution emission of the electronic *push-push* fluorophore was carried over to the solid state. The electrochemical reversibility and the fluorescence intensity modulation of the fluorophore proved that small organic fluorophores can be both electrochromic in the visible region with electrofluochromism of fluorescence off/on in deep red region.

The studied fluorophore was synthesized by a former trainee student Mathieu Frémont.

The crystal structure of the fluorophore was resolved by Dr. Maris Thierry

My contribution in this paper was the complete characterization of the fluorophore, including photophysical, electrochemical, and spectroeletrochemical property evaluation in addition to single crystal growth. Furthermore, I successfully made a working device that showed the dual role properties of the fluorophore, thus illustrating its potential as an active layer in electrochromic/electofluorochormic devices.

Electrochromic and Electrofluorochromic Dual Role of a Red Emissive Fluorophore

Chengzhang Yao, Mathieu Frémont, W. G. Skene

[1]Laboratoire de caractérisation photophysique des matériaux conjugués Département de Chimie, Pavillon JA Bombardier, Université de Montréal, CP 6128, succ. Centre-ville, Montréal, Québec, Canada H3C 3J7

3.1 Abstract

An asymmetric benzothiadiazole fluorophore with two different electron rich termini was investigated as a dual-role active material for electrochromism and electrofluorochromism. Its fluorescence yield (Φ_{fl}) and emission wavelength were dependent on solvent polarity. It fluoresced appreciably (Φ_{fl}=40%) in an electrolyte gel that is commonly used in electrochromic devices, as a film on a glass substrate (Φ_{fl}=20%), and in a working dual electrochromic/electrofluorochormic device (Φ_{fl}=13%). It underwent two stepwise oxidations. The first oxidation resulted in a 1000 nm red shift in the absorption to broadly absorb in the NIR. Whereas, the second oxidation led to a perceived green color at 715 nm. The fluorescence intensity could reversibly be modulated electrochemically. The emission intensity of the fluorophore was modulated with applied potential in both device-like conditions and in an operating device. Both the dual electrochromic and the electrofluorochromic behavior of the fluorophore were demonstrated.

3.2 Introduction

Materials that respond to external stimuli have found diverse applications. These include therapeutics with the encapsulating polymer releasing its drug cargo upon command.[1] Stimuli used for triggering a given responsive in materials include pH,[2] light,[3] and redox reactions.[4] The latter play an important role in biochemical reactions. Redox responsive materials have also been used as coatings in various commercial applications.[5] In such cases, the color of the coating reversibly changes with applied potential.[6] This stimuli responsiveness has been applied to smart-buildings.[7] In these applications, the light entering the building through the windows can be modulated by the coating whose transmission can be adjusted with an applied potential. This electrochromic layer has the advantage of reducing heating and cooling costs, resulting in both economic and ecological benefits.[8]

Both the color of the neutral and redox states of organic electrochromic materials can be adjusted to span the visible spectrum.[9] Absorptions in the visible region are typically achieved with conjugated donor-acceptor aromatics.[10] This is also possible when electron donating and accepting groups are conjugated, giving rise to intramolecular charge transfer.[11] Such is the case when a benzothiadiazole is conjugated with electron rich aromatics such as triphenylamines.[12] An added benefit of conjugated benzothiadiazoles (BZT) is its intrinsic fluorescent.[13] Its emission wavelength can be adjusted contingent on the type of aromatics to which it is coupled. For example, benzothiadiazoles strongly emit in the visible when they are coupled with triphenylamines.[14] The intramolecular charge transfer state that occurs with such electronic *push-pull* fluorophores upon photoexcitation is sensitive to polarity.[15] Emission color tuning is therefore possible by solvent polarity.

The intrinsic electroactivity of the triphenylamine can also be taken advantage for modifying the properties of conjugated benzothiadiazoles.[16] With applied potentials, the spectroscopic properties of triarylamine benzothiadiazoles can be modulated. This electrochromic behavior results in visible absorption changes with the color of both the neutral and oxidized states being contingent on the electronic groups.[17]

Fluorescence modulation is also possible with applied potential.[18] In general, this can proceed by two modes of actions. In one case, the electrochemically generated state efficiently deactivates the intrinsic emissive state.[19] In the other mode, the absorption of electrochemically generated state is significantly different from the neutral state. With applied potential, the neutral state bleaches and fewer excited states are produced when exciting at the neutral specie's absorption wavelength. Electrofluorescent devices have been prepared using fluorophores coupled with electroactive triphenylamines.[20] While the fluorescence of these devices is reversibly switched between their *off* and *on* states with applied potential, the emission of the triphenylamine fluorophores derivatives has been limited to the blue region of the visible spectrum. Extending the spectroscopic properties to the red region and into the near infrared regions are of importance for telecommunication switches and light emitting devices.[21] We were therefore motivated to investigate an electrofluorescent material having an emission in the red region of the visible spectrum. **1** (**Figure 3.1**) was targeted because its electronic *push-pull-push* structure was expected to address this criterion. It is also known to fluoresce in solution[22] and similar structures emit appreciably in thin films[23] in addition to undergoing aggregation induced emission.[24] The latter is a key property requirement for use in solid-state devices. Moreover, the terminal amines are expected to form a charge transfer state when excited. This would be extremely sensitive to polarity. The emission of **1** would therefore be solvent dependent, making it ideal for probing the polarity in operando in functioning electrofluorescent devices. The added advantage of shifting the emission to the red, is its absorption would also be bathochromically shifted deeper into the visible region. The color switching of **1** with

applied potential was therefore expected to be visibly detectable with the color of the oxidized state being shifted towards the NIR region. **1** was also expected to be both electrochromic and electrofluorescent with its color and emission bleaching with applied potential. Despite having properties that are ideally suited for its use in chromic devices, **1** is underexplored as an electroactive chromophore and fluorophore in such devices. To demonstrate its potential as dual-role active material in enabling devices with visibly detectable color changes and emission intensity variation with potential, the electrochromism and electrofluorochromism of **1** are herein reported. Its fluorescence and emission yield sensitivity towards polarity are also presented to illustrate its solid-state emission and to probe the polarity environment in operando.

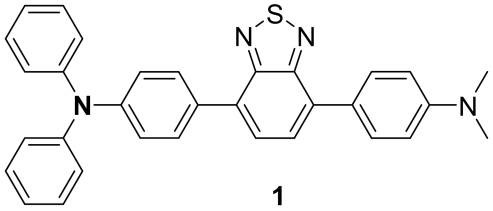

1

Figure 3.1. Fluorophore examined for use as a dual role electroactive material.

3.3 Results and Discussion

Structural Determination

To provide unequivocal evidence for the structure of **1**, notably is asymmetry regarding the end-capped amines, crystals for X-ray diffraction were prepared. Single crystals in the form of orange/red needles of the compound that were suitable for measurement were obtained by the slow evaporation of a dichloromethane solution. Two unique compounds of **1** were found per unit cell (**Figure 3.2**), with both molecules having similar bond distances and angles. Of importance, the asymmetry of **1** can be confirmed by the resolved X-ray structure, consisting of a NMe_2 moiety at one end and a triphenylamine group on the opposite end. The different electron donating strengths of the two unique end-capping units were expected to affect the bond R_2N–phenyl lengths. Indeed, the Me_2N–phenyl bond distance for both molecules of **1** was shorter than the corresponding distance with the triphenylamine moiety. For example, the N3A-C10 bond length was 1.374(2) Å, compared to 1.423(2) Å for its N4A-C18A counterpart. These contrast with the C7A-C3A and C6A-C15A bond distances that were longer (1.76(2) Å). Another feature of the crystallized structure of **1** is the dihedral angles. The phenyl–BZT angles of **1** were different for the NMe2 side being 16.5(3)º larger than the Ph_2N flank. The Me_2N–phenyl was less twisted than the corresponding Ph_2N angle, owing to the reduced steric hindrance between the *ortho* hydrogen of the phenyl and NR_2 moieties (See Table S4).

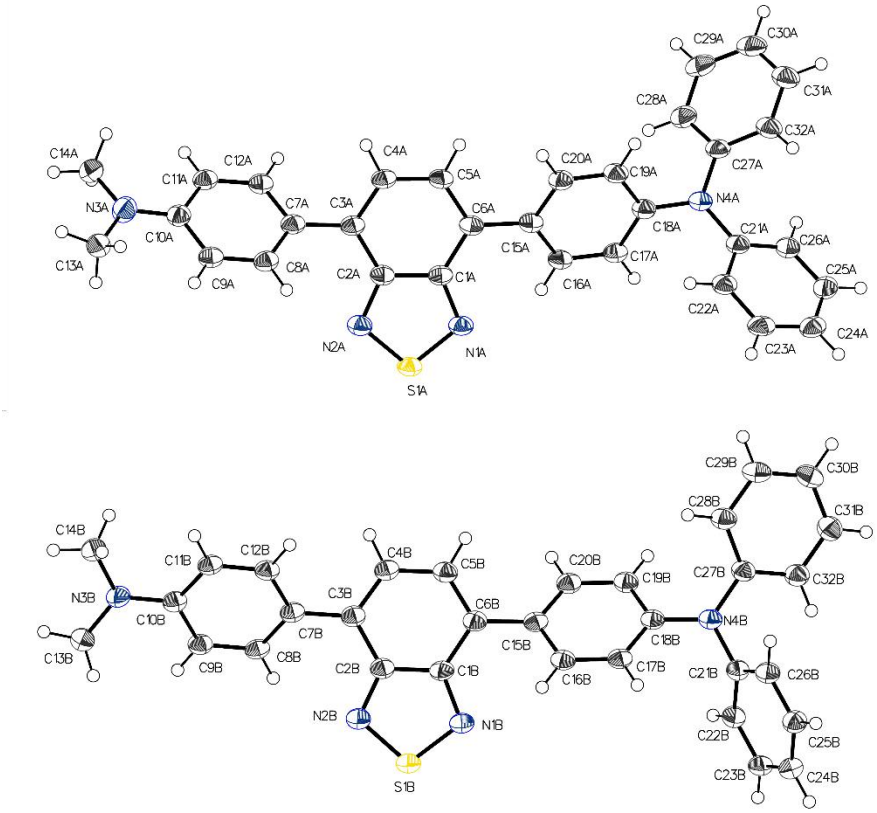

Figure 3.2. ORTEP diagram of the two distinct molecules of **1** resolved in the unit cell along with their corresponding atom numbering.

Spectroscopy

Amino end-capped benzothiadiazole derivatives such as **1** are known to be highly fluorescent in solution.

This is indeed the case of **1**.[22a, 25] The electron rich amine end-group conjugated with the electron deficient benzothiadiazole core were also expected to render **1** solvatochromic. This is courtesy of an intramolecular excited state charge transfer between the electron donating amine and benzothiadiazole acceptor, which is typical with electronic *push-pull* systems.[26] Both the emission wavelength and intensity should vary with solvent polarity, with the polar excited state being stabilized with polar solvents. Given the previous spectroscopic studies of **1** were limited exclusively to dichloromethane and toluene, its spectroscopic properties were evaluated in a range of solvents of varying polarity. These were to also benchmark the properties when evaluating the electrochromic and electrofluorochromic properties and the performance of **1** under device-like conditions. The absorption of the **1** varied by 10 nm (Table 1 and **Figure 3.7**). This confirms that the ground state is only slight perturbed by solvent polarity. The perceived color that persisted in the solvents examined was yellow. In contrast, the emission wavelength was dependent on the solvent. The emission wavelength varied by 125 nm in the solvents examined. This confirms that a highly polar state is formed upon excitation. This results from the intramolecular charge transfer between the electron rich termini and the deficient core. The solvatochromic shift also results in large Stokes shifts in most of the solvents examined. Aprotic polar solvents were exclusively investigated to avoid solute-solvent hydrogen bonding spectroscopic effects. The solvents investigated are also ideal for electrochemistry, including acetonitrile, dichloromethane, DMF, and THF. The observed spectroscopic behavior should therefore be similar under electrochromic and electrofluorochromic device-like conditions. This aside, the perceived emission color of **1** varied from bright yellow through to deep red, contingent on solvent, as per the inset of **Figure 3.3**. This is in contrast to unconjugated triphenylamines whose emission is hypsochromically shifted with a perceived blue emission.[27] An emission was also observed when **1** was deposited as a thin film on glass. According to Table 1, the solid-state emission was between that of Dichloromethane and THF. This confirms that the intrinsic moderate polarity of **1**. Its emission dependency makes **1** suitable as a probe for assessing the polarity in operating devices (vide infra).

Table 1. Spectroscopic properties of **1** contingent on solvent.

Solvent	**λ_{abs} (nm)**	**λ_{em}(nm)**	**Φ_{fl} (%)**[a,b]	**Stoke's shift(cm^{-1})**
Toluene	465	620	77 (50)	5040 (4850)
Diethyl ether	460	615	78	5700 (5950)
THF	465	655	64	6100 (5980)
Dichloromethane[d]	465	685	45 (23)	7000 (7250)
Acetonitrile	455	730	20	7870 (7610)
DMF	470	735	17	7470 (7320)
Solid-state[e]	450	660	20[c]	6300 (6500)

[a] Absolute values measured with an integrating sphere. [b] Values in parentheses are from literature using fluorescein as an actinometer.[22a, 25] [c] Corrected for λ^2; values in parentheses corrected for λ^4. [d] With 0.1 M tetrabutylammonium hexafluorophosphate. [e] Spin coated on a glass slide. Φ_{fl} is an average of three measurements of the same substrate.

While the solvatochromic properties of **1** were expected,[22a] a key performance to benchmark was the emission yield (Φ_{Fl}). This is of importance as high emissions that can be visually detected are desired. Appreciable emission in thin films is also required for using the fluorophores in solid-state devices. The challenge is maintaining a Φ_{Fl} in polar environments, where the solvent induced excited state stabilizing narrows the energy gap and increases non-emissive deactivation modes. Towards this end, the absolute Φ_{Fl} was measured with an integrating sphere. The differences in refractive index difference are not required for the absolute method, in contrast to relative actinometry. As per Table 1, the Φ_{Fl} is solvent dependent. A decrease in Φ_{Fl} with increasing solvent polarity is consistent with intramolecular charge transfer.[28] While the observed trend is not surprising, the moderate Φ_{Fl} even in DMF is atypical. The

solid-state emission is also unusual. Typically, intrinsically highly fluorescent fluorophores in solution emit poorly in the solid-state because of efficient self-quenching. **1** therefore behaves as a typical fluorophore in solution by being highly emissive, while also emitting as a thin film. The thin film emission is ideal for use in solid-state devices, where the fluorophore must remain emissive when cast a film with a gel electrolyte. Given the high electrolyte concentration that is required to make the solution conductive for electrochemical measurements, it can potentially deactivate the fluorophore's emission. To ensure this was not the case, the Φ_{fl} of **1** in dichloromethane with the electrochemical supporting electrolyte was measured. The fluorophore's emission was maintained. The collective emissive properties of **1** are ideally suited as an emitting mater in an electrofluorochromic device.

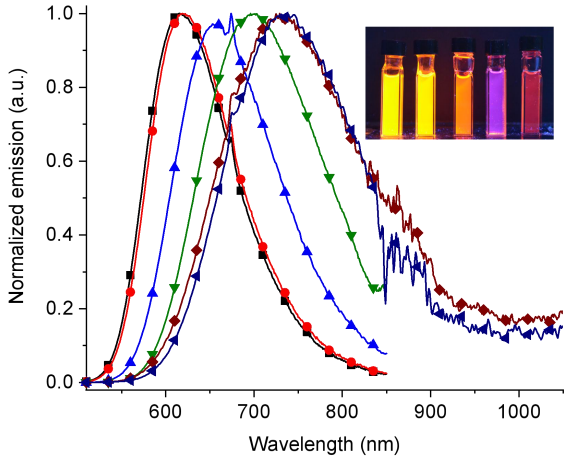

Figure 3.3. Normalized emission spectra of **1** in anhydrous solvents exciting at the maximum red-shifted absorption: diethyl ether (■), toluene (●), THF (▲), dichloromethane (▼), acetonitrile (♦), and DMF (◀). Insert: picture of **1** in vials of diethyl ether, toluene, THF, acetonitrile, and DMF (from left to right) when irradiated with a hand-held UV lamp at 365 nm.

To further assess the concentration dependent spectral properties of **1**, its emission was measured at various concentration in THF. No absorption shift was observed when varying the concentration over an order of concentration. Its emission also did not decrease with increasing concentration across the concentration range that was used for the concentration dependent absorption measurements.(**Figure 3.8** and **Figure 3.9**) This behavior contrasts with what is expected for typical fluorophores. For conventional fluorophores, their fluorescence is quenched at high concentrations by inner filter effects and self-quenching, while changes in their absorption spectra arise from intermolecular effects. The observed behavior is consistent with an aggregation induced emitter. The aggregation induced emission (AIE) of **1** was examined in varying vol% of water in THF.(**Figure 3.10**) The Φ_{fl} decreased by an order of magnitude with increasing water volume added to THF compared to neat THF. At 80% and 90% volume of water, the emission increased upwards of 40% (Table S1), consistent with an AIE behavior. The emission also red-shifted ca. 55 nm with decreasing temperature (**Figures 3.10**). This is consistent with a highly stabilized excited state forming at low temperatures, possible by favoring coplanarization of the aromatics and promoting intramolecular charge transfer. A monoexponential lifetime of 7.7 ns (^{2}=0.85; **Figure 3.11**) for **1** was also observed. This is consistent with only one species being responsible for the observed emission. The collective spectroscopic measurements, including the concentration and temperature dependent studies, confirm that the emission of **1** of highly sensitive to polarity and temperature. Moreover, its appreciable fluorescence when cast as a thin film, when aggregated, and in solution confirm its unique behavior as both an intrinsic fluorophore and AIE emitter. The latter is an ideal property for its use as the emitting layer in a solid-state electrofluorochromic device.

Electrochemistry

Given that the electrochromic and the electrofluorochromic properties are contingent on the electroactivity of the fluorophore, the electrochemistry of **1** was assessed. The electron donating property of the two amines was expected to collectively confer an anodic behavior to **1** that would occur within the electrochemical working window for the solvent. **1** was therefore expected to be oxidized. Moreover, its oxidation was expected to be reversible. This is a key property for its ultimate use as an electrochromic material. Irreversible oxidation would otherwise lead to products whose oxidation would be different from **1**. This would be compounded with undesired spectroscopic and fluorescence changes. The cyclic voltammetry of **1** was done to evaluate both its oxidation potential and its electrochemical reversibility. At the arbitrary scan speed of 100 mV/sec, one oxidation process was observed for **1** at 880 mV vs. Fc/Fc^+ (**Figure 3.16**). The process was reversible, based on the apparent equal peak current for the forward and reverse waves. The two amine end groups were expected to have different electronic donating strengths. Two stepwise processes were therefore expected. Although one process was observed at the given scan speed, **1** was further investigated by square wave voltammetry. This was to probe whether an additional anodic process occurred and was hidden in the cyclic voltammetry measurements. Indeed, a second oxidation processes was resolved by square wave voltammetry (**Figure 3.17**), occurring at 960 mV vs. Fc/Fc^+. Fitting for two Gaussian peaks and correcting for the baseline, the peaks were of equal area. This points towards the two processes being reversible. While the explicit processes cannot be assigned, they are assumed to be two sequential one-electron transfer processes, corresponding to the radical cation followed by the dication (vide infra). The electrochemical data confirm that **1** has the key properties for its as the active. The explicit processes of the two sequential one-electron transfer processes however cannot be unequivocally assigned. This aside, their overlapping potentials, taken together with the similar electron donating capacity of the two terminal groups, suggest the two oxidations occur at these sites. The first oxidation results in the radical cation at one terminus. Subsequent oxidation similarly gives rise to the radical cation on the opposite terminus, resulting in the overall bis(radical dication) of **1** (vide infra). The electrochemical data confirm that **1** has the key properties for it to be used as the active material in electrochromic devices, being it electroactivity and reversible oxidation

Spectroelectrochemistry

The collective electroactivity of **1** and its color in the visible spectrum that can be tracked by the user are suitable for its use as an active material in electrochromics. To assess this, the spectroelectrochemistry was evaluated. This entailed monitoring the change in absorption with applied potential. Given the two oxidation processes that were observed by square wave voltammetry of **1**, the absorption change at the two discrete potentials was monitored. The absorption at 450 nm bleached with an applied potential of 0.9 V concomitant with the broad absorption at 1500 nm. The NIR absorption grew over time with a constant potential of 0.9 V. Both the broad featureless absorption and the wavelength are consistent with an intervalence charge transfer with the triphenylamine radical intermediate.[29] Increasing the potential to 1.3 V caused additional changes in the spectrum. Notably, the broad absorption dissipated. This was replaced with a strong absorption in the visible region at 715 nm (**Figure 3.4**). The narrow absorption of the red-shifted induced color change is consistent with a dication. The dication is also based on the absorption of 1500 nm, being converted to the 900 nm absorption. The red/yellow color, corresponding to the 450 nm absorption further bleached. **1** therefore undergoes visible color bleaching with the radical cation absorbing out to the NIR region. Meanwhile, the perceived color changed from yellow to green when increasing the potential to the reach second oxidation peak that was measured by cyclic voltammetry.

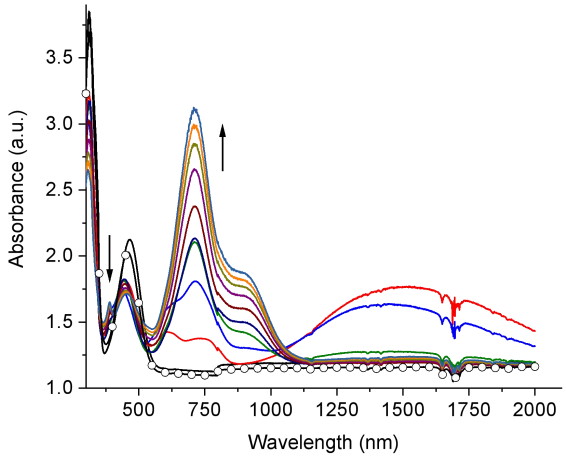

Figure 3.4. Change in absorbance spectra of **1** with applied potential of 1.3 V measured at 10 sec internals in anhydrous and deaerated dichloromethane with 0.1 M $TBAPF_6$. After 90 sec, a negative potential of -0.1 V was applied for 3.5 min (○).

Calculations

Theoretical calculations have proven to be viable tools for correlating structural modification of benzothiadiazole derivatives, such as benzobis(1,2,5-thiadiazole), on their properties[30] Theoretical calculations were therefore used to better understand the electrochemically generated intermediates and to evaluate their spectroscopic properties. In particular, the electronic transitions were calculated to help assign the absorption spectra of the radical cation and dication intermediates (**Figure 3.14**). First, the ground state geometry was calculated by CAM-DFT[31] with the 6-311+G(d,p) basis set. Next, the time-dependent DFT (TD-DFT)[32] was used to calculate the electronic transitions and excitation energies (**Figure 3.13**). In turn, these were used to generate the corresponding absorption spectra. To best mimic the experimental conditions, dichloromethane was used as the solvent continuum for all the calculations. The absolute energy, and hence, the absorbance spectra cannot be accurately calculated. Nonetheless, the errors are systematically scaled. Therefore, the difference in a series of compounds can be calculated with relative accuracy. Small errors, downwards of 0.1 eV, between the experimental and the calculated excited transitions are possible by TD-DFT.[33]

Of interest are the bond distances and dihedral angles that were measured from the crystal structure of **1**. The corresponding bond distances and angles of the theoretically calculated optimized structure of the neutral state were consistent with those from the X-ray data (vide supra). Notably, the bond lengths of the Me_2N–phenyl and Ph_2N–phenyl were asymmetric and they were consistent with the experimental data (Table S4). The corresponding bonds distances for the radical cation and dication were shorter than the neutral state, confirming their increased degree of conjugation. The corresponding dihedral angles for the two charged states were also smaller than the neutral state. In fact, the angles were smaller for the dication, further indicating its increased degree of conjugation via coplanarization of the aromatics.

The most red-shifted absorption of the neutral state **1** was calculated to occur at 418 nm. The principle theoretical absorption is therefore hypsochromically shifted relative to the measured value. The main electronic transition for the radical cation was 993 nm, while the dication was 648 nm. The trend in absorption shift with the redox state is consistent with the spectroelectrochemical results. Of interest is the spin density of the radical cation (**Figure 3.13**). The radical is unevenly distributed across the structure. It is polarized over the Me_2N–Ph and the benzothiadiazole portions of **1**, rather than being equally distributed over the entire conjugated framework. Similarly, the orbitals of the ground state that were

involved in the lowest energy electronic transitions of the neutral and the radical cation of **1** were mainly localized over the N-phenyl-benzothiadiazole-N-phenyl conjugated framework. In contrast, the HOMO of the dication was distributed over the entire framework with it extending out to the diphenylamino terminus. Meanwhile, the excited state orbitals were concentrated over benzothiadiazole core for the neutral. This aside, the calculations corroborate the electrochemical assignment of two sequential one-electron transfers to form first the radical cation followed by the dication.

Electrochromism/Electrofluorochromism

Chronoamperometry of **1** was investigated to further evaluate its potential use in a working electrochromic device. This involved monitoring the change in transmittance at a given wavelength with changes in applied potential. Both the radical cation and dication were monitored over time. As per **Figure 3.5B**, the absolute difference between the *off* and *on* states for the dication that was monitored at 695 nm is constant over a period of 2 hours. Interestingly, the transmission difference was over 80% when switching the potential at 30 sec intervals(**Figure 3.5A**). Taking the total area of the 19-well honeycomb working electrode as 0.24 cm^2, the coloration efficiency of **1** was calculated to be 530 and 780 $cm^2\ C^{-1}$ at 715 nm for the radical cation and 1400 nm for the dication, respectively. The coloration values are consistent with triphenylamine electrochromic polymers that vary between 200 and 600 $cm^2\ C^{-1}$, contingent on their structure.[34] The chronoabsorptometric data further demonstrate the capacity of **1** to sustain multiple oxidation/neutralization cycles while maintaining a constant coloration over 120 cycles.

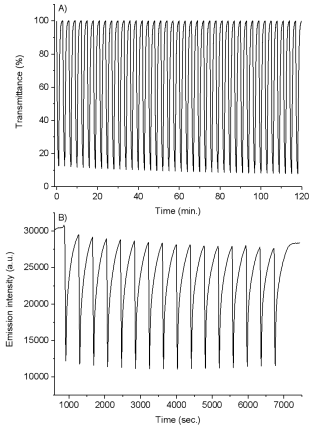

Figure 3.5. A) Change in percent transmittance of **1** measured at 1400 nm in anhydrous and deaerated dichloromethane with 0.1 M $TBAPF_6$ with applied potentials of +0.95 V for 30 sec, and then -0.1 V for 2 min intervals. B) Change in emission intensity of **1** in anhydrous and nitrogen purged dichloromethane with 0.1 M $TBAPF_6$ excited at 465 nm and monitored at 695 nm with applying potential of +1.3 V for 30 sec, and then -0.1 V for 6 min, respectively.

To fully characterize the electrochromic performance of **1**, its contrast ratio was also examined. This was to determine the optimal applied potential for the maximum transmittance difference between the neutral and oxidized state. With this parameter, the performance of similar electrochromes can be directly compared, although they may have been measured under different conditions.[35] The contrast ratio was measured by varying the time that the potential was applied to generate the oxidized state and monitoring the resulting transmittance change. For **1**, a 950 mV potential was applied between 1 and 60 sec and the resulting transmittance change at 715 and 1400 nm was monitored. The optimal time (τ) for maximum coloration of the dication and radical cation were 7.2 and 16.8, respectively.

The chronoamperometric transmittance difference confirms the electrochromic properties of **1**. To

demonstrate the true dual role of **1**, being both an electrochrome and electrofluorochrome, the electrochemically mediated fluorescence was also investigated. In this case, the variation in fluorescence intensity was monitored with applied potential. A rectangular transparent ITO electrode was placed in the front of a spectroscopic cuvette containing **1** and the electrolyte solution. The ITO coated surface faced the cuvette wall and it was held in place with the Teflon widget with the distance between the cuvette wall and the electrode being 5 mm. The counter and pseudo-reference electrodes were placed on the glass side of the transparent electrode and the cell was sealed with parafilm. The cuvette was placed as 45^{o} to both the incident beam and the detector. The emission from the surface could be measured with the orientation without any scattering. The resulting emission spectrum was consistent with the one measured in solution with a conventional setup, with the emission maximum at 695 nm. Of importance is the emission yield, which was maintained in the electrolyte solution (Φ_{fl}=40%). Given a pseudo-reference was used, precluding the knowing the exact potential applied, a reference square wave was measured. This was to determine the oxidation potential of **1** under the electrofluorochromic cell conditions. The measured potential was then used as the threshold value at which to modulate the fluorescence intensity. The resulting fluorescence change with applied potential is found in **Figure 3.5B**. Upon oxidizing **1**, its fluorescence bleached. This is owing to the depletion of the neutral state that would otherwise absorb the light at the given excitation wavelength. The fluorescence can then be turned-on by neutralizing the oxidation state. A complete emission spectrum of the oxidized state was also measured by exciting at its absorption maximum (450 nm). This was to ensure that the excited did not emit. Indeed, the oxidized state of **1** did not emit. The fluorescence quenching is therefore a result of both the spectral shift and the quenched emission of the radical intermediated. The fluorescence could be repeatedly quenched and restored with applied potential. A 70% change in the fluorescence *off* and *on* intensities can be seen in **Figure 3.5B**. This, taken together, with the consistent transmittance difference, demonstrate the electrochemical robustness of **1**. They further illustrate the dual role of **1**, being capable of both electrochemically mediated reversible color change and fluorescence intensity modulation.

A functioning sandwich device was prepared with **1** to further illustrate its dual role in an operating device. This was done by depositing it on a 2.5 cm x 2.5 cm ITO coated glass electrode. The other electrode was coated with the gel electrolyte.[36] The two substrates were pressed together and sealed with epoxy after removing any air bubbles. Both the emission spectra and emission yield were measured. These were to benchmark any changes in the emission properties of **1** in the device relative to in solution. In the assembled device, **1** emitted at 650 nm. Given the intrinsic polarity sensor property of **1**, the polarity of the device is consistent with that of dichloromethane with the supporting electrolyte.[22a] The Φ_{fl} was 13% in the device. While the emission was less than the as-cast film, it nonetheless appreciably fluoresced. In fact, the emission of the device was visible to the common user when exciting with a hand-held UV lamp. The fluorescence of the device could be switched with applied potential. The response was slower in the device for turning the fluorescence on compared to when measured in solution (**Figure 3.6**), although the fluorescence turn-off response was similar. The Φ_{fl} also decreased to 8% after operating the device. While the exact mechanism responsible for the slow turn-on cannot be addressed with the simple device fabricated it nonetheless serves as a proof-of-principle that an intrinsic fluorophore can be used as an electrofluorochrome in a solid-state device. The visible color switching of **1** was also possible. This is illustrated in the inset of **Figure 3.6** where **1** was patterned on the surface. The resulting smiling face switched between its orange and blue states, corresponding to the neutral and oxidized states, respectively. The collective visible color and emission changes possible with the operating device demonstrate the dual role of **1** and its suitability as a combined electroactive and electrofluorochromic material.

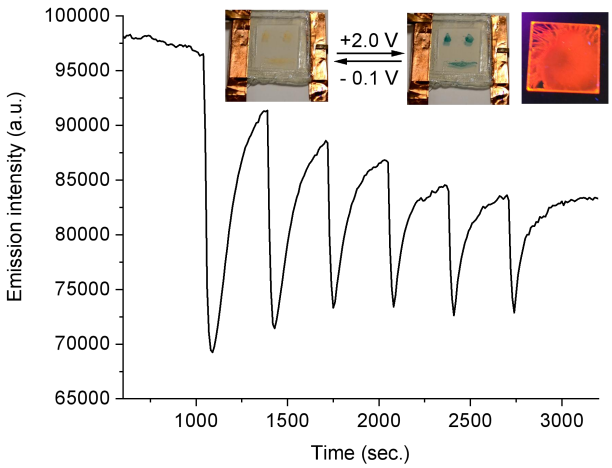

Figure 3.6. Spectroelectrofluorescence of the operating device prepared with **1** by exciting at 460 nm and monitoring at 650 nm when switching between -0.1 V for 5 min and +1.9 V at 30 sec. intervals. Inset: photographs of an electrochromic device prepared from **1** patterned with a smiling face in the neutral (left) and oxidized (middle) states along with **1** spin coated on a glass substrate irradiated with a hand-held UV lamp (right).

3.4 Conclusion

The emission yield and wavelength of an asymmetric fluorophore consisting of two different electron rich termini and a benzothiadiazole core were contingent on the solvent. It was also emissive in an electrolyte solution for spectroelectrochemical measurements. In fact, it remained fluorescent even as a thin film on a substrate and in a working electrochromic device. The visible color and emission intensity of fluorophore were both modulated with applied potential, courtesy of its electroactive terminus. The fluorophore therefore can play a dual role: an electrochrome and an electrofluorochrome, leading to a device having two properties that can be adjusted with applied potential. With optimization, devices capable of extended color switching and turning their fluorescence *off* and *on* are expected. Meanwhile, tuning of the perceived color and emission wavelength are possible by structurally modifying the fluorophore. Combined electrochromic and electrofluorochromic devices that display and emit a range of colors and even multiple colors will therefore be possible.

3.5 Acknowledgments

Both the Natural Sciences and Engineering Council Canada and the Canada Foundation for Innovation are acknowledged for Discovery and infrastructure grants, respectively, that enabled this work. Compute Canada (www.computecanada.ca) and their partners, Compute Ontario (computeontario.ca) and WestGrid (www.westgrid.ca), are also thanked for access to both computational resources and software for theoretical calculations. CY thanks MITACS for both a visiting and graduate scholarships. CY also thanks the Université de Montréal for a J. & M. Lemay graduate scholarship. The former Center for Self-Assembled Chemical Structures and the Quebec Centre for Advanced Materials are also acknowledged for access to infrastructure and equipment used for measurements. L. Walach is also thanked for preliminary solution emission measurements.

Conflicts of interest
There are no conflicts to declare.

References

[1] A. W. Chan, R. J. Neufeld, *Biomaterials* **2010**, *31*, 9040-9047.
[2] B. J. Deibert, J. Li, *Chem. Commun.* **2014**, *50*, 9636-9639.
[3] J. Li, K. Pu, *Chem. Soc. Rev.* **2019**, *48*, 38-71.
[4] T. Suga, H. Ohshiro, S. Sugita, K. Oyaizu, H. Nishide, *Adv. Mater.* **2009**, *21*, 1627-1630.
[5] J. Winsberg, T. Hagemann, T. Janoschka, M. D. Hager, U. S. Schubert, *Angew. Chem., Int. Ed.* **2017**, *56*, 686-711.
[6] M. H. Chua, Q. Zhu, K. W. Shah, J. Xu, *Polymers* **2019**, *11*, 98.
[7] J. W. Xu, L. Toppare, Y. Li, C. Xu, E. Kim, Y.-W. Zhong, C. Zhang, A. Beneduci, M. Ak, S.-H. Hsiaob, Royal Society of Chemistry, **2019**.
[8] M. H. Chua, T. Tang, K. H. Ong, W. T. Neo, J. W. Xu, in *Electrochromic Smart Materials: Fabrication and Applications* (Eds.: J. W. Xu, M. H. Chua, K. W. Shah), The Royal Society of Chemistry, **2019**, pp. 1-21.
[9] C. J. Barile, D. J. Slotcavage, M. D. McGehee, *Chem. Mater.* **2016**, *28*, 1439-1445.
[10] D. T. Christiansen, S. Ohtani, Y. Chujo, A. e. L. Tomlinson, J. R. Reynolds, *Chem. Mater.* **2019**, *31*, 6841-6849.
[11] P. Ledwon, P. Zassowski, T. Jarosz, M. Lapkowski, P. Wagner, V. Cherpak, P. Stakhira, *J. Mater. Chem. C* **2016**, *4*, 2219-2227.
[12] Y. Yang, J. Zhang, Y. Zhou, G. Zhao, C. He, Y. Li, M. Andersson, O. Inganäs, F. Zhang, *J. Phys. Chem.* **2010**, *114*, 3701-3706.
[13] F. F. Oliveira, D. C. Santos, A. A. Lapis, J. R. Corrêa, A. F. Gomes, F. C. Gozzo, P. F. Moreira Jr, V. C. de Oliveira, F. H. Quina, B. A. Neto, *Bioorganic & Medicinal Chemistry Letters* **2010**, *20*, 6001-6007.
[14] L. Shi, C. He, D. Zhu, Q. He, Y. Li, Y. Chen, Y. Sun, Y. Fu, D. Wen, H. Cao, *J. Mater. Chem.* **2012**, *22*, 11629-11635.
[15] R. D. Telore, M. A. Satam, N. Sekar, *Dyes Pigm.* **2015**, *122*, 359-367.
[16] S. Zeng, L. Yin, C. Ji, X. Jiang, K. Li, Y. Li, Y. Wang, *Chem. Commun.* **2012**, *48*, 10627-10629.
[17] H.-J. Yen, G.-S. Liou, *Polym. Chem.* **2018**, *9*, 3001-3018.
[18] a) Y. Kim, E. Kim, G. Clavier, P. Audebert, *Chem. Commun.* **2006**, 3612-3614; b) K. Kanazawa, K. Nakamura, N. Kobayashi, in *Luminescence in Electrochemistry: Applications in Analytical Chemistry, Physics and Biology* (Eds.: F. Miomandre, P. Audebert), Springer International Publishing, Cham, **2017**, pp. 175-213.
[19] S. I. Yang, S. Prathapan, M. A. Miller, J. Seth, D. F. Bocian, J. S. Lindsey, D. Holten, *J. Phys. Chem. B* **2001**, *105*, 8249-8258.
[20] K. Justin Thomas, J. T. Lin, Y.-T. Tao, C.-W. Ko, *Chem. Mater.* **2002**, *14*, 1354-1361.
[21] S. Wang, X. Yan, Z. Cheng, H. Zhang, Y. Liu, Y. Wang, *Angew. Chem., Int. Ed.* **2015**, *54*, 13068-13072.
[22] a) S.-i. Kato, T. Matsumoto, M. Shigeiwa, H. Gorohmaru, S. Maeda, T. Ishi-i, S. Mataka, *Chem. Eur. J.* **2006**, *12*, 2303-2317; b) M. Shigeiwa, H. Gorohmaru, S. Maeda, S.-i. Kato, T. Ishi-i, T. Thies, S. Mataka, *Nonlinear Opt., Quantum Opt.* **2005**, *34*, 171-174.
[23] Y.-C. Lo, T.-H. Yeh, C.-K. Wang, B.-J. Peng, J.-L. Hsieh, C.-C. Lee, S.-W. Liu, K.-T. Wong, *ACS Appl. Mater. Interfaces* **2019**, *11*, 23417-23427.
[24] a) J. Qi, C. Sun, D. Li, H. Zhang, W. Yu, A. Zebibula, J. W. Y. Lam, W. Xi, L. Zhu, F. Cai, P. Wei, C. Zhu, R. T. K. Kwok, L. L. Streich, R. Prevedel, J. Qian, B. Z. Tang, *ACS Nano* **2018**, *12*, 7936-7945; b) J. Fan, Y. Zhang, K. Zhang, J. Liu, G. Jiang, F. Li, L. Lin, C.-K. Wang, *J. Mater. Chem. C* **2019**, *7*, 8874-8887.
[25] S.-i. Kato, T. Matsumoto, T. Ishi-i, T. Thiemann, M. Shigeiwa, H. Gorohmaru, S. Maeda, Y. Yamashita, S. Mataka, *Chem. Commun.* **2004**, 2342-2343.

[26] a) M. Wałęsa-Chorab, M.-H. Tremblay, M. Ettaoussi, W. G. Skene, *Pure Appl. Chem.* **2016**, *87*, 649-661; b) T. Khanasa, N. Prachumrak, R. Rattanawan, S. Jungsuttiwong, T. Keawin, T. Sudyoadsuk, T. Tuntulani, V. Promarak, *J. Org. Chem.* **2013**.

[27] a) Y. A. Skryshevski, A. Y. Vakhnin, *Mol. Crystal. Liq. Cryst.* **2005**, *427*, 207/[519]-216/[528]; b) X.-Y. Hou, T. C. Li, C.-R. Yin, H. Xu, J. Lin, Y.-R. Hua, D.-Y. Chen, L.-H. Xie, W. Huang, *Synth. Met.* **2009**, *159*, 1055-1060.

[28] J. R. Lakowicz, *Principles of Fluorescence Spectroscopy*, 3rd ed., Springer, New York, **2006**.

[29] a) S.-H. Hsiao, H.-Y. Lu, *Journal of The Electrochemical Society* **2018**, *165*, H638-H645; b) C. Lambert, G. Nöll, *J. Am. Chem. Soc.* **1999**, *121*, 8434-8442.

[30] a) B. Zhou, Z. Hu, Y. Jiang, C. Zhong, Z. Sun, H. Sun, *PCCP* **2018**, *20*, 19759-19767; b) A. Thomas, K. Bhanuprakash, K. M. M. K. Prasad, **2011**, *24*, 821-832.

[31] a) T. Yanai, D. P. Tew, N. C. Handy, *Chem. Phys. Lett.* **2004**, *393*, 51-57; b) P. J. Stephens, F. J. Devlin, C. F. Chabalowski, M. J. Frisch, *J. Phys. Chem.* **1994**, *98*, 11623-11627; c) S. H. Vosko, L. Wilk, M. Nusair, *Can. J. Phys.* **1980**, *58*, 1200-1211; d) A. D. Becke, *Phys. Rev. A* **1988**, *38*, 3098-3100.

[32] M. E. Casida, in *Recent Advances in Density Functional Methods, Vol. 1* (Ed.: D. P. Chong), World Scientific, Singapore, **1995**, pp. 155-192.

[33] a) A. D. Laurent, D. Jacquemin, *Int. J. Quantum Chem* **2013**, *113*, 2019-2039; b) M. J. G. Peach, P. Benfield, T. Helgaker, D. J. Tozer, *J. Chem. Phys.* **2008**, *128*, 044118.

[34] a) O. Negru, L. Vacareanu, M. Grigoras, *Express Polymer Letters* **2014**, *8*, 647-658; b) N. Sun, F. Feng, D. Wang, Z. Zhou, Y. Guan, G. Dang, H. Zhou, C. Chen, X. Zhao, *RSC Adv.* **2015**, *5*, 88181-88190; c) N. Sun, S. Meng, D. Chao, Z. Zhou, Y. Du, D. Wang, X. Zhao, H. Zhou, C. Chen, *Polym. Chem.* **2016**, *7*, 6055-6063; d) Y. Wang, Y. Liang, J. Zhu, X. Bai, X. Jiang, Q. Zhang, H. Niu, *RSC Adv.* **2015**, *5*, 11071-11076; e) H. J. Yen, C. J. Chen, G. S. Liou, *Adv. Funct. Mater.* **2013**, *23*, 5307-5316; f) H.-J. Yen, G.-S. Liou, *J. Mater. Chem.* **2010**, *20*, 9886-9894; g) Y. Zhang, F. Liu, Y. Hou, H. Niu, *Synth. Met.* **2019**, *247*, 81-89; h) R. Zheng, J. Zhang, C. Jia, Z. Wan, Y. Fan, X. Weng, J. Xie, L. Deng, *Polym. Chem.* **2017**, *8*, 6981-6988.

[35] S. Hassab, D. E. Shen, A. M. Österholm, M. Da Rocha, G. Song, Y. Alesanco, A. Viñuales, A. Rougier, J. R. Reynolds, J. Padilla, *Sol. Energy Mater. Sol. Cells* **2018**, *185*, 54-60.

[36] M. Wałęsa-Chorab, R. Banasz, M. Kubicki, V. Patroniak, *Electrochim. Acta* **2017**, *258*, 571-581.

3.6 Experimental Details

Theoretical calculations

Calculations were done with Gaussian 16, Revision B.01.[1] The geometries were optimized with CAM-B3LYP[2] with the 6-311+G(d,p) basis set. Time-dependent DFT (TD-DFT)[3] was used to calculate the excitation energies and the resulting absorption spectra. The solvent continuum model (scrf) was used with dichloromethane and the geometry connectivity was specified. The orbitals were biorthogonalized and the Natural transition orbital (NTO)[3] analyses was done for the first transition of the singlet transition to visualize the principle transition in the absorption spectrum. In all the cases, the first energy transition corresponding to the lowest energy electronic transition.

Spectroscopic measurements

Absorption measurements were done with a combined UV-visible-NIR spectrophotometer from Varian 500.with four-window quartz cuvettes. The solvent used was anhydrous dichloromethane, unless stated otherwise. The emission measurements were done with a combined steady-state/lifetime fluorimeter. Samples were degassed by bubbling with nitrogen for at least 20 minutes. The samples were afterwards sealed with a screw top with a Teflon coating silicone elastomer septum. Emission spectra were recorded by exciting at the red-shifted maximum absorption. Quantum yield measurements were done with a calibrated integrating sphere. The samples had an absorbance of 0.1 at the red-shifted absorption wavelength for Φ_{fl} measurements. The same solvent that was used for the Φ_{fl} measurements was used neat for the instrument response scattering. In the case of the operating devices, the emission spectra and Φ_{fl} were done with the device after sandwiching the two transparent electrodes together without copper tape the epoxy sealing glue. The latter were avoided as they fluoresce and they increase the background emission in the integrating sphere. The device was laid flat on the designated sphere support in the integrating sphere. A similar ITO native substrate was used as the reference for the substrate scattering. Both the direct and indirect emission were used for calculating the emission yield over the entire visible spectrum. Temperature dependent studies were done with a CoolSpek cryostat using liquid nitrogen and a temperature controller. Lifetime measurements with done by TCSPC with a 405 nm ps-LED.

Electrochemical measurements

In anhydrous dichloromethane (5 mL), was dissolved **1** (2.5 mg) and tetrabutylammonium hexafluorophosphate ($TBAPF_6$; 194 mg) to make a 1 mM solution. Ferrocene (37.2 mg) and $TBAPF_6$ (77.6 mg) were dissolved in dichloromethane (2 mL) to give a 100 mM solution. The solutions were degassed with nitrogen for at least 15 minutes. Afterwards, the solution of **1** (1.5 mL) was added to a small volume vial with a commercially available all-in-one ceramic electrode that was connected to a potentiostat. The ceramic electrode consisted of a printed platinum working electrode, platinum counter electrode, and Ag/AgCl reference electrode. Either a blanket of nitrogen was maintained over the cell or it was hermetically sealed with parafilm. Scans from -1.6 V to +1.5 V with a scan speed of 100 mV/s were done for cyclic voltammetry measurements. A volume (15 μL) of the concentrated ferrocene stock solution was added after the measurements as an internal reference and then the cyclic voltammograms remeasured. For square wave measurements, the same solution was used as the cyclic voltammetry analyses by applying +1.5 V, P_H=10 mV, P_W=50 ms, S_H= 5 mV and the parameters.

For the spectroelectrochemical measurements, the same stock solution that was used for the cyclic voltammetry measurements was measured. The measurements were done with a 10 x 10 mm quartz cuvette with a narrow optical path length. A commercially available ceramic honeycomb working electrode was used. The electrode consisted of 19 gold plated low volume wells along with a printed platinum counter electrode. A polished silver wire was used as was pseudo-reference electrode. The solution was degassed with nitrogen for at least 20 minutes before transferring it to a cuvette. The cuvette was hermetically sealed with parafilm after placing it in the UV-visible-NIR spectrometer. The given

potential was applied for a fixed period of time, afterwards the resulting absorption spectrum was measured. Similarly, the switching was done by continuously measuring the transmittance at a given wavelength and the applied potential was repeatedly switched between the neutral and oxidized states. The potentials for switching between the oxidized and neutral states were applied for a given interval.

Chronoabsorptometric measurements were done by applying a potential of +1.3 V for 30 sec and -0.1 V for 3 min. This was repeated for 30 cycles and the transmittance difference at 715 nm during the switching cycles was monitored. The transmittance difference at 1400 nm was also monitored with switching potentials of +0.95 V for 60 sec and -0.1 V for 2 min over 40 cycles. The contrast ratio fittings were done similar to the conventional chronoabsorptometric measurements. A potential of 1.3 V was applied for 1, 2, 5, 10, 15, 20 , 25, 30, and 35 sec. and the transmittance was continuously monitored at 715 nm. A potential of 0.95 V was applied for 1, 2, 5, 10, 15, 20, 25, 30, 35, 40, 50, 60, 70, and 80 sec. and the transmittance was also continuously monitored at 1400 nm. The corresponding τ values were obtained by fitting the data to $\Delta T=\Delta T_{max}(1-\exp(-t/\tau))$.[4]

The spectroelectrofluorescence was done with the electrochemical stock solution of **1** that was used for the cyclic voltammetry measurements. The cuvette that was used for the spectroelectrochemical measurements was also used for the spectroelectrofluorescence measurements. In this case, the working electrode was a rectangular shaped ITO coated glass slide. The electrode was placed in the cuvette in the thin optical slit. A platinum counter electrode coil wire was placed behind the electrode and a silver wire was used as the pseudo reference electrode. Copper tape was applied to the ITO electrode to connect to the potentiostat with an alligator clip. The sample was hermetically sealed with parafilm, afterwards the electrodes were connected to the potentiostat. A specialized open face sample holder was used. This ensured a large surface area for absorbing the excitation light and the sample was oriented towards the detector for the emission. For this, the front face of the cuvette was placed at a right angle to the excitation light. Two types of measurements were done: emission and kinetics. In both cases, the excitation wavelength was the longest wavelength absorption (465 nm). The instrument was adjusted to give the optimal signal under these conditions. For the emission measurements, an oxidation potential was then applied for a given amount of time. After each potential, the complete emission spectrum was measured. For the kinetic scans, the emission at a single wavelength (695 nm) was continuously monitored for a given time frame during which the potential was consistently cycled between the oxidized and neutral states by applying potentials of +1.3 and -0.1 V, respectively at 30 sec intervals. The chosen time frame of 6 minutes was arbitrarily selected, during which time 15 complete oxidation/neutralizations were continuously monitored.

Functioning electrochromic/electrofluorochromic devices of **1** were fabricated with a sandwich architecture. The electrolyte gel consisted of $LiClO_4$ (300 mg) and PMMA (120 kDa, 700 mg) that were added to acetonitrile (5 mL). The mixture was heated until a homogeneous solution was obtained. Next, propylene carbonate (2 g) was added to the mixture and it was stirred overnight to yield a highly viscous and transparent gel. Two ITO coated glass substrates were used to fabricate the device. First, **1** was spray coated on one substrate. Next, the conductive electrolyte gel was spread over the other ITO electrode. The two plates were sandwiched together and held in place with a metal clip. A commercial glass/metal glue was applied at the interface of the plate to seal the device. Caution was taken to ensure the glue did not contact either the gel or **1** and to ensure it did not diffuse into the device before it was cured. Copper tape was then applied to each substrate for connecting to the potentiostat with alligator clips. The devices were operated by applying potentials of +2.0 V for 1 min followed by -0.1 V for 7minutes.

3.7 Supporting information

Synthetic Details

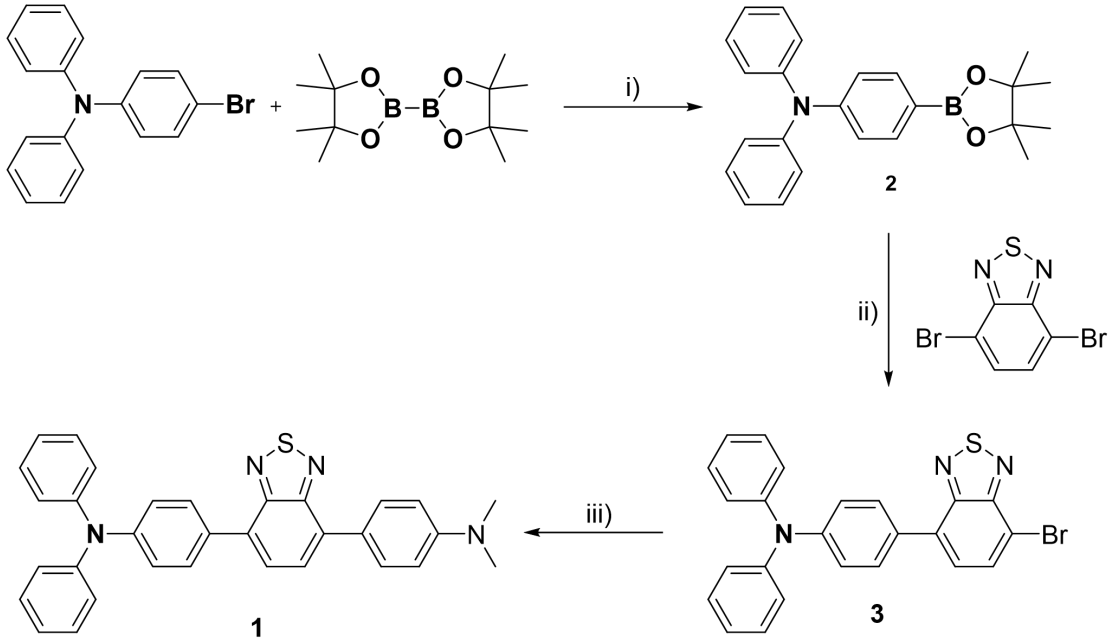

Scheme S1. Synthetic pathway for the preparation of the electrofluorochrome: i) $Pd(dppf)Cl_2$, CH_3CO_2K, dioxane, 90° C, overnight; ii) $Pd(PPh_3)_4$, Na_2CO_3, Bu_4NBr, toluene/H_2O, 90° C, overnight; iii) 4-(Dimethylamino)phenylboronic acid, $Pd(PPh_3)_4$, Na_2CO_3, Bu_4NBr, toluene/H_2O, 120° C 3 hrs.

***N*,*N*-diphenyl-4-(4,4,5,5-tetramethyl-1,3,2-dioxaborolan-2-yl)aniline (2)**.[5] Potassium acetate (906 mg, 9.24 mmol, 3 eq) and diborane bis(pinacolato) (939 mg, 3.7 mmol, 1.2 eq) were added to a solution of 4-bromo-*N*,*N*-diphenylaniline (1 g, 3.08 mmol) in dioxane (20 mL). The solution wan then bubbled with nitrogen for 20 minutes. Afterwards, [1,1'-bis (diphenylphosphino) ferrocene] dichloropalladium (II) (76 mg, 0.093 mmol, 0.03 eq) was added and the solution was refluxed for 24 hours under nitrogen. Afterwards, the reaction mixture cooled to room temperature, filtered, and then diluted with ethyl acetate. The organic phase was washed with water, extracted, dried with magnesium sulfate, filtered, and then concentrated. The crude product was purified by silica gel chromatography (hexane/dichloromethane) with a gradient ranging from 10% to 40% dichloromethane. The title compound was obtained as a white solid (937 mg, 82%). ^{1}H NMR ($CDCl_3$, 400 MHz) δ (ppm) = 7.70 (d, 2H), 7.28 (m, 4H), 7.14 (m, 4H), 7.07 (m, 4H), 1.36 (s, 12H). ^{13}C NMR ($CDCl_3$, 100 MHz) δ (ppm) = 150.4, 147.2, 135.7, 129.1, 124.8, 123.2, 121.6, 83.3, 24.7. ESI-MS [M+H$^+$] m/z: calcd for $C_{24}H_{26}BNO_2$, 371.21, found 371.21.

4-(7-Bromobenzo[c][1,2,5]thiadiazol-4-yl)-*N*,*N*-diphenylaniline (3).[6] Sodium carbonate (2.79 g, 26.4 mmol, 4.9 eq), 4,7-dibromobenzo[c]-1,2,5-thiadiazole (1.58 g, 38 mmol, 1 eq), and tetra-*n*-butylammonium bromide (5 mg) were added to a solution of **2** (2 g, 5.38 mmol) in a toluene:water (30:10 mL) mixture. The solution was then deoxygenated by three freeze-pump-thaw cycles. Then tetrakis(triphenylphosphine)palladium (621 mg, 0.54 mmol, 0.1 eq) was added to the solution and it was then heated at 90° overnight. The mixture was cooled to room temperature and then diluted with dichloromethane. The organic phase was washed with water, extracted, dried over magnesium sulfate, filtered, and then concentrated. The crude product was purified by silica gel chromatography (hexane/ether, 100:0 to 98:2) to give an orange solid (1.25 g, 51%). ^{1}H NMR ($CDCl_3$, 400 MHz) δ (ppm) = 7.90 (d, 1H), 7.80 (m, 2H), 7.55 (d, 1H), 7.30 (dd, 4H), 7.19 (m, 6H), 7.08 (t, 2H). ^{13}C NMR ($CDCl_3$, 100 MHz) δ (ppm) = 154.1, 153.3, 148.6, 147.5, 133.7, 132.5, 130.1, 130, 129.6, 127.5, 125.2, 123.6,

122.7, 112.3. ESI-MS [M+H$^+$] m/z: calcd for $C_{24}H_{17}BrN_3S$, 458.03, found 458.10.

4-(7-(4-(Dimethylamino)phenyl)benzo[c][1,2,5]thiadiazol-4-yl)-N,N-diphenylaniline (1).[7] 4-(Dimethylamino)phenylboronic acid (179 mg, 1.09 mmol, 1 eq), sodium carbonate (566 mg, 5.34 mmol, 4.9 eq), and tetra-*n*-butylammonium bromide (5 mg) were added to a solution of **2** (0.5 g, 1.09 mmol) in a toluene:water (15:5 mL) mixture in a microwave tube. The solution was degassed with nitrogen for 20 minutes, followed by the addition of tetrakis(triphenylphosphine)palladium (125 mg, 0.109 mmol, 0.1 eq). The solution was heated in the microwave at 120^o C for 3 hours. The mixture was cooled to room temperature and then diluted with dichloromethane. The organic phase was washed with water, extracted, dried over magnesium sulfate, filtered, and then concentrated. The crude product was purified by silica gel chromatography (hexane/dichloromethane, 50:55) to give a red solid (249 mg, 46%). ^{1}H NMR ($CDCl_3$, 400 MHz) δ (ppm) = 7.93 (d, 2H), 7.88 (d, 2H), 7.72 (d, 2H), 7.29 (dd, 4H), 7.21 (m, 6H), 7.06 (t, 2H), 6.90 (d, 2H), 3.05 (s, 6H). ^{13}C NMR ($CDCl_3$, 100 MHz) δ (ppm) = 154.5, 154.3, 150.5, 147.9, 147.7, 133.1, 131.5, 131.3, 130.2, 130.0, 129.45, 127.8, 126.5, 125.5, 124.95, 123.3, 123.2, 112.5, 40.6. ESI-MS [M+H$^+$] m/z: calcd for $C_{32}H_{27}N_4S$, 499.19, found 499.3.

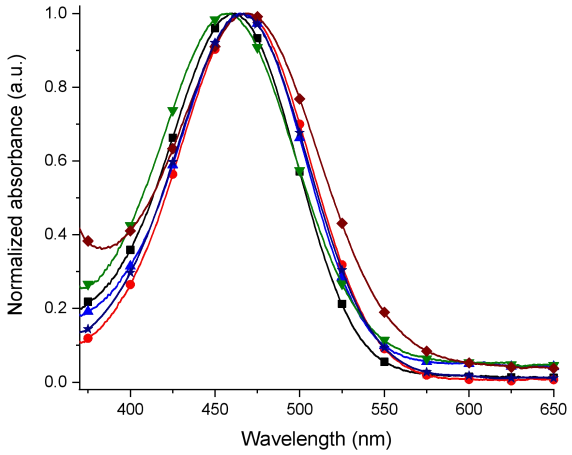

Figure 3.7. Normalized absorbance spectra of **1** in different anhydrous solvent: diethyl ether (■), THF (●), toluene (▲), acetonitrile (▼), DMF (♦), and dichloromethane ( ).

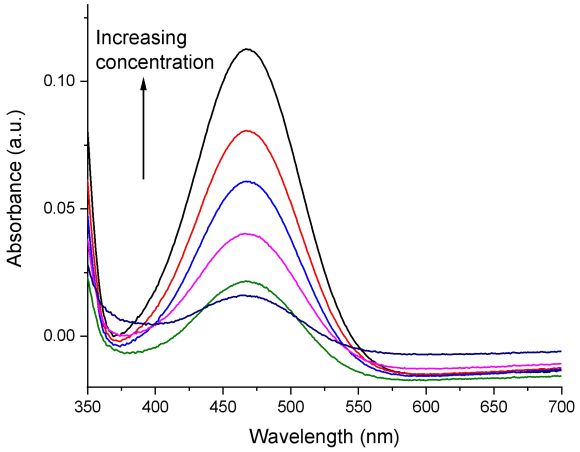

Figure 3.8. Concentration dependent absorption of **1** sequentially diluted from a 1 mM stock solution in THF.

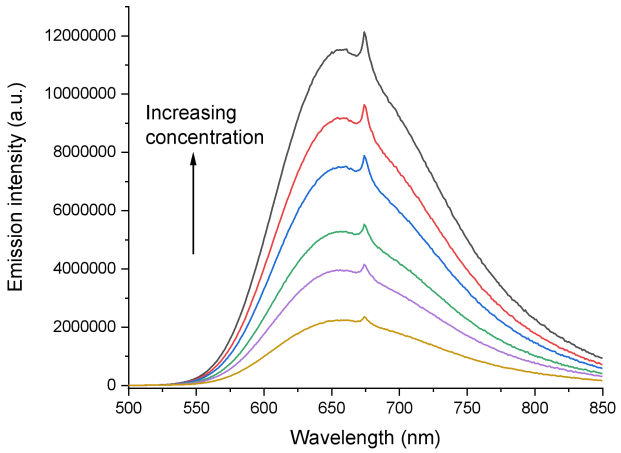

Figure 3.9. Concentration dependent emission of **1** in THF, exciting at 465 nm with the various solutions from.

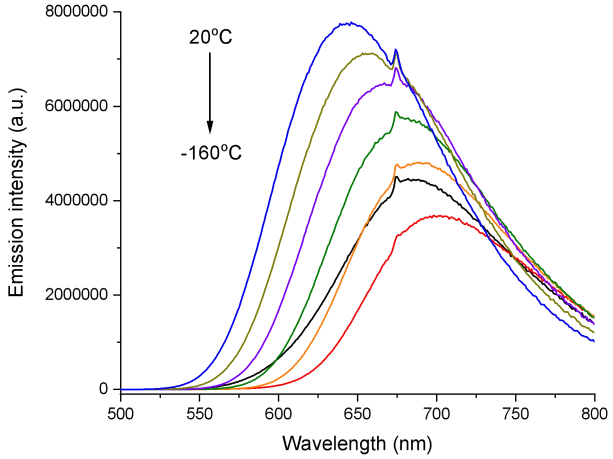

Figure 3.10. Temperature dependent emission of **1** in 2-methyltetrahydrofuran between -160° and 20° C, exciting at 465 nm. The temperature was equilibrated for a least 5 min. at each temperature: 20° (—), -10° (—), -40° (—), -70° (—), -100° (—), -130° (—), 160° C (—).

Table S2. Emission wavelength and emission yield of **1** as a function of various vol% water in THF.

THF vol. %	Φ_{fl} (%)	Emission (nm)
100	63	655
80	7.0	705
60	6.0	715
40	2.5	690
20	39	655
10	45	645

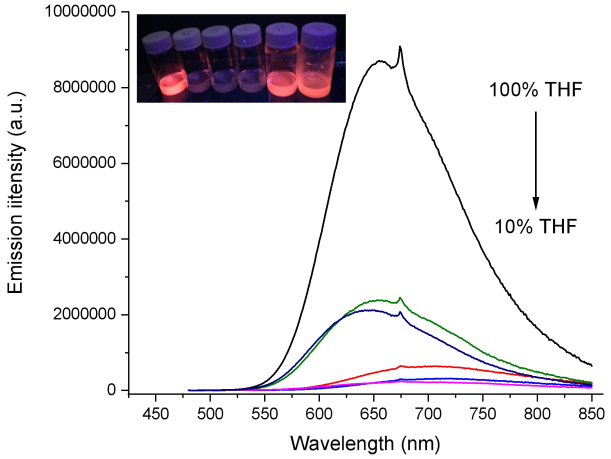

Figure 3.11. Emission spectra of **1** in various vol.% of water in THF. Inset: photograph of **1** in vials irradiated with a handheld UV lamp with vol.% water of 0%, 20%, 40%, 60%, 80%, and 90% (from left to right) in THF.

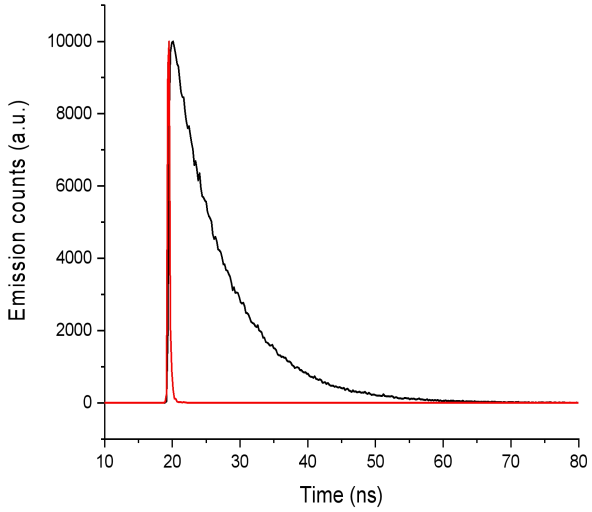

Figure 3.12. Singlet excited state kinetic decay of **1** (—) and the instrument response frequency (—)

measured in degassed THF and exciting at 405 nm.

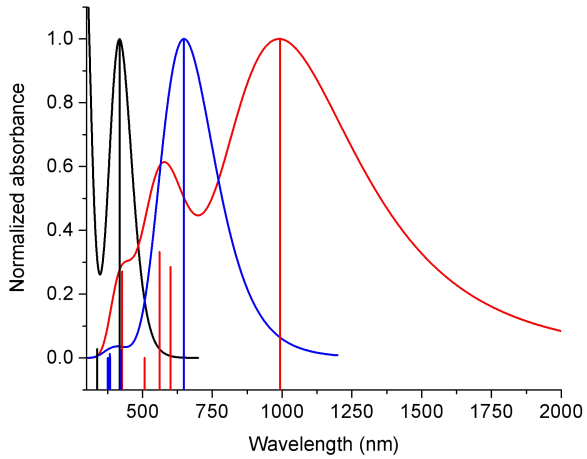

Figure 3.13. Calculated absorption spectra of the neutral (black), dication (blue), and radical cation (red) of **1** by DFT-TD means with CAM-B3LYP with the 6-311G*(d,p) basis set.

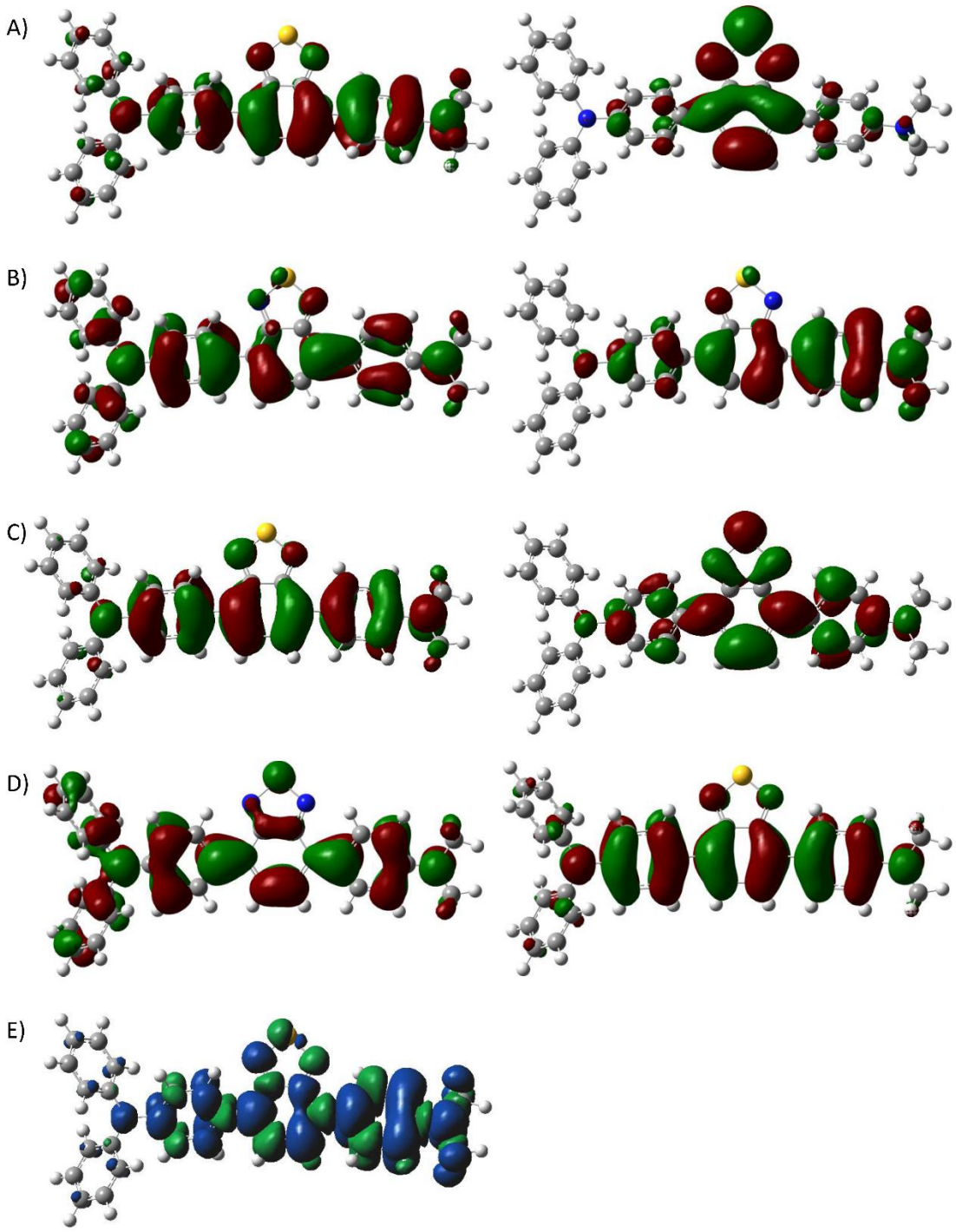

Figure 3.14. HOMO (left) and LUMO (right) from the natural transition orbital analysis calculated from the first singlet transition by TD-DFT of the neutral (A), -radical cation orbital (B), -radical cation orbital (C), the dication (D), and the spin density (E) of **1**.

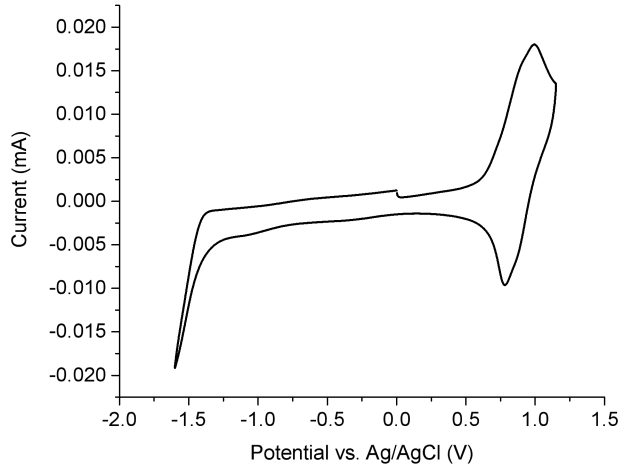

Figure 3.15. Cyclic voltammogram of **1** measured at 100 mV/sec in anhydrous and degassed dichloromethane with 0.1 M $TBAPF_6$.

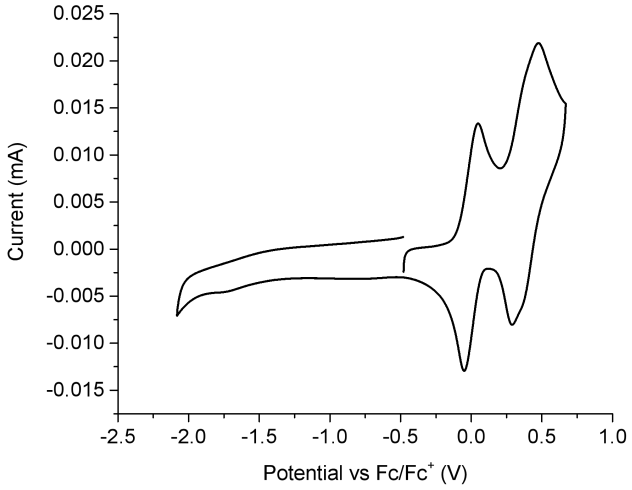

Figure 3.16. Cyclic voltammogram of **1** measured at 100 mV/sec in anhydrous and degassed dichloromethane with 0.1 M $TBAPF_6$ and equimolar ferrocene added an internal reference.

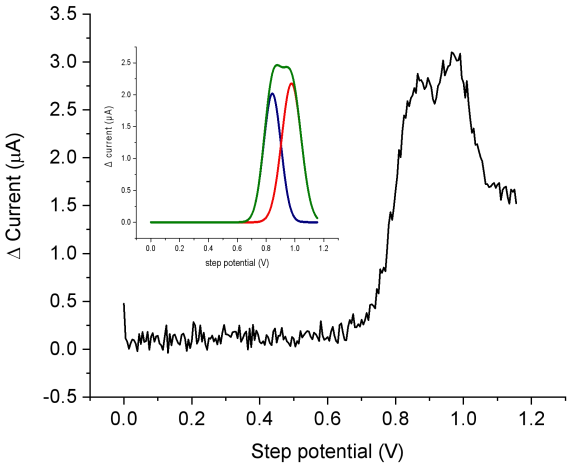

Figure 3.17. Square wave voltammogram of **1** measured in anhydrous and degassed dichloromethane with 0.1 M $TBAPF_6$. Inset: mathematically deconvoluted experimental square wave voltammogram with baseline correction into two constitutional components (red and blue) along with the refitted peak (green) of two deconvoluted gaussian peaks.

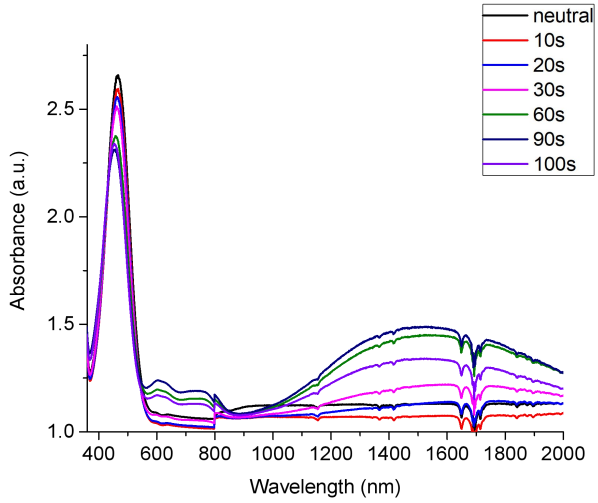

Figure 3.18. Change in absorption spectra of **1** with applied potential of 0.95 V between 10 and 100 sec in anhydrous and deaerated dichloromethane with 0.1 M $TBAPF_6$.

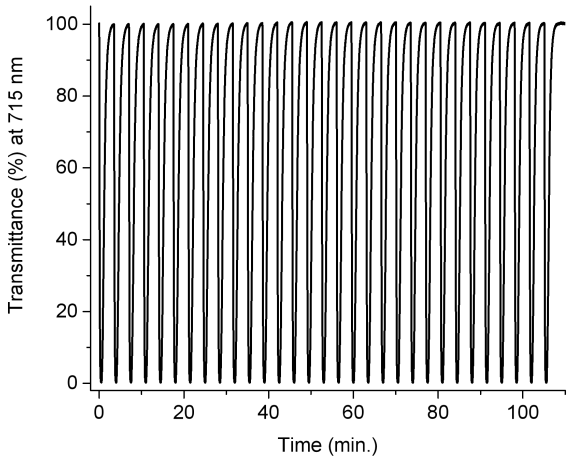

Figure 3.19. Change in percent transmittance of **1** at 715 nm measured in anhydrous and deaerated dichloromethane with 0.1 M $TBAPF_6$ with applied potential switching between +1.3 and -0.1 V at 30 sec. intervals.

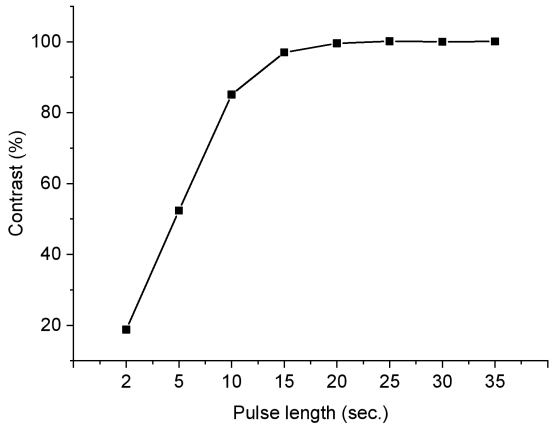

Figure 3.20. Calculated contrast ratio of **1** in anhydrous and degassed dichloromethane with 0.1 M $TBAPF_6$ at 715 nm derived by measuring the percent transmittance with different pulse durations.

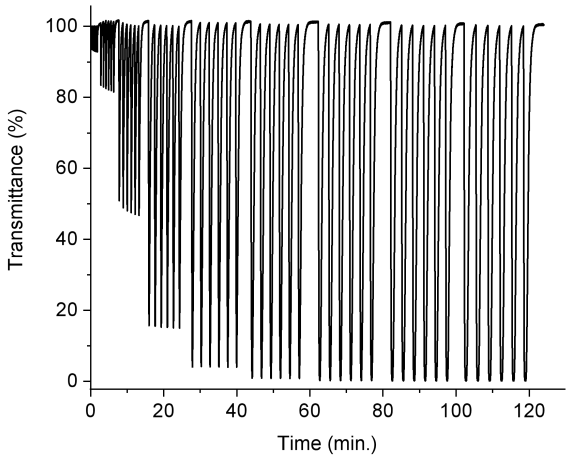

Figure 3.21. Variation of percent transmittance of **1** in anhydrous and degassed dichloromethane with 0.1 M $TBAPF_6$ monitored at 715 nm with switching the applied potential between +1.3 and -0.1 V six times per given switching interval: 1, 2, 5, 10, 15, 20, 25, 30, and 35 sec.

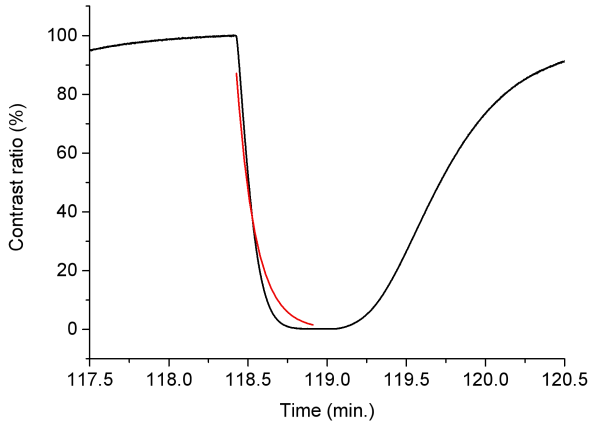

Figure 3.22. Contrast ratio of **1** in anhydrous and degassed dichloromethane with 0.1 M $TBAPF_6$ monitored at 715 nm: experimental (—) and theoretically (—) fitted curves.

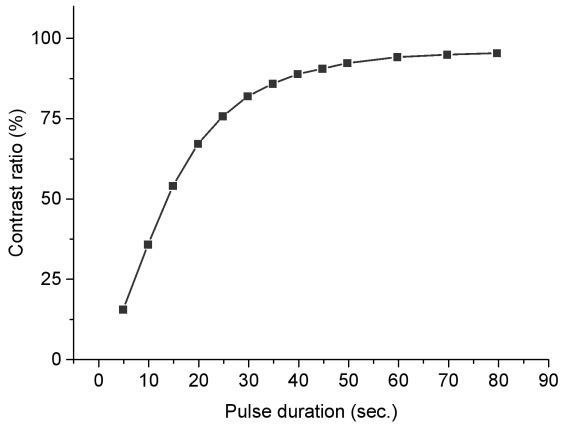

Figure 3.23. Calculated contrast ratio of **1** in anhydrous and degassed dichloromethane with 0.1 M $TBAPF_6$ at 1400 nm derived from measuring the percent transmittance with different pulse durations.

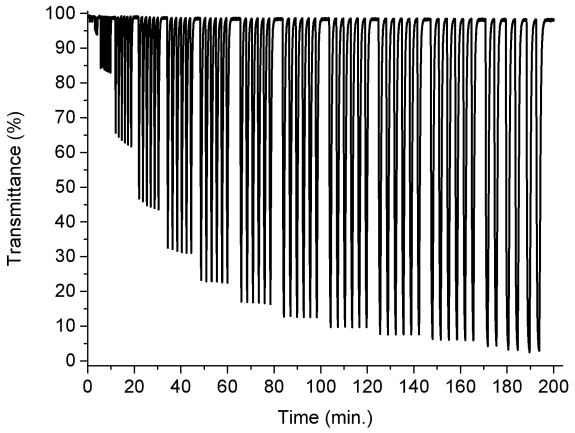

Figure 3.24. Variation of percent transmittance of **1** in anhydrous and degassed dichloromethane with 0.1 M $TBAPF_6$ monitored at 1400 nm with switching the applied potential between +0.95 and -0.1 V six times per switching interval: 1, 2, 5, 10, 15, 20, 25, 30, 35, 40, 45, 50, and 60 sec.

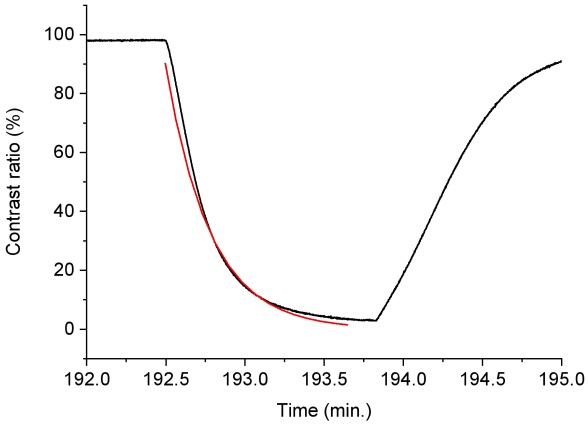

Figure 3.25. Contrast ratio of **1** in anhydrous and degassed dichloromethane with 0.1 M $TBAPF_6$ monitored at 1400 nm: experimental (▬) and theoretically (▬) fitted curves.

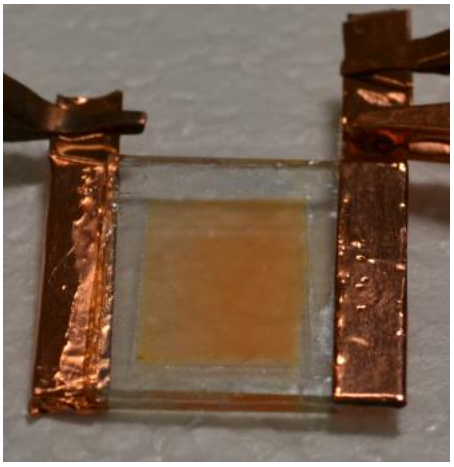

Figure 3.26. Photograph of the operating dual electrochromic and electofluorochromic operating sandwich device prepared from **1**.

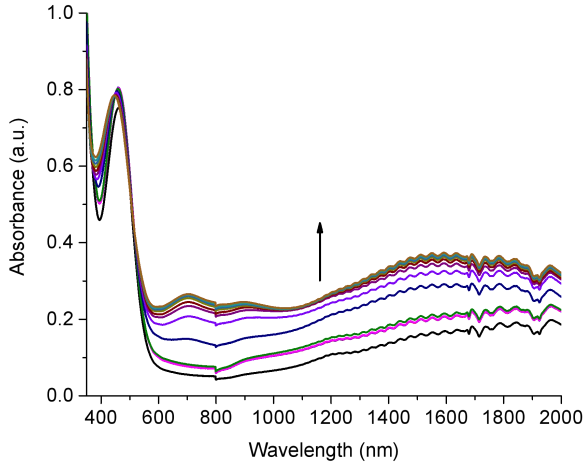

Figure 3.27. Change in absorption spectra of the operating device prepared from **1** with increasing applied potential from 0 to 2.5 V measured at 2 min. intervals.

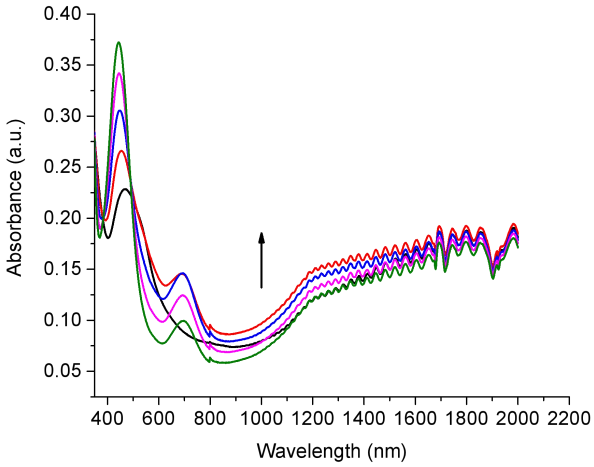

Figure 3.28. Change in absorption spectra of the device prepared from **1** with applied potential of 1.9 V measured at 15 sec. intervals.

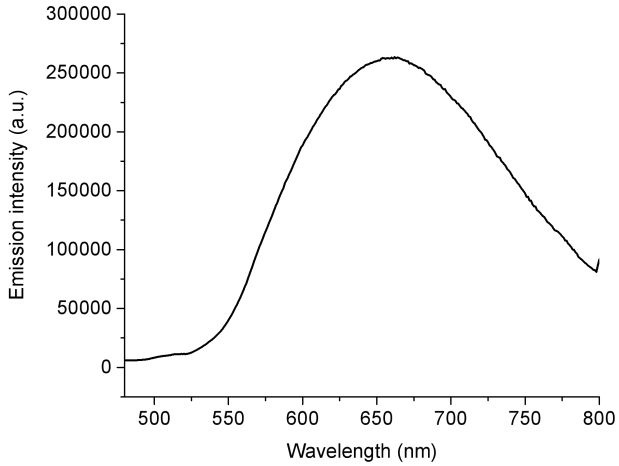

Figure 3.29. Emission spectrum of the assembled operating dual electrochromic electrofluorochromic sandwich device prepared from **1** when excited at 460 nm.

Table S3. Coordinates of the optimized geometry of the neutral **1** calculated by CAM-B3LYP with the 6-311+G(d,p) basis set.

Atom	x	y	z
S	2.27198	3.26152	0.04705
N	0.99626	2.25842	0.01991
N	3.46938	2.16661	0.02869
N	9.28778	-0.81079	-0.08381
N	-5.03207	-0.24286	0.00319
C	1.46544	1.01455	0.00038
C	2.91055	0.96065	-0.00499
C	3.60819	-0.29427	-0.03287
C	2.81117	-1.40575	-0.0583
H	3.27568	-2.38345	-0.09886
C	1.38953	-1.3527	-0.0462
H	0.85242	-2.29358	-0.04746
C	0.67932	-0.185	-0.02254
C	5.08111	-0.38657	-0.02126
C	5.89192	0.48695	-0.74953
H	5.43849	1.28488	-1.32202
C	7.26868	0.35888	-0.76811
H	7.84169	1.06282	-1.35398
C	7.91783	-0.66162	-0.04732
C	7.10234	-1.52512	0.70814
H	7.5419	-2.30701	1.31012
C	5.72617	-1.38737	0.70828
H	5.13988	-2.06696	1.31614

C	10.10135	0.24261	-0.66155
H	9.84409	0.40897	-1.70946
H	11.14613	-0.0579	-0.62516
H	9.99693	1.19571	-0.12679
C	9.92796	-1.71957	0.84828
H	9.77724	-1.42471	1.89518
H	10.99699	-1.73615	0.64792
H	9.55478	-2.73789	0.72308
C	-0.79836	-0.16669	-0.02968
C	-1.53082	0.71466	0.76904
H	-1.01183	1.42263	1.40069
C	-2.91421	0.68266	0.79085
H	-3.45529	1.36358	1.43543
C	-3.6201	-0.21876	-0.00796
C	-2.89655	-1.0923	-0.82103
H	-3.42224	-1.78871	-1.4617
C	-1.51257	-1.06802	-0.82231
H	-0.97735	-1.74453	-1.47808
C	-5.76606	0.9677	0.08822
C	-5.39042	2.07923	-0.6665
H	-4.53232	2.01342	-1.32361
C	-6.10854	3.26239	-0.57504
H	-5.80322	4.11679	-1.16751
C	-7.21953	3.35121	0.25479
H	-7.78214	4.27439	0.31945
C	-7.60108	2.24243	1.00006
H	-8.46207	2.29849	1.65567
C	-6.87755	1.06121	0.92594
H	-7.17341	0.20394	1.51765
C	-5.72456	-1.47776	-0.07843
C	-5.30471	-2.57635	0.672
H	-4.44506	-2.48057	1.32342
C	-5.98177	-3.78376	0.58467
H	-5.64284	-4.62748	1.1742
C	-7.09528	-3.91043	-0.23689
H	-7.62604	-4.85251	-0.29821
C	-7.52092	-2.8149	-0.97783
H	-8.38451	-2.90028	-1.62681
C	-6.83854	-1.60916	-0.90768
H	-7.16879	-0.76205	-1.49579

Table S4. Coordinates of the optimized geometry of the radical cation of **1** calculated by CAM-B3LYP with the 6-311+G(d,p) basis set.

Atom	x	y	z
S	2.2672	3.32092	-0.01946
N	1.00723	2.3045	-0.01902
N	3.47177	2.23381	0.02337
N	9.22905	-0.79279	-0.04861
N	-4.99407	-0.25546	-0.00715
C	1.48365	1.06602	0.02126
C	2.92742	1.02405	0.03137
C	3.63251	-0.23392	0.06653
C	2.81804	-1.35842	0.08868
H	3.2726	-2.33949	0.09474
C	1.41682	-1.31252	0.06929
H	0.88679	-2.2549	0.10306
C	0.69418	-0.13655	0.03667
C	5.07204	-0.35079	0.05622
C	5.91519	0.67984	-0.43566
H	5.47119	1.59117	-0.80338
C	7.26981	0.54148	-0.4785
H	7.86396	1.34331	-0.88999
C	7.90077	-0.64951	-0.00938
C	7.05991	-1.68344	0.50527
H	7.49331	-2.58821	0.90352
C	5.70843	-1.53197	0.5264
H	5.11522	-2.32797	0.9538
C	10.09104	0.29166	-0.52197
H	9.91641	0.48504	-1.58153
H	11.12661	-0.00046	-0.38579
H	9.90727	1.20197	0.04801
C	9.86701	-2.03858	0.38024
H	9.73171	-2.18904	1.45255
H	10.92868	-1.97876	0.16709
H	9.44987	-2.88726	-0.16111
C	-0.7689	-0.13311	0.01109
C	-1.52921	0.87008	0.62712
H	-1.03243	1.68435	1.13398
C	-2.90811	0.82569	0.63374
H	-3.46112	1.60285	1.14358
C	-3.59903	-0.21601	-0.00019

C	-2.8457	-1.21614	-0.63174
H	-3.34872	-2.02024	-1.15141
C	-1.46792	-1.17503	-0.61494
H	-0.92296	-1.9502	-1.13938
C	-5.76131	0.9419	0.0755
C	-5.4834	2.01953	-0.76296
H	-4.67343	1.94605	-1.47808
C	-6.2414	3.1783	-0.68141
H	-6.01673	4.00997	-1.33843
C	-7.29304	3.26828	0.22249
H	-7.88792	4.17154	0.27918
C	-7.57749	2.18964	1.05028
H	-8.39381	2.24942	1.7601
C	-6.81314	1.03347	0.9839
H	-7.0315	0.19552	1.63433
C	-5.6897	-1.49514	-0.09931
C	-5.36427	-2.55293	0.74722
H	-4.57318	-2.43014	1.47659
C	-6.05201	-3.75413	0.65633
H	-5.7914	-4.56977	1.32017
C	-7.08055	-3.9071	-0.26548
H	-7.62101	-4.84347	-0.32946
C	-7.41275	-2.84862	-1.10156
H	-8.21171	-2.9574	-1.82516
C	-6.71842	-1.64969	-1.02544
H	-6.97377	-0.82714	-1.68203

Table S5. Coordinates of the optimized geometry of the dication of **1** calculated by CAM-B3LYP with the 6-311+G(d,p) basis set.

Atom	x	y	z
S	2.28356	3.35156	-0.28252
N	1.0178	2.33421	-0.2846
N	3.46732	2.24059	-0.22001
N	9.15963	-0.80165	0.26882
N	-4.90959	-0.25713	0.05296
C	1.47664	1.10027	-0.22342
C	2.9157	1.04464	-0.18684
C	3.63889	-0.22684	-0.18333
C	2.77734	-1.37214	-0.34463
H	3.22032	-2.35408	-0.39022

C	1.42767	-1.31798	-0.38431
H	0.90696	-2.26013	-0.4525
C	0.65746	-0.10728	-0.26345
C	5.01316	-0.36196	-0.04041
C	5.8774	0.74242	0.30146
H	5.43746	1.70935	0.48182
C	7.21344	0.60352	0.41965
H	7.80718	1.46055	0.69815
C	7.85126	-0.66646	0.19212
C	7.00256	-1.7874	-0.12015
H	7.43656	-2.76052	-0.28851
C	5.66741	-1.63792	-0.21955
H	5.09107	-2.51319	-0.47601
C	10.02529	0.34493	0.57209
H	9.89354	1.12936	-0.17268
H	11.05816	0.01584	0.55168
H	9.8038	0.73966	1.5637
C	9.80251	-2.10358	0.0505
H	9.46135	-2.82709	0.7907
H	10.87509	-1.98264	0.15108
H	9.58571	-2.47365	-0.95153
C	-0.73017	-0.12981	-0.18364
C	-1.50799	1.01926	0.20376
H	-0.99566	1.92801	0.47442
C	-2.85556	0.98298	0.28267
H	-3.39723	1.85451	0.61894
C	-3.57837	-0.21777	-0.01883
C	-2.82376	-1.37764	-0.39736
H	-3.34536	-2.28334	-0.66788
C	-1.47758	-1.32929	-0.47104
H	-0.9674	-2.21601	-0.81514
C	-5.7034	0.94288	0.15423
C	-5.65657	1.88284	-0.86681
H	-5.0185	1.71941	-1.72647
C	-6.44459	3.02114	-0.77568
H	-6.41669	3.75587	-1.57031
C	-7.27191	3.21018	0.32337
H	-7.88771	4.09834	0.38991
C	-7.31616	2.25808	1.33504
H	-7.96143	2.40404	2.192
C	-6.53442	1.11607	1.2532

H	-6.56519	0.36713	2.03452
C	-5.64231	-1.49903	0.03007
C	-5.41905	-2.44733	1.02005
H	-4.6916	-2.25817	1.79974
C	-6.14729	-3.62816	1.0034
H	-5.98096	-4.36967	1.77452
C	-7.09153	-3.85133	0.00999
H	-7.66016	-4.77277	0.00148
C	-7.31349	-2.89031	-0.96926
H	-8.05083	-3.06195	-1.74316
C	-6.59245	-1.7063	-0.96135
H	-6.76225	-0.95014	-1.7174

Table S6. Crystallographic data of **1**.

Chemical formula	$C_{32}H_{26}N_4S$
M_r	498.63
Crystal system, space group	Triclinic, *P*
Temperature (K)	100
a, *b*, *c* (Å)	9.8712 (6), 12.0146 (7), 21.2768 (12)
α, β, γ (°)	97.631 (3), 94.569 (3), 100.912 (3)
V (Å^3)	2441.5 (2)
Z	4
Radiation type	Cu *K*α
μ (mm^{-1})	1.40
Crystal size (mm)	0.38 × 0.15 × 0.07
Data collection	
Diffractometer	Bruker Smart *APEX*
Absorption correction	Multi-scan *SADABS2016*/2 (Bruker,2016/2) was used for absorption correction. wR2(int) was 0.1490 before and 0.0598 after correction. The Ratio of minimum to maximum transmission is 0.5553. The λ/2 correction factor is Not present.
T_{min}, T_{max}	0.179, 0.322
No. of measured, independent and observed [$I > 2\sigma(I)$] reflections	48944, 9032, 7877
R_{int}	0.044
$(\sin \theta/\lambda)_{max}$ (Å^{-1})	0.610
Refinement	
$R[F^2 > 2\sigma(F^2)]$, $wR(F^2)$, *S*	0.045, 0.138, 1.07
No. of reflections	9032
No. of parameters	671
No. of restraints	504
H-atom treatment	H-atom parameters constrained
$\Delta\rho_{max}$, $\Delta\rho_{min}$ (e Å^{-3})	0.32, −0.38

Table S7. Selected dihedral angles and bond lengths from the X-ray crystallographic data of **1** and the optimized structures calculated by theoretical means.[1]

Atoms in dihedral angle	Angle (°)	Atoms in bond distance	Bond length (Å)
C8A-C7A-C3A-C2A	46.1(3)	C7A-C3A	1.476(2)
C8B-C7B-C3B-C2B	-40.3(3)	C7B-C3B	1.471(2)
Neutral state[1]	-40.1	Neutral state[1]	1.47
Radical cation[1]	-21.9	Radical cation[1]	1.44
Dication[1]	8.52	Dication[1]	1.44
C1A-C6A-C15A-C16A	29.6(3)	C6A-C15A	1.476(2)
C1B-C6B-C15B-C16B	-37.2(3)	C6B-C15B	1.472(2)
Neutral state[1]	-41.7	Neutral state[1]	1.47
Radical cation[1]	-33.5	Radical cation[1]	1.46
Dication[1]	-12.2	Dication[1]	1.46
C14A-N3A-C10A-C11A	8.4(3)	N3A-C10A	1.374(2)
C14B-N3B-C10B-C11B	6.1(3)	N3B-C10B	1.374(2)
Neutral state[1]	11.9 and -10.9	Neutral state[1]	1.38
Radical cation[1]	2.7 and 2.6	Radical cation[1]	1.34
Dication[1]	-0.5 and -0.8	Dication[1]	1.34
C19A-C18A-N4A-C27A	-51.6(2)	C18A-N4A	1.423(2)
C19B-C18B-N4B-C27B	27.5(3)	C18B-N4B	1.407(2)
Neutral state[1]	38.4 and 38.3	Neutral state[1]	1.41
Radical cation[1]	27.7 and 49.5	Radical cation[1]	1.39
Dication[1]	13 and 61.4	Dication[1]	1.39

[1]Optimized geometry calculated by CAM-B3LYP with the 6-311+G(d,p) basis set.

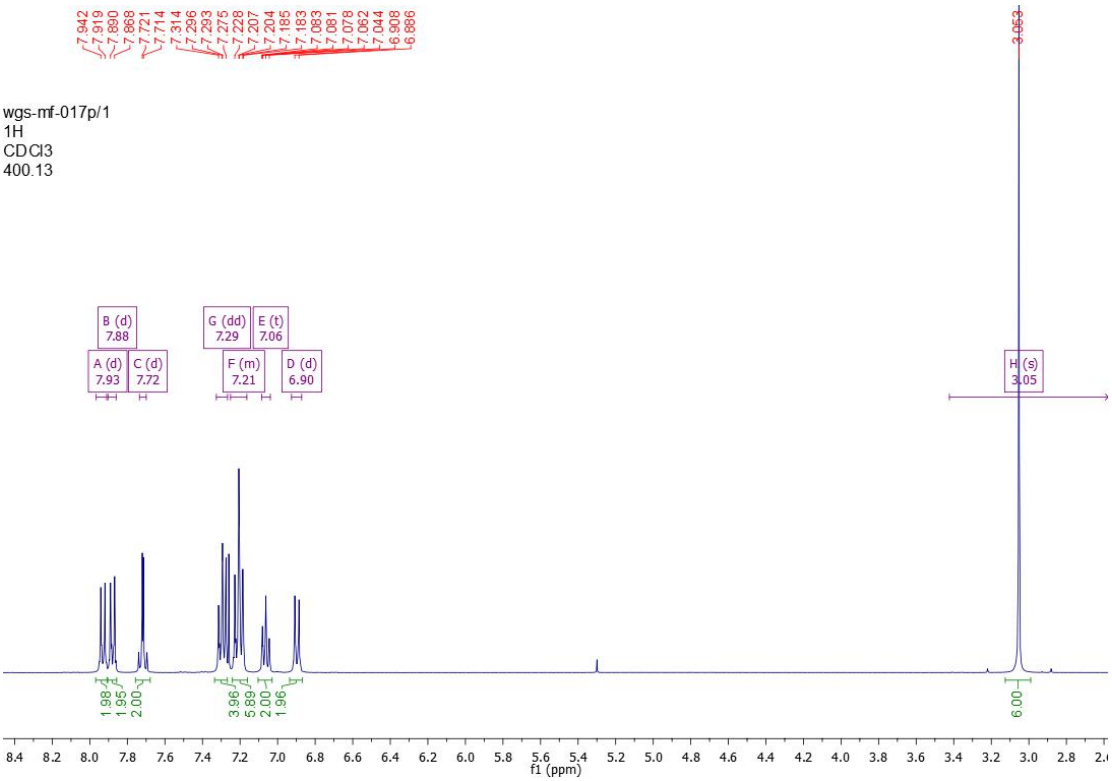

Figure 3.30. ^{1}H NMR spectrum of **1** recorded in $CDCl_3$.

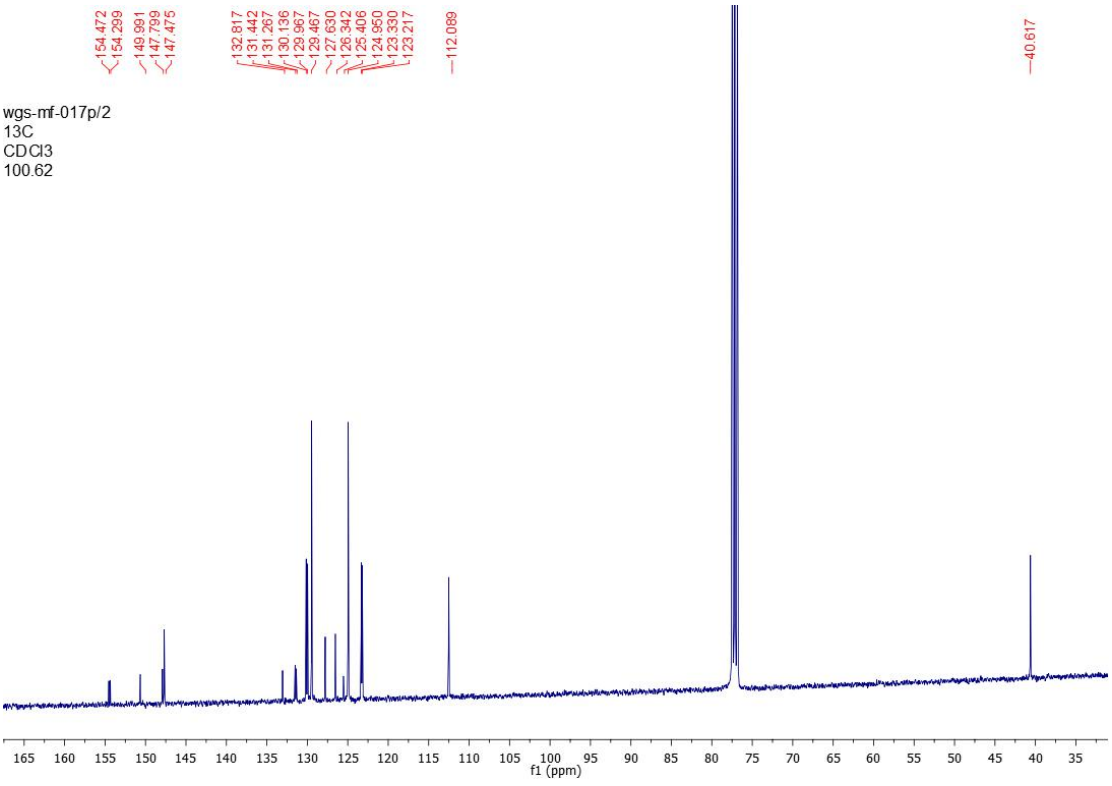

Figure 3.31. ^{13}C NMR spectrum of **1** recorded in $CDCl_3$

.

References

S[1] M. J. Frisch, G. W. Trucks, H. B. Schlegel, G. E. Scuseria, M. A. Robb, J. R. Cheeseman, G. Scalmani, V. Barone, G. A. Petersson, H. Nakatsuji, M. C. X. Li, A. V. Marenich, J. Bloino, B. G. Janesko, R. Gomperts, B. Mennucci, H. P. Hratchian, J. V. Ortiz, A. F. Izmaylov, J. L. Sonnenberg, D. Williams-Young, F. Ding, F. Lipparini, F. Egidi, J. Goings, B. Peng, A. Petrone, T. Henderson, D. Ranasinghe, V. G. Zakrzewski, J. Gao, N. Rega, G. Zheng, W. Liang, M. Hada, M. Ehara, K. Toyota, R. Fukuda, J. Hasegawa, M. Ishida, T. Nakajima, Y. Honda, O. Kitao, H. Nakai, T. Vreven, K. Throssell, J. J. A. Montgomery, J. E. Peralta, F. Ogliaro, M. J. Bearpark, J. J. Heyd, E. N. Brothers, K. N. Kudin, V. N. Staroverov, T. A. Keith, R. Kobayashi, J. Normand, K. Raghavachari, A. P. Rendell, J. C. Burant, S. S. Iyengar, J. Tomasi, M. Cossi, J. M. Millam, M. Klene, C. Adamo, R. Cammi, J. W. Ochterski, R. L. Martin, K. Morokuma, O. Farkas, J. B. Foresman, D. J. Fox, Gaussian, Inc., Wallingford CT, **2016**.

[2] a) T. Yanai, D. P. Tew, N. C. Handy, *Chem. Phys. Lett.* **2004**, *393*, 51-57; b) P. J. Stephens, F. J. Devlin, C. F. Chabalowski, M. J. Frisch, *J. Phys. Chem.* **1994**, *98*, 11623-11627; c) S. H. Vosko, L. Wilk, M. Nusair, *Can. J. Phys.* **1980**, *58*, 1200-1211; d) A. D. Becke, *Phys. Rev. A* **1988**, *38*, 3098-3100.

[3] M. E. Casida, in *Recent Advances in Density Functional Methods, Vol. 1* (Ed.: D. P. Chong), World Scientific, Singapore, **1995**, pp. 155-192.

[4] S. Hassab, D. E. Shen, A. M. Österholm, M. Da Rocha, G. Song, Y. Alesanco, A. Viñuales, A. Rougier, J. R. Reynolds, J. Padilla, *Sol. Energy Mater. Sol. Cells* **2018**, *185*, 54-60.

[5] A. Medina, C. G. Claessens, G. M. A. Rahman, A. M. Lamsabhi, O. Mó, M. Yáñez, D. M. Guldi, T. Torres, *Chem. Commun.* **2008**, 1759-1761.

[6] M. Velusamy, K. R. Justin Thomas, J. T. Lin, Y.-C. Hsu, K.-C. Ho, *Org. Lett.* **2005**, *7*, 1899-1902.

[7] S.-i. Kato, T. Matsumoto, M. Shigeiwa, H. Gorohmaru, S. Maeda, T. Ishi-i, S. Mataka, *Chem. Eur. J.* **2006**, *12*, 2303-2317.

4. Study of a series of red chromophores

In this chapter, three benzothiadiazole (BZT) derivatives with a triphenylamine (TPA) were studied. This series of compounds had different electron withdrawing groups that were coupled to the conjugated BZT-TPA core. The photophysical and electrochemical properties of these electronic *push-pull* compounds were fully demonstrated. By taking advantage of the intrinsic emission of the BZT core and the reversible electrochemical redox property of the TPA moiety, the compounds showed a reversible redox process as well as solid state emission. Compounds **1** and **2** were further used as the active layer for fabricating working layers in electrofluorochromic devices.

The compounds studied were synthesized by a former trainee student, Mathieu Frémont.

The single crystal X-ray diffraction was resolved by Dr. Maris Thierry.

The spectroscopic properties of compound 3 were assessed by various group members: Alexandre Malinge, Lei Hu, Coralie Cambe, Georges Turner, and Laurie Walach.

My contribution in this work was the full characterization of compounds **1** and **2**, including photophysical properties, electrochemical properties, spectroeletrochemical properties, single crystal growth. The electrochemical properties and spectroeletrochemical properties of compound **3.** Furthermore, we successfully made working device of compound **1** and **2** as electroluminochromic layers and showed the '*turn on and off*' properties. I also compiled the collective data of compound 3 and assembled the supporting information of the compounds.

Influence of electron-withdrawing groups on the Benzothiadiazole derivatives as electrochromic materials.

Chengzhang Yao, Mathieu Frémont, Alexandre Malinge, Lei Hu, Coralie Cambe, Georges Turner, Laurie Walach, and W. G. Skene

Abstract
Three conjugated fluorophores consisting a central benzothiadiazole flanked with triphenylamine on one side and a phenyl substituted with different electron withdrawing groups on the other side were investigated. The effect of three electron withdrawing groups (-NO_2, -CN, and -CHO) on the spectroscopic properties were assessed. The electronic *push-pull* fluorophores were solvatochromic with Stokes shifts upwards of 10 000 cm^{-1}. Their emissions spanned from 540 nm the visible spectrum to the NIR region continent on solvent. Their emission yields were also near unity in apolar solvents for a local excited state and decreased in polar solvents with intramolecular charge transfer. The emission yield of the -NO_2 fluorophore was ca. 9-fold less than its -CN and -CHO counterparts in the solid state. The reversible redox behavior of the triphenylamine enabled electrochemically mediated visible color changes. New absorptions at ca. 550 nm and in NIR region were formed with electrochemical oxidation. The electrochemically generated states could be reversibly generated for upwards of 60 min, illustrating their usefulness as electrochromic materials. Similarly, their intrinsic emission intensity could be modulated with applied potential. The emission off/on behavior could be carried over to operating devices with the -NO_2 and -CN fluorophores. The collectively electrochemically mediated color switching and emission intensity modulation along with their solid-state emission demonstrate that benzothiadiazole fluorophores can play a dual role in chromic devices.

Graphical Abstract

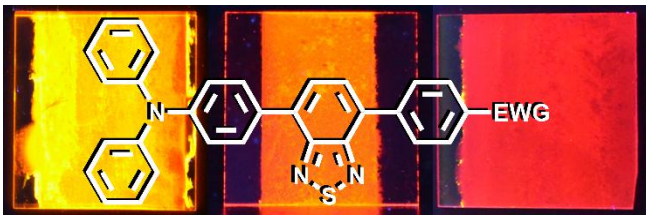

The effect of the electron withdrawing group (EWG) on the emission of benzothiadiazoles was investigated and their electrofluorochromic response.

4.1 Introduction

Electrochemically mediated color changes enable light filtering coatings in smart-windows.[1] These true applications have an ecological advantage. This is by reducing building cooling costs by modulating the transmitted light that otherwise heats the internal air.[2-3] The active component in these devices is a metal oxide, such as tungsten oxide.[4-5] While the coating is robust and can undergo extended duty cycle that is required for long-term use in functional applications, the perceived color change is limited to blue hues and colorless for tungsten oxides.[6-7] In contrast, an extended palette of colors that span the visible spectrum and extend to the NIR is possible with conjugated organic polymers.[7-9] Access to these colorful polymers has been enabled by recent advances in synthetic methods such as direct arylation.[10-11] These catalytic advances also have the benefit of being environmentally friendlier preparation methods compared to conventional coupling protocols.[12]

Extended degrees of conjugation are required for organic polymers to absorb in the visible region. The resulting narrow energy gap between their HOMO and LUMO energy levels for visible absorption can lead to efficient excited state deactivation by non radiative modes.[13-14] While conjugated polymers have been successfully used as the color switching material in electrochromic devices, they have played a limited role as a fluorophore in electrofluorochromic devices. These are devices whose emission intensity can be electrochemically mediated when they are excited by light.[15]

It is of interest to have an active material that has both an absorption in the visible and fluoresces. It could therefore play a dual-role in an operating device; as an electrochrome and an electrofluorochrome. It would be capable of undergoing both visible color changes and emission intensity modulation with applied potential that can be tracked a common user. Appreciable emission yield (Φ_{Fl}) both in the solid state and when cast as a thin film along with reversible electroactivity are additional keys properties that are required of fluorophores for their use as active dual-role layers in chromic devices. These preclude conventional fluorophores for use as fluorochromes. Although the rigid structures of conventional fluorophores prevent unwanted emission quenching by non radiative means such as bond rotations in solution, their intrinsic fluorescence is quenched by intermolecular deactivation processes and filter effects in the solid state.

Benzothiadiazoles are ideal candidates for dual-role materials in chromic devices. This is in part because of their absorptions in the visible spectrum.[16-19] Access to colorful small molecules can be done using catalytic methods along the lines of their polymer counterparts.[20-21] The emissive wavelength of small molecules of benzothiadiazoles such as dyads and triads can be adjusted with both the type of aromatic and electronic groups that are conjugated with a central benzothiadiazole,[16, 22-23] co-assembled structures[24], and polarity.[25-26] Most importantly, conjugated benzothiadiazoles behave as conventional fluorophores with high emission yields (Φ_{Fl}) in solution.[27] In contrast to conventional fluorophores, the intrinsic emission of benzothiadiazoles can be carried over to the solid-state.[28-29] The solid-state emission has been exploited for using benzothiadiazoles in various applications, including imaging,[30] electrochemiluminescent sensing,[31] solid-state lasers,[32] and emitting devices.[28, 33-34] However, benzothiadiazoles are intrinsically electrochemically inert within the working limits of solvents that are commonly used for the electrochemical measurements. The electroactivity that is required for their use in electrochromic applications is possible by covalently coupling an electroactive group to the intrinsic electron accepting benzothiadiazole. For example, a reversible oxidation behavior within the working limits of common electrochemical solvents is possible by the covalent attachment of triphenylamine to benzothiadiazoles.[35] The added benefit of the electroactive moiety is its electron donating property. The electroactive moiety can undergo intramolecular charge transfer with an electron accepting group when the chromophore is irradiated, leading to intense emission in the visible region.[36] The emission

wavelength of the resulting intramolecular charge transfer can be adjusted with the strength of the accepting group.

The visible color, solid-state emission, and reversible electroactivity of benzothiadiazoles make them ideal dual-mode candidates for use in electrochromic/electrofluorochromic devices. Despite these collective properties and the myriad uses of benzothiadiazoles as functional materials, their use as dual-role materials in chromic devices remains in its infancy. More specifically, their electrochemically mediated emission intensity modulation for their ultimate use in electrofluorochromic devices is underexplored.[37-38] Towards this end, the impact of electron acceptors of varying strength (-NO_2, -CN, and -CHO) on the emission of benzothiadiazoles (Chart 1) and the use of these electronic *push-pull* electroactive fluorophores as dual-role materials are herein evaluated. This knowledge is beneficial for designing subsequent dual-role chromes that have prescribed electrochemically mediated color changes, emission wavelength, and emission intensity modulation for use as the active layers in functioning chromic devices.

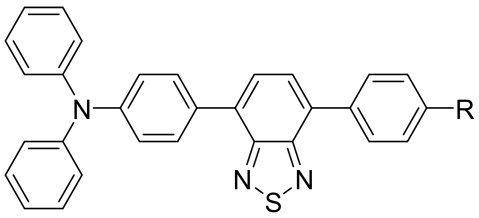

1 R=NO_2
2 R=CN
3 R=CHO

Chart 1. Benzothiadiazoles with electron withdrawing groups of varying strength prepared and investigated as dual-role role electrofluorochromic materials.

4.2 Results and Discussion

Crystallographic Data

X-ray diffraction of small crystals was used for two-fold reasons. One was to provide complementary data for confirming the identity of **3**. The other reason was to investigate the intermolecular effects and provide insight about the intermolecular effects on the photophysical properties. This is of importance because intermolecular π-π stacking can quench the emission of intrinsic fluorophores. According to **Figure 4.1A**, the resolved crystal structure confirms the identify of **3**, notably the aldehyde terminus. **3** was resolved as a single crystal structure with four compounds occur within the unit cell (**Figure 4.1B**). The phenyls are twisted from the central benzothiadiazole to minimize the steric hindrance between the *ortho*-hydrogens on the aromatics. This is illustrated in the dihedral angles of the phenyls with respect benzothiadiazole. These angles were 37.6(3)° and -29.8(3)° for the triphenylamine and phenyl-CHO segments, respectively. While the angles are consistent with other phenyl substituted benzothiadiazoles, they are expected to decrease upon excitation owing to bond elongation that occurs in the excited state.[22] The planarization concomitant with the intramolecular charge transfer between the termini are also expected to give rise to an appreciable emission in the visible region. The aldehyde group is further coplanar with its adjacent phenyl with a dihedral angle of 9.5(3)° for O1-C31-C28-C27. This indicates that the terminal group is indeed conjugated with the phenyl to which it is covalently attached. The resonance is further expected to give rise to excited charge transfer and enhance the visible emission.

The molecular attributes of the single crystal structure are not surprising in that they are consistent with similar 4-triphenylamine,7-phenyl substituted benzothiadiazoles.[22, 38] What is of importance are the intermolecular effects that occur in the solid-state packing. Of particular interest in the absence of any stacking. It is noteworthy that two anti-parallel molecules of **3** are superimposable by an inversion center are present in the unit cell, yet their aromatics do not overlap. Although the two compounds are nearly coplanar (180.0(3)°), they are slipped by 0.528(3) Å. Moreover, the centroid-to-centroid distance defined by the all-carbon aromatic portion of the benzothiadiazole is 3.536(2) Å. These collective attributes do not meet the criteria for π stacking. The extended packing structure of **3** is a herringbone arrangement (Figure 4.1D) as seen along the a-axis. This is a result of multiple CH-aryl interactions. For example, **3** forms three CH-aryl interactions. More specifically, C15 and C18 interact with the terminal phenyl of the TPA moiety of a different molecule, while C29 interacts with the phenyl moiety of the benzothiadiazole core of a third molecule. The C-aryl distances are 3.557(2), 3.462(2) and 3.430(2) Å for C15, C18, and C29, respectively. The aryl-TPA interactions are nearly orthogonal (143 and 139°), while the C29-benzothiadiazole angle is more obtuse (119°; **Figure 4.6**), corresponding to the planar anti-parallel structure in **Figure 4.1B**. The aldehyde of the oxygen also forms an intermolecular contact. In this case, it forms a contact with C16, which is located on the one of the terminal phenyls of the TPA segment, located 3.186 (2) Å away.

Additional contacts also take place. These involve another molecule of **3** in the unit cell to form a head-to-head dimer with a separate molecule having a symmetry operator of -x, 1-y, -z. The dimer forms two bonds between S1•••N1 that are 3.148(2) Å in length, along with a S1•••C8 bond with a distance of 3.479(2) Å. These are illustrated as the blue dotted lines in **Figure 4.1C**. The resulting 2S–2N square dimer that is adopted is typical for chalcogens.[39-40] The bond lengths are within the range what is expected for 2S–2N square. In fact, the distance is within the 3.42 Å mean of a series of benzothiadiazole 2S-2N dimers.[41] The dimer is atypical in that the arrangement is limited to only two molecules and it does not expand to other molecules to form donor-acceptor arrays. From the collective crystallographic data, it is apparent that **3** does not have any supramolecular arrangements such as π-stacking that promote emission

self-quenching. It is therefore expected to emit in the solid-state (vide infra) and not suffer from concentration induced emission deactivation, unlike conventional fluorophores. The series of benzothiadiazole fluorophores form Chart 1 are therefore expected to emit in the solid-state, making it suitable for use as an active layer in electrofluorochromic devices.

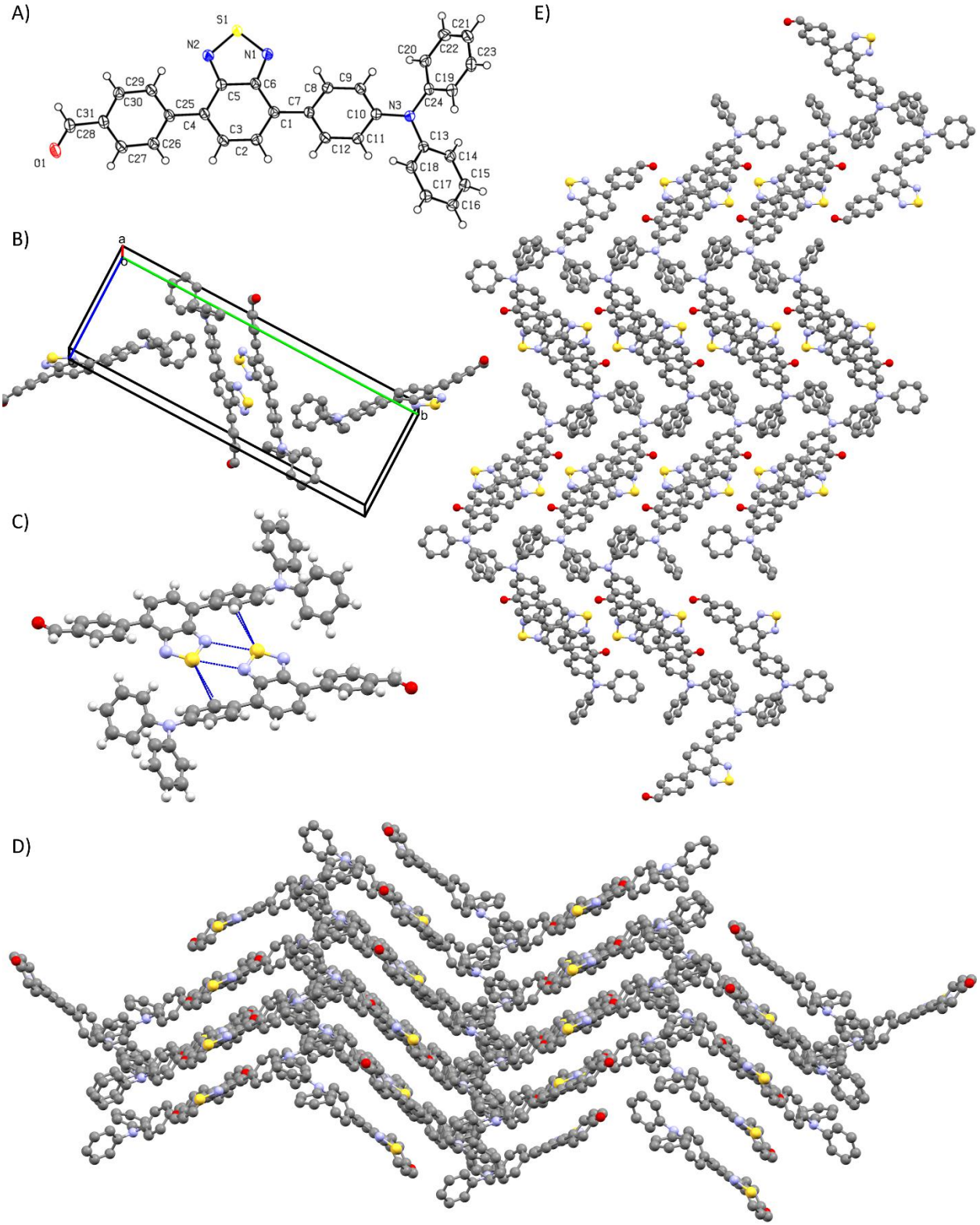

Figure 4.1. Resolved X-ray crystallographic structure of **3**: A) illustrated as the ORTEP diagram with the

ellipsoids drawn at 50% probability and the atom numbering; B) unit cell packing, C) supramolecular 2S–2N square dimer, D) herringbone packing structure shown along the a^*-axis, and E) extended solid-state packing shown along the c-axis. The hydrogens have been omitted (B, D, and E) for clarity with the supramolecular contacts shown as blue lines (B).

Spectroscopic Properties

The spectroscopic properties of **1-3** were investigated to assess their suitability as active fluorophores in a dual working electrochromic/electrofluorochromic devices. To better evaluate the effect of the electron withdrawing nitrile and nitro groups on the electronic *push-pull* chromophore, the spectroscopic properties were compared to the known **1** with a withdrawing substituent of moderate strength.[34] Although various spectroscopic properties of **2** and **3** have been reported,[22, 34] they were remeasured for benchmarking the extending properties of **1** and **2** under similar conditions. Comparing the solvatochromic data in different solvents, notably the emission yields (Φ_{fl}), is challenging by relative means because the refractive index of solvents must be taken into account. This can be overcome by absolute emission yields that are done with an integrating sphere. In this case, the absolute solvent refractive indices are not required. Rather, they are factored into the Φ_{fl} measurement when measuring the sphere response with a given solvent. The solvatochromism and the solvent dependent Φ_{fl} can therefore be directly compared among the three *push-pull* fluorophores of varying electron withdrawing strength.

The electron donor-acceptor of the termini are known to promote intramolecular charge transfer when irradiated. The degree of transfer is contingent on the solvent polarity, resulting in spectroscopic shifts. Both the absorption and emission solvent dependent spectra were evaluated. According to Table 8, the absorption of **1** varies by 32 nm. The shift is not pronounced because the ground state is neutral and therefore it is less perturbed by solvent polarity. **1** is nonetheless sensitive to solvent polarity as illustrated by its negative solvatochromism. This is a hypsochromic shift in the spectra arising from stabilization of the HOMO with polar solvents. Both **2** and **3** similarly undergo a negative solvatochromism of ca. 25 nm (**Figures 4.10 and 4.14**). Since the charge transfer is generated in the excited state, the solvent dependent emission wavelength is typically more pronounced than the ground state solvent induced shifts. This is indeed the case. This is apparent when taking hexane as a benchmark for **1** where only the localized state is generated and not the charge transfer state. The emission of **1** shifts bathochromically with increasing solvent polarity upwards of 180 nm in the solvents investigated. The solvent perturbation on the spectroscopic properties is further evident with the Stokes shift, which is upwards of 9600 cm^{-1}. Similarly, both **2** and **3** are solvatochromic with Stokes shifts upwards of 11 000 cm^{-1}. The perceived emission ranges from green in apolar solvents and shifts to the near-infrared region with increasing polarity (inset **Figure 4.2**). The solvatochromic behavior of the three fluorophores is consistent. This aside, the solvent dependent spectral shifts are more pronounced for **1** than they are for **2** and **3**. This implies the charge transfer for **1** is greater than for **2** and **3**. This is owing to the enhanced electron withdrawing character of the nitro group relative to the nitrile and aldehyde substitutions. In contrast, the similar shifts of **2** and **3**, imply their comparable electronic withdrawing character. This is supported by the calculated (vide infra) dipole difference between the ground and excited states. The absolute dipole cannot be accurately calculated owing to experimental-theory correlation errors. However, the relative values within a series can be accurately calculated because of systematic errors, providing the same level of theory and basis sets are used for the calculations. In the case of **1**, its dipole difference between the excited and ground states is 17.6 D. In contrast, the dipole for **2** and **3** is smaller, 16.0 and 15.1 D, respectively. The difference between the excited and ground state dipole moments can be used to rank the strength of the electron withdrawing group. Accordingly, they can be ranked by increasing order according to: **3**, **2**, and **1**.

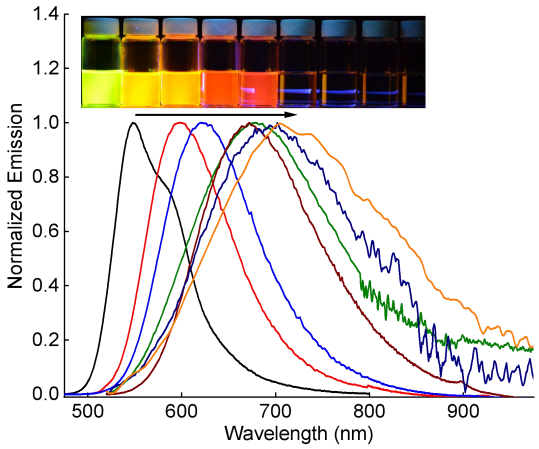

Figure 4.2. Normalized emission spectra of **1** in hexane (black), toluene (red), diethyl ether (blue), dichloromethane (green), ethyl acetate (wine), acetonitrile (navy blue), and DMSO (orange) irradiated at the most red-shifted absorbance. Inset: photograph of vials of **1** irradiated with a handheld UV lamp at 365 nm in hexane, toluene, chloroform, dichloromethane, diethyl ether, ethyl acetate, THF, acetone, acetonitrile, methanol, and DMSO (left to right).

The solvent emission that is of particular interest is dichloromethane and THF. We previously established that the polarity of dichloromethane resembles that of the environment in a working solid-state electrochromic device.[38] Therefore, the emission in dichloromethane can be used to predict the color perceived by the common user when operating the electrofluorochromic device. The emission of the three fluorophores is consistent in dichloromethane with a perceived color of red in the cusp of the visible spectrum. There is no perceived difference between the various fluorophores despite the enhanced solvatochromic behavior of **1**.

The temperature dependent emission was also evaluated to assess the effect of the electron withdrawn group. 2-Methyl-THF was used as the solvent because it forms a transparent glass matrix when frozen, allowing to measure the emission from room temperature to -160 ºC. The emission of the three fluorophores red-shifted with decreasing temperature. In the case of **2** and **3**, the emission red-shifted by 65 nm, whereas the spectral shift of **1** is more pronounced (87 nm; **Figure 4.21 and 4.23**). The observed shifts are consistent with increasing stabilization of the excited state with decreasing temperature. This can arise by planarization of the terminal phenyls with the benzothiadiazole core and ultimately favoring intramolecular charge transfer. The emission intensity also degreases upon lowering the temperature. Not taking the temperature dependent refractive index variation of the solvent into account, the emission of **2** and **3** decrease ca. two-fold at low temperature. The effect is more pronounced with **1**, whose emission decreases four-fold at low temperature. Bond rotations are restricted at low temperatures along with reduced vibrational modes. If these modes are efficient excited state deactivation modes, their suppression should result in fluorescence enhancement at reduced temperatures. Given the opposite effect is observed, deactivation at low temperature is from efficient non-radiative deactivation by coupling of the LUMO and HOMO energy levels (vida infra).

Three key properties that the fluorophores must possess for their use in working combined electrochromic and electrofluorochromic devices is both color changes and emission in the visible spectrum along with appreciable emission yields (Φ_{Fl}). The fluorophore's must also appreciably emit with minimal fluorescence quenching in the solid state. Given the pronounced solvatochromic effect of the fluorophores, their solvent dependent Φ_{Fl} was investigated. This was to ensure that the fluorophores appreciably emitted

under conditions that mimic an operating device. This is of importance because the Φ_{Fl} typically decreases with increasing polar environments because the narrowing of the LUMO-HOMO energy gap increases non-radiative excited state deactivation.[13] As expected, the Φ_{Fl} of **1** is affected by the solvent polarity. The values range from near unity (91%) in apolar hexane, where only the local excited state can form, to essentially being quenched (1%) in methanol. The quenching in polar solvents is consistent with efficient non-radiative deactivation. This is supported by the lifetime measurements. Both **2** and **3** have similar excited state lifetimes in THF, 7.34 and 7.02, respectively (**Figures 4.19 and 4.20**). In contrast, the lifetime of **1** is shorter (4.15 ns). This tracks with its decrease in Φ_{fl}, relative to **2** and **3**. To further compare the lifetimes with the Φ_{fl}, the kinetics of **3** were measured in several solvents. Its longest lifetime is shortened with increasing solvent polarity; 6.15 ns for toluene, 2.71 ns for acetone, and 1.12 ns acetonitrile (**Figure 4.19**). The shorter lifetime is consistent with faster excited state deactivation, and in turn, lower emission yields.

Of interest is the Φ_{Fl} in solvents of marginal polarity such as dichloromethane, chloroform, and THF. This is because they are commonly used solvents for electrochemical measurements, especially spectroelectrofluorescence. Appreciable emission is these solvents is desired for accurately monitoring the electrochemically mediated fluorescence changes. In the case of **2** and **3**, their fluorescence is maintained. In contrast, **3** appreciably fluoresces in only THF. The reduced fluorescence is confirmed both by absolute and relative means and is most likely from solvent-solute interactions involving the nitro group. The fluorophores nonetheless emit in sufficient yields in a solvent that can be used to evaluate their electrochemically mediated fluorescence.

While high Φ_{fl} is an ideal property for fluorophore use in electrofluorescent devices, high values in solution do not directly carry over to the solid-state. This is because conventional fluorophores self-deactivate at high concentrations, especially in thin films. Emission in the latter is a required property from an active layer in electrofluorescent devices. This is possible with fluorophores that undergo aggregation induced emission (AIE).[42] This is the case of most conjugated benzothiadiazoles.[29] The strength of the electron acceptor was expected to affect the AIE behavior the fluorophores, given the effect of the other emission properties. The AIE of both **1** and **3** were assessed in varying volume ratios of THF and acetonitrile and THF water. These solvents were chosen because of their contrasting Φ_{Fl}. In the case of **1** in THF, the Φ_{Fl} decreases eight-fold with increasing water until it is aggregated in 90% water. Similarly, the Φ_{Fl} of **3** in THF is quenched with increasing amounts of acetonitrile. However, its emission is restored to half its original value when aggregated in 90% acetonitrile compared to pristine THF. The Φ_{Fl} of the fluorophores were also evaluated in the solid state by drop casting a concentrated solution onto glass slides. Both **3** and **2** appreciably emit in the solid state. In contrast, the emission of **1** is an order of magnitude less than its counterparts. It is worthy to note that fluorescence yields can be affected by oxygen. This is problematic with the integrating sphere used in this study because the measurements are done under ambient conditions. To avoid oxygen related quenching and to validate whether oxygen indeed affected the emission yields, a sample of **3** was prepared under an oxygen-free environment. This was done by placing it in a polyethylene bag. Afterwards it was evacuated to remove any oxygen and then sealed under vacuum. The wrapping used was impermeable to oxygen, ensuring the measurements were indeed done in the absence of oxygen. Any emission of the plastic wrapping is eliminated from the measurements by measuring a blank glass slide that was prepared under similar vacuum sealed conditions. Moreover, the minimal background emission from the plastic wrapping occurred in the UV region that was outside the spectral window used for the measurements. The vacuum sealed sample is identical to the measurement (±5%) done under ambient conditions, confirming deactivation of the excited state by oxygen is negligible from **3**. Meanwhile, both the AIE and the solid-state emission confirm that the fluorophores can be adjusted by tuning the strength of the their electron withdrawing group. This aside, solid-state emission of **2** and **3** confirm they have ideal properties for their use as active layers in electrofluorochromic devices. In contrast, a device prepared by **1** would not be as performant as its counterparts because of its muted solid-state emission.

The aldehyde of **3** is advantageous because it can further react to modify the fluorophore's properties. For example, it can condense with amines to form an imine. The resulting heteroatomic bond extends the conjugated framework, impacting both the absorption and the emission. The imine bond is also known to efficient deactivate the excited state by combined photoisomerization and electron transfer, resulting in a significant decrease in the emission yield.[43-45] Arylamines are also efficient excited state deactivators by reducing the excited fluorophore.[46] The photoreactivity of **3** was evaluated by quenching it with aniline when excited (**Figure 4.24**). The resulting bimolecular rate constant was diffusionally controlled ($>10^{10}$ $M^{-1}s^{-1}$), confirming **3** is efficiently deactivated by aniline. This illustrates that the conjugated benzothiadiazoles are photoreactive.

Table 8. Photophysical properties of the fluorochromes in various solvents.

	1				**2**				**3**			
Solvent	λ_{abs} (nm) [a]	λ_{em} (nm) [b]	Φ_{fl} (%) [c]	Stoke's shift[d] (cm^{-1})	λ_{abs} (nm) [a]	λ_{em} (nm)[b]	Φ_{fl} (%)[c]	Stoke's shift[d] (cm^{-1})	λ_{abs} (nm) [a]	λ_{em} (nm)[b]	Φ_{fl} (%) [c]	Stoke's shift[d] (cm^{-1})
Hexane	456	548	91	3800	450	542	90	5000	450	540	94	3700
Toluene	455	600	87	5400	451	591	80	5700	452	590	95	5200
Acetone	443	730	0.9[e]	9400	432	732	20	11 000	438	707	17	9000
Diethyl ether	447	625	83	6700	447	608	85	6200	444	606	77	6000
THF	452	678	40	8000	444	658	71	8000	445	654	63	7200
Dichloromethane	457	672	1.5[e]	9000	446	672	65	8100	445	673	63	7600
Chloroform	465	660	3.5 [e]	7100	452	654	70	7200	453	642	74	6500
Acetonitrile	440	700	0.2[e]	10 000	432	732	7	10 000	428	743	4	9900
Ethyl acetate	443	672	44	9600	427	650	65	8500	435	650	60	7600
Methanol	433	660	0.3 0.9[e]	7700	439	696	0.2 [e]	9500	429	710	1	9200
DMSO	455	712	0.1[e]	9000	428	740	4[e]	10 500	443	750	3	9250
Solid state[h]	490	675	6	5750	445	625 (610) [i]	50 (60) [i]	5700	460	640 (638) [j]	54 (54) [j]	6030

[a]Maximum absorbance at longest wavelength. [b]Maximum emission at longest wavelength. [c]Absolute quantum yields measured with an integrating sphere. [d]Conversion from nm to cm^{-1} corrected for λ^2. [e]Quantum yield relative to ruthenium tris(bipyridine) dichloride (Φ_{fl}=2.8% in water).[34, 47] [h] Φ_{fl} measured with an integrating sphere as a thin film on glass slides. [i]From literature as-prepared powder.[22] [j]From literature as thin film.[34]

Electrochromism/Electrofluorochromism

Desired electrochemical properties of the fluorophores are moderately low oxidation potentials and a reversible redox behavior. The latter is to sustain multiple electrochemically induced color switching cycles. Of interest, is the oxidation potential given that triphenylamines are known for their exclusive anodic behavior.[48] The cyclic voltammograms of the fluorophores were measured to evaluate both the oxidation potentials and the reversibility oxidized intermediate. Ferrocene was used as an internal reference for easy comparison of the electrochemical properties and to eliminate any concentration dependent variations in the potential that can occur with the silver wire pseudo-reference. The redox potentials of the three fluorophores are consistent. This is expected given that the oxidation occurs on the triphenylamine. While the anodic behavior is of exclusive interest, the fluorophores could be electrochemically reduced. Only one oxidation process was observed with the scanned electrochemical window (**Figure 4.3**). The oxidation potential for the forward waves of **2** and **1** are 590 and 630 mV vs. Fc/Fc^+, respectively. Their corresponding E_{ox}, taken as the average of the forward and reverse potentials are 530 and 540 mV, respectively. The terminal electron withdrawing groups affect the oxidation only to a minor degree. The slight difference in the oxidation potential between **2** and **1** is due to the stronger electronic accepting capacity of the nitro group, relative to the nitrile substituent. Along with calibrating the redox potential, the number of electrons transferred and the reversibility can be evaluated with equimolar ferrocene. According to the peak current differences between ferrocene and the fluorophores, the anodic process corresponds to a one-electron transfer. Whereas, the similar peak currents for the forward and reverse waves implies electrochemical reversibility under the scanned rates used. The same electrochemical properties were found for **3**, being consistent with those previously reported.[34]

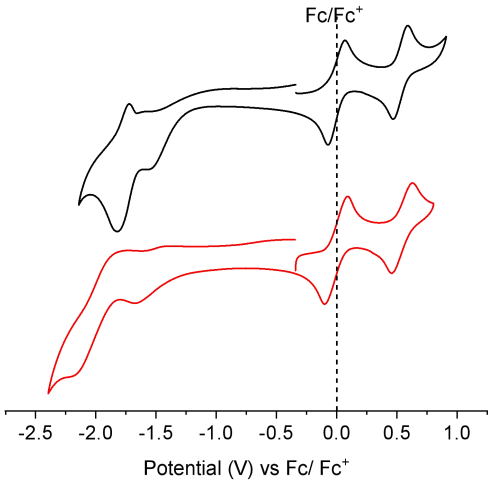

Figure 4.3. Cyclic voltammograms of **2** (black) and **1** (red) in 0.1 $TBAPF_6$ and degassed anhydrous dichloromethane measured at 100 mV/sec vs. the reversible ferrocene/ferrocenium redox couple.

A critical property that the fluorophores must possess for their use as the active layer in electrochromic devices is a change in color with applied potential. This can be evaluated by spectroelectrochemistry. This is the change in absorption with applied potential. The absorption of the neutral fluorophores bleach with applied potential. The absorption in the blue region of the visible spectrum of the neutral is replaced with two new absorptions in the red region of the spectrum. Specifically, **2** exhibits two broad absorptions between 536 and 600 nm along with one at 900 nm. As for **1**, the visible region absorption was narrower, being centered at 604 nm, with the NIR absorption occurring at 865 nm (**Figure 4.4A**). In both cases, the NIR absorption increase with increasing times of applied potential is more intense than the

electrochemically induced change in the visible region. The perceived color for **2** and **1** changes from yellow in the neutral state to green and orange, respectively for the oxidized state. The perceived color of the oxidized is according to the most red-shifted absorption in the visible region. With increasing times of applied potential, the perceived color bleaches, resulting in a visible-to-invisible color change. The fluorophores therefore act as visible switches with detectable on/off colors.

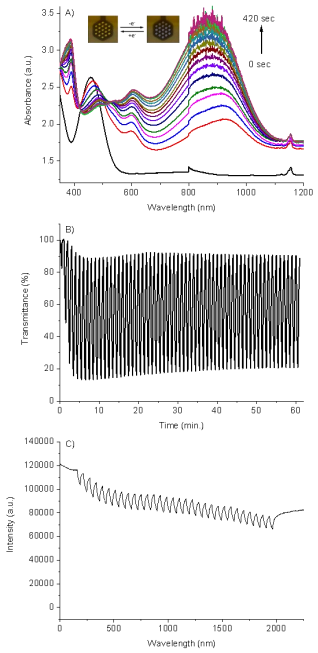

Figure 4.4. A) Change in absorption of **1** with an applied potential of +1.15 V in 0.1 M $TBAPF_6$ in degassed and anhydrous dichloromethane measured at 30 sec. intervals. Inset: photographs of the honeycomb working of **1** in the neutral (left) and oxidized states (right). B) Transmittance % change of **1** in anhydrous and degassed dichloromethane monitored at 917 nm with applied potentials between +1.3 and -0.1 V switched at 30 sec intervals. C) Change in fluorescence intensity of **1** excited at 450 nm and monitored at 690 nm in 0.1 M $TBAPF_6$ in degassed dichloromethane with applied potentials of +1.35 and -0.1 V for 30 s for **1**, respectively.

Theoretical calculations were done to complement the spectroelectrochemical studies and further understand the effect of the withdrawing groups on the electronic transitions. For this, dichloromethane was chosen as a solvent continuum to mimic the spectroelectrochemical conditions. Similar to the dipole moments (vide supra), the absolute electronic transitions cannot be accurately calculated. However, the trend between the series of compounds that are calculated in the similar way can be relatively known.

Subtle differences in the electronic transitions were calculated for the three compounds (**Figure 4.33**). For example, the most red-shifted absorption for the ground state varies by only 9 nm between the three fluorophores. While both **2** and **3** have similar absorptions, **1** is the most red shifted, as expected because of the stronger electron withdrawn substituent. Specifically, the absorption is centered at 404, 413 and 407 nm for **2**, **1**, and **3**, respectively. As expected, the absorption of the radical cations is red-shifted relative to the neutral state. Given the spin for the radical cation is located on the triphenyl amine segment, the orbitals involved in the electronic transition of the fluorophores are concentrated at this

segment. This is confirmed by the natural transition orbital (NTO) calculation that facilitates visualization of the principal HOMO and LUMO energy levels that involved the given electronic absorption. Indeed, the NTO HOMO is located on the triphenyl amine segment and it extends to the benzothiadiazole core (**Figure 4.32**). The orbitals of the LUMO extend slightly out to the other phenyl substituent. Despite this, there is little interplay of the terminal electronic group in the orbitals. This aside, the absorption of the radical cation of **3** is 21 nm red-shifted compared to **1** and **2**. The electronic transition of the radical cation for **2**, **1**, and **3** is 764, 762, and 783, respectively. For the dications, both the HOMO and LUMO orbitals involve the terminal electron withdrawn group to a greater degree for the dication than with the radical cation. As a result, absorption of the dication, that can be formed by the two-electron oxidation of the compounds, is red-shifted compared to the radical cation. In fact, the calculated electronic absorption occurs in the NIR for the three fluorophores at ca. 835 nm. While there is little difference in the absorptions of the similar states for the three fluorophores, the relative difference between their respective neutral and radical cation states are unique. The difference increases according to the order of **3**, **1**, and **2**. Of noteworthy is the epsilon that was calculated for the three states of fluorophores. The epsilon of the radical cation for the three fluorophores is consistently half of the corresponding epsilon for the neutral state. In contrast, the dication is four-fold more intense than the radical cation. Correlating these findings with the spectroelectrochemical experimental results, the electrochemically induced red-shifted absorption in the visible is consistent with the radical cation, while the more intense NIR absorption can be attributed to the dication. The formation of two distinct oxidized species can result from disproportionation of a singly oxidized species with the neutral state. Both the calculations and the electrochemical data confirm that significant spectral changes nonetheless occur upon electrochemical oxidization. The absorptions of the electrochemically oxidized fluorophores in the visible and NIR regions that are significantly different than the neutral states illustrate the usefulness of the fluorophores as electrochromophores that can be tracked by common users.

The spectroelectrochemistry confirms that the fluorophores are both electroactive and they change perceived colors with applied potential. This points towards them as being suitable for use as electroactive layers in electrochromic devices. However, their true performance under device-like conditions cannot be derived from the spectroelectrochemical measurements. Insight into the colorfast of the fluorophores, notably their capacity to repeatedly switch colors over extended periods of times is possible by monitoring the transmittance % at a given wavelength with switching the applied potentials between the neutral and oxidized states. The NIR absorption of 917 nm was chosen to examine the duty cycle of the materials. Both **2** and **1** can switch between their neutral and oxidized states for up to 2 hours at 30 sec. switching intervals (**Figure 4.4B**). During these periods, the transmittance % of the two states is regenerated. The materials can therefore sustain multiple switching between the two states, confirming their suitability as electroactive layers in operating electrochromic devices.

The modulation of the fluorescence intensity with applied potential was also examined. This was to assess their suitability as dual role active materials; capable of both electrochemically mediated color switching and fluorescence intensity quenching. This was done by monitoring the change in fluorescence intensity with potential applied in a solution of dichloromethane with the corresponding electrolyte. Dichloromethane was the solvent of choice because it can be made conductive for the electrochemical measurements with the additional of a supporting electrolyte. It was also to mimic the conditions that were used for the spectroelectrochemical and the duty cycle measurements. The emission spectra were first measured to see the effect of the supporting electrolyte on the emission relative to pristine dichloromethane. The measured emission maximum is 670 nm for **2** and 690 nm for both **1** and **3**. Only in the cases of **1** and **3** is the emission red shifted by 20 nm, relative to pristine dichloromethane. This implies that the electrolytic solution perceived by these two fluorophores is more polar than pristine dichloromethane. The shifts further demonstrate that the type of electron withdrawn group that is conjugated with the benzothiadiazole senses its environment differently and it affects the emission. Although the fluorescence of **1** is significantly less than **2** in this solvent, it nonetheless fluoresces

sufficiently for its intensity variation with applied potential to be measured. The electrochemically mediated change in fluorescence is evident in **Figure 4.4C** for **1** with its emission being reduced when generating the oxidized state.

The fluorescence is regenerated when reducing the oxidized state to the neutral state. The emission reduction upon oxidation is a result of the charged stated deactivating the intrinsic fluorescence of the neutral state with the concomitant red-shifted absorption of oxidized state. The latter decreases the absorption of the monochromatic wavelength that excites the neutral state. The fluorescence initially decreases by 4, 13, and 50% for **2**, **1**, and **3**, respectively. Although the absolute emission intensity decreases during the cycling period, the difference between the emissive *on* and *off* states for the three fluorophores is consistent. The residual emission with applied positive potential implies that neutral state does not completely deplete upon oxidation. This is in part owing to a mismatch between the surface area of the spiral counter electrode surface and the planar ITO glass working electrode. This is exacerbated by diffusional effects in the cuvette. The neutral fluorophore can continuously diffuse to the working electrode during with the measurements to replenish the oxidized fluorophore, resulting in no perceived reduction in emission intensity. This effect can be mitigated by either reducing the volume of the cell such as with a honeycomb-type electrode or in a working device. This aside, the intrinsic emission of the fluorophores can be reversibly modulated electrochemically.

Working devices were fabricating to further investigate the fluorescence intensity modulation with applied potential. The emission maximum of **2** and **1** in the devices is comparable to that in pristine dichloromethane. Compared to their emission in as cast films, the emission in devices is shifted by 15 nm. Surprisingly, the emission of **1** is blue shifted, whereas that of **2** is red shifted compared to the as-cast films on glass slides. This further illustrates the unique sensing capacities of the different electron withdrawing groups towards their environment. The absolute emission yields of the device were benchmarked to compare the effect of the different components on deactivating the excited state. In the case of **1**, there is little effect as the Φ_{Fl} is consistent with that in pristine dichloromethane (Φ_{Fl} =2%). In contrast, the emission of **2** decreases to 16%, compared to pristine dichloromethane. Similar to what was observed in the half-fluorochromic device, the emission intensity of the fluorophores is reversible in the operating device with switching the applied potentials between the neutral and oxidized. The devices were operated for 30 minutes, afterwards the Φ_{fl} were remeasured. For **1**, the value before and after switching is unchanged (**Figure 4.5**), whereas it decreases to 12% for **2**. The working devices demonstrate that the intrinsic fluorophore fluorescence can be preserved when they are used as electroactive layers. Their fluorescence intensity can also be reversibly switched electrochemically. The overall decrease of the fluorescence intensity with operating time is most likely a result of irreversible migration of the fluorophore towards the cathode, resulting in memory effects. This can potentially be addressed by immobilizing the fluorophore on the anode and by using a complementary cathodically active film as a charge storage layer.

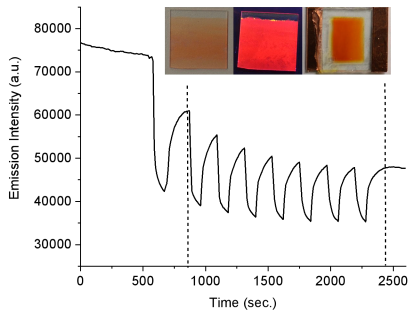

Figure 4.5. Change in emission intensity of the operating electrofluorochromic device prepared with **1** as

the active layer with applied potential switching between + 2.0 V for 90 s and -1.5 V for 130 s in the region delimited by the dashed lines. Excited at 470 nm and monitored 645 nm. Inset: photographs of **1** spray coated on a glass slide and irradiated under ambient light (left) and a UV handheld lamp (middle) along with a fully assembled electrofluorochromic device prepared with **1** as the active layer (right).

4.3 Conclusion

It was confirmed that the strength of the electron withdrawing group has pronounced effects on the spectroscopic properties. This provides the means to tune the emission wavelength with solvent polarity. Ultimately the sensor-like properties are ideal for reporting the environment to which the fluorophore are exposed. This is beneficial for evaluating the *in operando* environment of working electrochromic devices. Subtitle changes in the withdrawing group impact significantly the emission yield, especially in solvents commonly that are used for electrochemical measurements. Nonetheless, the fluorophores underwent colors changes in the visible spectrum, with their absorption shifting from the blue region of the visible spectrum to the NIR region with applied potential. Their intrinsic emission intensity can also be modulated with applied potential. Not only does the benzothiadiazole fluorophores emit appreciably in the solid-state, but their emission intensity can be electrochemically mediated in functioning devices. The device performance, specifically the consistent off/on emission intensity, can potentially be improved by immobilizing the chromophore on the anode. The tuneability of the color and both the emission wavelength and solid-state intensity of benzothiadiazoles makes them ideal active dual-mode materials for use in electrofluorochromic devices. Ultimately, devices emitting across the visible spectrum that are capable of electrochemically mediated emission intensity modulation are possible by tuning the functional group that is conjugated with the benzothidiazole core and the triphenylamine terminus.

4.4 Experimental

Synthesis

***N*,*N*-diphenyl-4-(4,4,5,5-tetramethyl-1,3,2-dioxaborolan-2-yl)aniline** (**5**).[49] Potassium acetate (906 mg, 9.24 mmol, 3 eq) and diborane bis (pinacolato) (939 mg, 3.7 mmol, 1.2 eq) were added to a solution of 4-bromo-*N*,*N*-diphenylaniline (1 g, 3.08 mmol) in dioxane (20 mL). The solution was then bubbled under nitrogen for 20 minutes. Next, [1,1'-bis (diphenylphosphino) ferrocene] dichloropalladium (II) (76 mg, 0.093 mmol, 0.03 eq) was added and the solution was refluxed for 24 hrs. After cooling, the mixture was filtered and then diluted with ethyl acetate. The organic phases were washed with water, dried with magnesium sulfate and then concentrated. The crude product was purified by chromatography column on silica (hexane / dichloromethane) with a gradient from 10 to 40% dichloromethane to afford the product as a white solid (937 mg, 82%). ^{1}H-NMR ($CDCl_3$, 400 MHz) δ ppm = 7.7 (2H, d), 7.28 (4H, m), 7.14 (4H, m), 7.07 (4H, m), 1.36 (12H, s). ^{13}C-NMR ($CDCl_3$, 100 MHz) δ ppm= 150.4, 147.2, 135.7, 129.1, 124.8, 123.2, 121.6, 83.3, 24.7. ESI-MS [M+H$^+$]: m/z calcd for $C_{24}H_{26}BNO_2$ 371.28, found 371.21.

4-(7-Bromobenzo[c][1,2,5]thiadiazol-4-yl)-*N*,*N*-diphenylaniline (**4**).[50] Sodium carbonate (2.79 g, 26.36 mmol, 4.9 eq), 4,7-dibromobenzo [c]-1,2,5-thiadiazole (1.58 g, 38 mmol, 1 eq), and tetra-*n*-butylammonium bromide (5 mg, 0.015 mmol) were added to a solution of **4** (2 g, 5.38 mmol) in a toluene:water (30/10 mL). Three cycles of freeze-pump-thaw were then done with the solution. Next, tetrakis(triphenylphosphine) palladium (621 mg, 0.538 mmol, 0.1 eq) was added and the mixture was heated at 90°C overnight. After cooling, the mixture was diluted with dichloromethane. The organic phases were washed with water, dried over magnesium sulfate, and then concentrated. The crude product was purified by chromatographic column of silica (hexane/ether, 100:0 to 98:2) to give the product as an

orange solid (1.25 g, 51%). ^{1}H NMR ($CDCl_3$, 400 MHz) δ ppm = 7.9 (1H, d), 7.8 (2H, m), 7.55 (1H, d), 7.3 (4H, dd), 7.19 (6H, m), 7.08 (2H, t). ^{13}C NMR ($CDCl_3$, 100 MHz) ppm = 154.1, 153.3, 148.6, 147.5, 133.7, 132.5, 130.1, 130, 129.6, 127.5, 125.2, 123.6, 122.7, 112.3. ESI-MS [M+H$^+$]: m/z calcd for $C_{24}H_{16}BrN_3S$ 458.37, found 458.1.

4-(7-(4-Nitrophenyl)benzo[c][1,2,5]thiadiazol-4-yl)-N,N-diphenylaniline (**1**). Sodium carbonate (339 mg, 21 mmol, 4.9 eq), 4-nitrophenylboronic acid (109 mg, 0.654 mmol, 1 eq), tetra-*n*-butylammonium bromide (5 mg, 0.015 mmol) were added to a solution of **5** (300 mg, 0.654 mmol) in toluene:water (10:3 mL) in a microwave tube. The solution was purged with nitrogen for 20 minutes. Then, tetrakis (triphenylphosphine) palladium (151 mg, 0.065 mmol, 0.1 eq) was added to the solution. The vial was next heated in a microwave at 120ºC for 3 hours. Upon cooling, the mixture was diluted with dichloromethane. The organic phase was washed with water and then extracted. It was dried over magnesium sulfate and then concentrated. The crude product was purified over silica (hexane/dichloromethane; 60:40) to afford the product as a violet solid (272 mg, 83%). ^{1}H NMR ($CDCl_3$, 400 MHz) δ ppm = 8.39 (2H, d), 8.18 (2H, d), 7.88-7.8 (4H, ddd), 7.31 (4H, t), 7.21 (6H, m), 7.09 (2H, t). ^{13}C NMR ($CDCl_3$, 100 MHz) δ ppm = 154.15, 153.8, 148.65, 147.5, 147.4, 143,9, 138.35, 134.8, 130.2, 130.0, 129.9, 129.55, 129.4, 128.45, 127.0, 125.2, 123.7, 122.6. ESI-MS [M+H$^+$]: m/z calcd for $C_{30}H_{20}N_4O_2S$ 500.57, found 501.2.

4-(7-(4-(Diphenylamino)phenyl)benzo[c][1,2,5]thiadiazol-4-yl)benzonitrile (**2**).[22] Similar to **1** with sodium carbonate (288 mg, 72 mmol, 4.9 eq), 4-cyanophenylboronic acid (81 mg, 0.556 mmol, 1 eq), tetra-*n*-butylammonium bromide (5 mg, 0.015 mmol), **5** (255 mg, 0.556 mmol), and tetrakis(triphenylphosphine) palladium (66.3 mg, 0.055 mmol, 0.1 eq). The product was purified over silica (hexane/dichloromethane; 50:50) to afford an orange solid (190 mg, 71%). ^{1}H NMR ($CDCl_3$, 400 MHz) δ ppm = 8.12 (2H, d), 7.89 (2H, d), 7.82 (4H, m), 7.3 (4H, dd), 7.21 (6H, m), 7.09 (2H, t). ^{13}C NMR ($CDCl_3$, 100 MHz) δ ppm = 154.1, 153.8, 148.5, 147.5, 142, 134.5, 132.5, 130.35, 130.3, 130.15, 129.9, 129.55, 129.1, 127.0, 125.2, 125.7, 122.7, 119.0, 111.8. ESI-MS [M+H$^+$]: m/z calcd for $C_{31}H_{20}N_4S$ 480.58, found 481.3.

4-(7-(4-Diphenylamino)phenyl)benzo[c][1,2,5]thiadiazol-4-yl)benzaldehyde (**3**).[51] Similar to **1** with sodium carbonate (339 mg, 3, 21 mmol, 4.9 eq), tetra-*n*-butylammonium bromide (5 mg, 0.015 mmol), 4-formylphenylboronic acid (98 mg, 0.654 mmol, 1 eq), **5** (300 mg, 0.654 mmol), and tetrakis (triphenylphosphine) palladium (151 mg, 0.065 mmol, 0.1 eq). The product was purified over silica (hexane/dichloromethane; 40: 60%) to give a red solid (170 mg, 53%). ^{1}H NMR ($CDCl_3$, 400MHz) δ ppm = 10.11 (1H, s), 8.17 (2H, d), 8.05 (2H, d), 7.90 (2H, d), 7.85 (1H, d), 7.78 (1H, d), 7.3 (4H, m), 7.21 (6H, m), 7.09 (2H, t). ^{13}C NMR ($CDCl_3$, 100 MHz) δ ppm = 191.9, 154.1, 153.9, 148.5, 147.5, 143,5, 135.8, 134.2, 131.0, 130.4, 130.1, 130.0, 129.9, 129.5, 129.1, 127.1, 125.2, 123.6, 122.7. ESI-MS [M+H$^+$]: m/z calcd for $C_{31}H_{21}N_3OS$ 483.58, found 484.3.

The spectroscopic, fluorescence, emission yields, spectroelectrochemical, and electrochemical measurements were done as previously reported.[38, 52] For the solid-state emission, the given sample was coated on a either a glass microscope coverslip or a rectangular 60 µL well quartz slide with a matching straight quartz plate. The emission yields were measured with an integrating sphere using either a native coverslip or an empty rectangular 60 µL well quartz slide as the reference substrate for measuring the scattering according to the direct and indirect methods.[53] For weakly emitting samples, the emission spectra were mathematically smoothed for esthetic purposes only and for locating the maximum. The quenching measurements were done in nitrogen saturated toluene of **3** to which was added given amounts of a concentrated solution of aniline in toluene. Lifetime measurements were done with a TCSPC system using a 405 nm ps-LED.

The electrofluorochromic measurements were done in 10 x 10 mm quartz cuvette with 7 x 50 mm ITO glass slide as the working electrode and a spiral platinum wire as the counter electrode. A special insert was used to maintain a distance of ca. 5 mm. between the cell wall and the ITO electrode. The cuvette was placed at 45^{o} to the incident light in the fluorometer to measure the emission. The electrochromic/electrofluorochromic device was prepared by spray coating the given fluorophore on a square 25 x 25 mm ITO coated glass slide. A stock solution of PMMA (MW~120 000 g/mol) was dissolved in acetonitrile (10 mL) along with the lithium perchlorate (300 mg, 2.82 mmol).[54] The solution was stirred overnight, afterwards, it was spread over a square ITO glass slide. The device was sealed with epoxy glue around the edges after pressing the slides were together. Contact of the glue with the active layer was avoided by preventing its diffusing into the device. Copper taper was adhered to each electrode to connect the device to a potentiostat via banana clips.

Theoretical calculations were done with Gaussian Rev. 16B.01[55] using the CAM-DFT[56] method along with the 6-311G+(d,p) basis set. Dichloromethane was used as the solvent continuum (IEFPCM) for all the calculations. This level of theory and the basis set were used to calculate the various states according by corrected linear response method.[57] In short, the ground state was first optimized, followed by the non equilibrated TD-DFT of the first 5 excited states to give the electronic absorption transitions. Next, the equilibrated TD-DFT of the first 5 excited states were calculated, followed by optimizing the geometry of the excited the state. For the electronic transitions, the TD-DFT method was used without the nonequilibrium keyword. The principal HOMO and LUMO involved in the electronic transitions were compiled using the Natural Transition Orbital calculation of the lowest energy transition. The NTOs were used for visual purposes.

Acknowledgements
The Natural Sciences and Engineering Council Canada and the Canada Foundation for Innovation are acknowledged for operating and infrastructure grants that enabled this work. CY expresses thanks to MITACS, UdeM, and J. & M. Lemay for a Globalink undergraduate and graduate awards that supported this work. CC and LW thank the French regional governments for travel awards to undertake the presented research. Sincere thanks are expressed to Drs. S. Simard and D. Chartrand for assistance with the X-ray crystallography of **3**. The former CSACS is also acknowledged for access to equipment. Compute Canada (www.computecanada.ca) and their partners, Compute Ontario (computeontario.ca) and WestGrid (www.westgrid.ca), are also thanked for access to both computational resources and software for theoretical calculations.

References

1. Chua, M. H.; Tang, T.; Ong, K. H.; Neo, W. T.; Xu, J. W., Introduction to Electrochromism. In *Electrochromic Smart Materials: Fabrication and Applications* Xu, J. W.; Chua, M. H.; Shah, K. W., Eds. **2019**; Chapter 1.
2. Granqvist, C. G., Electrochromics for smart windows: Oxide-based thin films and devices. *Thin Solid Films* **2014**, *564*, 1-38.
3. Warner, J. L. R.; M.S.Selkowitz, S. E.; Arasteh, D. K., Utility and Economic Benefits of Electrochromic Smart Windows. Lawrence Berkeley National Laboratory: **1992**.
4. Ma, D.; Wang, J., Inorganic electrochromic materials based on tungsten oxide and nickel oxide nanostructures. *Sci. China Chem.* **2017**, *60* (1), 54-62.
5. Cong, S.; Geng, F.; Zhao, Z., Tungsten Oxide Materials for Optoelectronic Applications. *Adv. Mater.* **2016**, *28* (47), 10518-10528.
6. Bange, K., Colouration of tungsten oxide films: A model for optically active coatings. *Sol. Energy Mater. Sol. Cells* **1999**, *58* (1), 1-131.
7. Dyer, A. L.; Thompson, E. J.; Reynolds, J. R., Completing the Color Palette with Spray-Processable Polymer Electrochromics. *ACS Appl. Mater. Interfaces* **2011**, *3* (6), 1787-1795.
8. Kerszulis, J. A.; Johnson, K. E.; Kuepfert, M.; Khoshabo, D.; Dyer, A. L.; Reynolds, J. R., Tuning the painter's palette: subtle steric effects on spectra and colour in conjugated electrochromic polymers. *J. Mater. Chem. C* **2015**, *3* (13), 3211-3218.
9. Beaujuge, P. M.; Ellinger, S.; Reynolds, J. R., The donor-acceptor approach allows a black-to-transmissive switching polymeric electrochrome. *Nat. Mater.* **2008**, *7* (10), 795-799.
10. Christiansen, D. T.; Ohtani, S.; Chujo, Y.; Tomlinson, A. L.; Reynolds, J. R., All Donor Electrochromic Polymers Tunable across the Visible Spectrum via Random Copolymerization. *Chem. Mater.* **2019**, *31* (17), 6841-6849.
11. Bura, T.; Beaupre, S.; Legare, M.-A.; Quinn, J.; Rochette, E.; Blaskovits, J. T.; Fontaine, F.-G.; Pron, A.; Li, Y.; Leclerc, M., Direct heteroarylation polymerization: guidelines for defect-free conjugated polymers. *Chem. Sci.* **2017**, *8* (5), 3913-3925.
12. Yu, S.; Liu, F.; Yu, J.; Zhang, S.; Cabanetos, C.; Gao, Y.; Huang, W., Eco-friendly direct (hetero)-arylation polymerization: scope and limitation. *J. Mater. Chem. C* **2017**, *5* (1), 29-40.
13. Jortner, J., Radiationless transitions. *Pure Appl. Chem.* **1971**, *27* (3), 389-419.
14. Nalwa, H. S., *Advanced Functional Molecules and Polymers: Electronic and Photonic Properties*. CRC Press: **2001**; Vol. 3.
15. Audebert, P.; Miomandre, F., Electrofluorochromism: From Molecular Systems to Set-Up and Display. *Chem. Sci.* **2013**, *4* (2), 575-584.
16. Wang, J.-L.; Xiao, Q.; Pei, J., Benzothiadiazole-Based D−π-A−π-D Organic Dyes with Tunable Band Gap: Synthesis and Photophysical Properties. *Org. Lett.* **2010**, *12* (18), 4164-4167.
17. Barnsley, J. E.; Shillito, G. E.; Mapley, J. I.; Larsen, C. B.; Lucas, N. T.; Gordon, K. C., Walking the Emission Tightrope: Spectral and Computational Analysis of Some Dual-Emitting Benzothiadiazole Donor–Acceptor Dyes. *J. Phys. Chem. A* **2018**, *122* (40), 7991-8006.
18. Misra, R.; Gautam, P., Tuning of the HOMO–LUMO gap of donor-substituted symmetrical and unsymmetrical benzothiadiazoles. *Org. Biomol. Chem.* **2014**, *12* (29), 5448-5457.
19. Pathak, A.; Tomer, T.; Thomas, K. J.; Fan, M.-S.; Ho, K.-C., Fine tuning the absorption and photovoltaic properties of benzothiadiazole dyes by donor-acceptor interaction alternation via methyl position. *Electrochim. Acta* **2019**, *304*, 1-10.
20. Wang, X.; Wang, K.; Wang, M., Synthesis of conjugated polymers via an exclusive direct-arylation coupling reaction: a facile and straightforward way to synthesize thiophene-flanked benzothiadiazole derivatives and their copolymers. *Polym. Chem.* **2015**, *6* (10), 1846-1855.

21. Zhang, J.; Parker, T. C.; Chen, W.; Williams, L.; Khrustalev, V. N.; Jucov, E. V.; Barlow, S.; Timofeeva, T. V.; Marder, S. R., C–H-Activated Direct Arylation of Strong Benzothiadiazole and Quinoxaline-Based Electron Acceptors. *J. Org. Chem.* **2015**.
22. Ishi-i, T.; Tanaka, H.; Youfu, R.; Aizawa, N.; Yasuda, T.; Kato, S.-i.; Matsumoto, T., Mechanochromic fluorescence based on a combination of acceptor and bulky donor moieties: tuning emission color and regulating emission change direction. *New J. Chem.* **2019**, *43* (13), 4998-5010.
23. Peng, Z.; Wang, Z.; Huang, Z.; Liu, S.; Lu, P.; Wang, Y., Expression of anti-Kasha's emission from amino benzothiadiazole and its utilization for fluorescent chemosensors and organic light emitting materials. *J. Mater. Chem. C* **2018**, *6* (29), 7864-7873.
24. Balakrishnan, K.; Hsu, W.-L.; Mataka, S.; Pau, S., Tunable light emission from co-assembled structures of benzothiadiazole molecules. *Chem. Commun.* **2014**, *50* (42), 5600-5603.
25. Wałęsa-Chorab, M.; Tremblay, M.-H.; Ettaoussi, M.; Skene, W. G., Photophysical, Electrochemical, and Spectroelectrochemical Investigation of Electronic *Push–Pull* Benzothiadiazole Fluorophores. *Pure Appl. Chem.* **2016**, *87* (7), 649-661.
26. Pazini, A.; Maqueira, L.; Santos, F. D.; Barreto, A. R. J.; Carvalho, R. D.; Valente, F. M.; Back, D.; Aucelio, R. Q.; Cremona, M.; Rodembusch, F. S.; Limberger, J., Designing highly luminescent aryloxy-benzothiadiazole derivatives with aggregation-induced enhanced emission. *Dyes Pigm.* **2020**, *178*, 108377.
27. Neto, B. A. D.; Carvalho, P. H. P. R.; Correa, J. R., Benzothiadiazole Derivatives as Fluorescence Imaging Probes: Beyond Classical Scaffolds. *Acc. Chem. Res.* **2015**, *48* (6), 1560-1569.
28. Fell, V. H. K.; Findlay, N. J.; Breig, B.; Forbes, C.; Inigo, A. R.; Cameron, J.; Kanibolotsky, A. L.; Skabara, P. J., Effect of end group functionalisation of small molecules featuring the fluorene–thiophene–benzothiadiazole motif as emitters in solution-processed red and orange organic light-emitting diodes. *J. Mater. Chem. C* **2019**, *7* (13), 3934-3944.
29. Yang, S.-Y.; Zhang, Y.-L.; Khan, A.; Yu, Y.-J.; Kumar, S.; Jiang, Z.-Q.; Liao, L.-S., Nondoped organic light-emitting diodes with low efficiency roll-off: the combination of aggregation-induced emission, hybridized local and charge-transfer state as well as high photoluminescence efficiency. *J. Mater. Chem. C* **2020**, *8* (9), 3079-3087.
30. Wu, W.; Yang, Y.; Yang, Y.; Yang, Y.; Zhang, K.; Guo, L.; Ge, H.; Chen, X.; Liu, J.; Feng, H., Molecular Engineering of an Organic NIR-II Fluorophore with Aggregation-Induced Emission Characteristics for In Vivo Imaging. *Small* **2019**, *15* (20), 1805549.
31. Li, Z.; Qin, W.; Wu, J.; Yang, Z.; Chi, Z.; Liang, G., Bright electrochemiluminescent films of efficient aggregation-induced emission luminogens for sensitive detection of dopamine. *Mater. Chem. Front.* **2019**, *3* (10), 2051-2057.
32. Mamada, M.; Komatsu, R.; Adachi, C., F8BT Oligomers for Organic Solid-State Lasers. *ACS Appl. Mater. Interfaces* **2020**.
33. Li, Y.; Wang, W.; Zhuang, Z.; Wang, Z.; Lin, G.; Shen, P.; Chen, S.; Zhao, Z.; Tang, B. Z., Efficient red AIEgens based on tetraphenylethene: synthesis, structure, photoluminescence and electroluminescence. *J. Mater. Chem. C* **2018**, *6* (22), 5900-5907.
34. Chen, X.; Yang, Z.; Li, W.; Mao, Z.; Zhao, J.; Zhang, Y.; Wu, Y.-C.; Jiao, S.; Liu, Y.; Chi, Z., Nondoped Red Fluorophores with Hybridized Local and Charge-Transfer State for High-Performance Fluorescent White Organic Light-Emitting Diodes. *ACS Appl. Mater. Interfaces* **2019**, *11* (42), 39026-39034.
35. Justin Thomas, K. R.; Lin, J. T.; Velusamy, M.; Tao, Y.-T.; Chuen, C.-H., Color Tuning in Benzo[1,2,5]thiadiazole-Based Small Molecules by Amino Conjugation/Deconjugation: Bright Red-Light-Emitting Diodes. *Adv. Funct. Mater.* **2004**, *14* (1), 83-90.
36. Pathak, A.; Justin Thomas, K. R.; Singh, M.; Jou, J.-H., Fine-Tuning of Photophysical and Electroluminescence Properties of Benzothiadiazole-Based Emitters by Methyl Substitution. *J. Org. Chem.* **2017**, *82* (21), 11512-11523.
37. Wałęsa-Chorab, M.; Skene, W. G., Visible-to-NIR Electrochromic Device Prepared from a Thermally Polymerizable Electroactive Organic Monomer. *ACS Appl. Mater. Interfaces* **2017**, *9* (25), 21524-21531.

38. Yao, C.; Frémont, M.; Skene, W. G., Electrochromic and Electrofluorochromic Dual Role of a Red Emissive Fluorophore *submitted* **2020**.
39. Eichstaedt, K.; Wasilewska, A.; Wicher, B.; Gdaniec, M.; Połoński, T., Supramolecular Synthesis Based on a Combination of Se···N Secondary Bonding Interactions with Hydrogen and Halogen Bonds. *Cryst. Growth Des.* **2016**, *16* (3), 1282-1293.
40. Biot, N.; Bonifazi, D., Chalcogen-bond driven molecular recognition at work. *Coord. Chem. Rev.* **2020**, *413*, 213243.
41. Ams, M. R.; Trapp, N.; Schwab, A.; Milić, J. V.; Diederich, F., Chalcogen Bonding "2S–2N Squares" versus Competing Interactions: Exploring the Recognition Properties of Sulfur. *Chem. Eur. J.* **2019**, *25* (1), 323-333.
42. Ji, Q.; Chao, C.; Dan, D.; Zhong, T. B., Aggregation-Induced Emission Luminogens: Union Is Strength, Gathering Illuminates Healthcare. *Adv. Healthcare Mater.* **2018**, *0* (0), 1800477.
43. Fischer, E.; Frei, Y., Photoisomerization Equilibria Involving the C[Double Bond]N Double Bond. *J. Chem. Phys.* **1957**, *27* (3), 808-809.
44. Ko, K. C.; Wu, J.-S.; Kim, H. J.; Kwon, P. S.; Kim, J. W.; Bartsch, R. A.; Lee, J. Y.; Kim, J. S., Rationally designed fluorescence 'turn-on' sensor for Cu2+. *Chem. Commun.* **2011**, *47* (11), 3165-3167.
45. Shyamal, M.; Mazumdar, P.; Maity, S.; Sahoo, G. P.; Salgado-Morán, G.; Misra, A., Pyrene Scaffold as Real-Time Fluorescent Turn-on Chemosensor for Selective Detection of Trace-Level Al(III) and Its Aggregation-Induced Emission Enhancement. *J. Phys. Chem. A* **2016**, *120* (2), 210-220.
46. Ghosh, T.; Chatterjee, S.; Prasad, E., Photoinduced Electron Transfer from Various Aniline Derivatives to Graphene Quantum Dots. *J. Phys. Chem. A* **2015**, *119* (49), 11783-11790.
47. Katsumi, N., Synthesis, Luminescence Quantum Yields, and Lifetimes of Trischelated Ruthenium(II) Mixed-ligand Complexes Including 3,3′-Dimethyl-2,2′-bipyridyl. *Bull. Chem. Soc. Jpn.* **1982**, *55* (9), 2697-2705.
48. Yen, H.-J.; Liou, G.-S., Recent advances in triphenylamine-based electrochromic derivatives and polymers. *Polym. Chem.* **2018**, *9* (22), 3001-3018.
49. Liang, A.; Wang, Y.; Liu, Y.; Tan, H.; Cao, Y.; Li, L.; Li, X.; Ma, W.; Zhu, M.; Zhu, W., Synthesis, Photophysical and Electrochemical Characterization of the Heteroleptic Iridium Complexes with Modified Ancillary Ligand by Carrier-transporting Groups. *Chin. J. Chem* . **2010**, *28* (12), 2455-2462.
50. Dutta, P.; Yang, W.; Eom, S. H.; Lee, W.-H.; Kang, I. N.; Lee, S.-H. J. C. C., Development of naphtho [1, 2-b: 5, 6-b′] dithiophene based novel small molecules for efficient bulk-heterojunction organic solar cells. *Chem. Commun.* **2012**, *48* (4), 573-575.
51. Sandanayaka, A. S.; Matsukawa, K.; Ishi-i, T.; Mataka, S.; Araki, Y.; Ito, O. J. T. J. o. P. C. B., Photoinduced charge separation and charge recombination in [60] fullerene-(benzothiadiazole-triphenylamine) based dyad in polar solvents. *J. Phys. Chem. B* **2004**, *108* (52), 19995-20004.
52. Wałęsa-Chorab, M.; Yao, C.; Tuner, G.; Skene, W. G., Electrochemical and Solvent Mediated Visible-to-Near Infrared Spectroscopic Switching of Benzoselenodiazole Fluorophores. *Chemistry - A European Journal* **2019**, *submitted*.
53. Leyre, S.; Coutino-Gonzalez, E.; Joos, J. J.; Ryckaert, J.; Meuret, Y.; Poelman, D.; Smet, P. F.; Durinck, G.; Hofkens, J.; Deconinck, G.; Hanselaer, P., Absolute determination of photoluminescence quantum efficiency using an integrating sphere setup. *Rev. Sci. Instrum.* **2014**, *85* (12), 123115-1 123115-9.
54. Wu, J.-H.; Liou, G.-S., High-Performance Electrofluorochromic Devices Based on Electrochromism and Photoluminescence-Active Novel Poly(4-Cyanotriphenylamine). *Adv. Funct. Mater.* **2014**, *24* (41), 6422-6429.
55. Frisch, M. J.; Trucks, G. W.; Schlegel, H. B.; Scuseria, G. E.; Robb, M. A.; Cheeseman, J. R.; Scalmani, G.; Barone, V.; Petersson, G. A.; Nakatsuji, H.; X. Li, M. C.; Marenich, A. V.; Bloino, J.; Janesko, B. G.; Gomperts, R.; Mennucci, B.; Hratchian, H. P.; Ortiz, J. V.; Izmaylov, A. F.; Sonnenberg, J. L.; Williams-Young, D.; Ding, F.; Lipparini, F.; Egidi, F.; Goings, J.; Peng, B.; Petrone, A.; Henderson, T.; Ranasinghe, D.; Zakrzewski, V. G.; Gao, J.; Rega, N.; Zheng, G.; Liang, W.; Hada, M.; Ehara, M.; Toyota,

K.; Fukuda, R.; Hasegawa, J.; Ishida, M.; Nakajima, T.; Honda, Y.; Kitao, O.; Nakai, H.; Vreven, T.; Throssell, K.; J. A. Montgomery, J.; Peralta, J. E.; Ogliaro, F.; Bearpark, M. J.; Heyd, J. J.; Brothers, E. N.; Kudin, K. N.; Staroverov, V. N.; Keith, T. A.; Kobayashi, R.; Normand, J.; Raghavachari, K.; Rendell, A. P.; Burant, J. C.; Iyengar, S. S.; Tomasi, J.; Cossi, M.; Millam, J. M.; Klene, M.; Adamo, C.; Cammi, R.; Ochterski, J. W.; Martin, R. L.; Morokuma, K.; Farkas, O.; Foresman, J. B.; Fox, D. J. *Gaussian 16, Revision B.01*, Gaussian, Inc.: Wallingford CT, **2016**.

56. Peach, M. J. G.; Tellgren, E. I.; Sałek, P.; Helgaker, T.; Tozer, D. J., Structural and Electronic Properties of Polyacetylene and Polyyne from Hybrid and Coulomb-Attenuated Density Functionals. *J. Phys. Chem. A* **2007**, *111* (46), 11930-11935.

57. Guido, C.; Caprasecca, S., *How to perform corrected Linear Response calculations in G09*. **2016**.

4.5 Supporting information

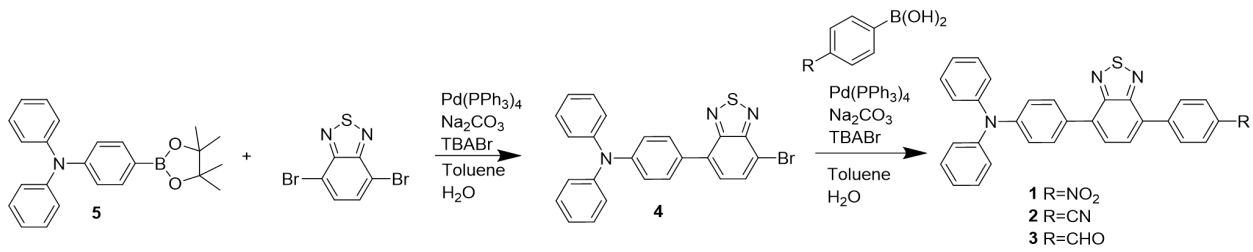

Scheme 2. Reaction scheme for the preparation of the fluorochromes.

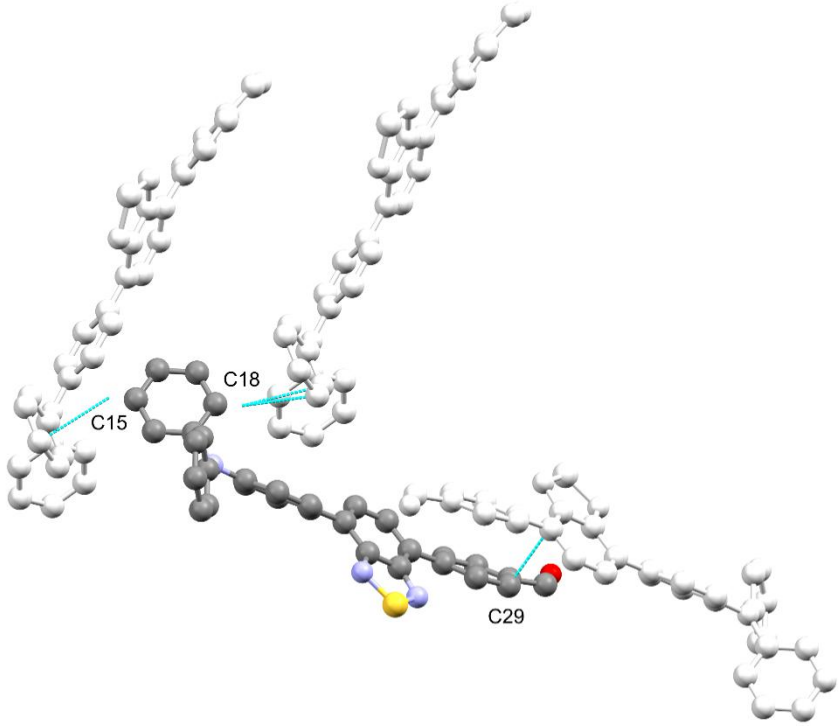

Figure 4.6. Intermolecular contacts (blue lines) of **3** in the resolved crystal structure. The molecules are bleached in color to focus attention on the central structure and its contacts.

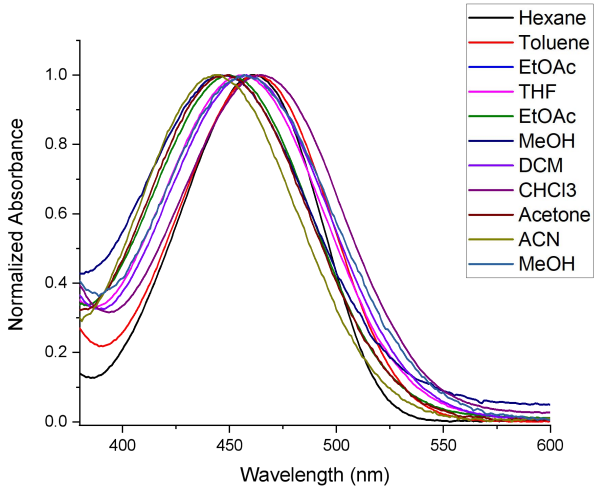

Figure 4.7. Normalized absorbance spectra of **1** in various solvents.

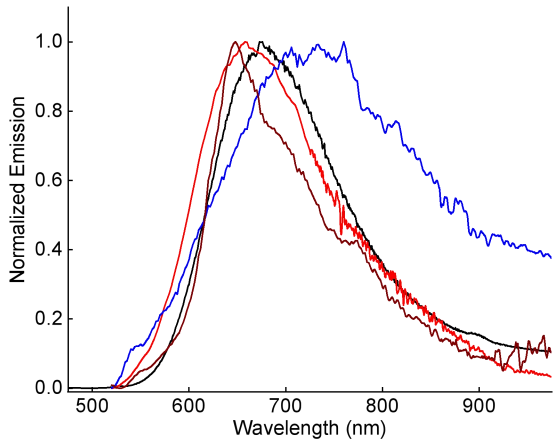

Figure 4.8. Normalized emission spectra of **1** in THF (black), chloroform (red), acetone (blue), and methanol (wine).

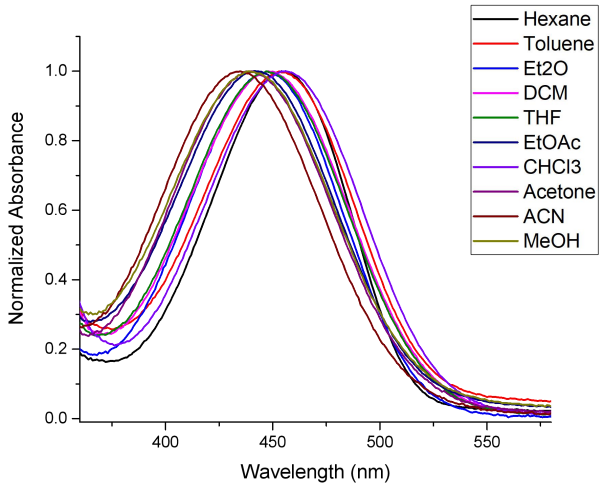

Figure 4.9. Normalized absorbance spectra of **2** in various solvents.

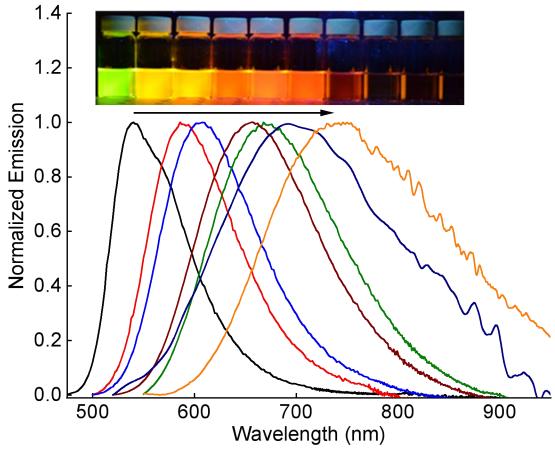

Figure 4.10. Normalized emission spectra of **2** in hexane (black), toluene (red), diethyl ether (blue), dichloromethane (green), THF (wine), methanol (navy blue), and DMSO (orange).

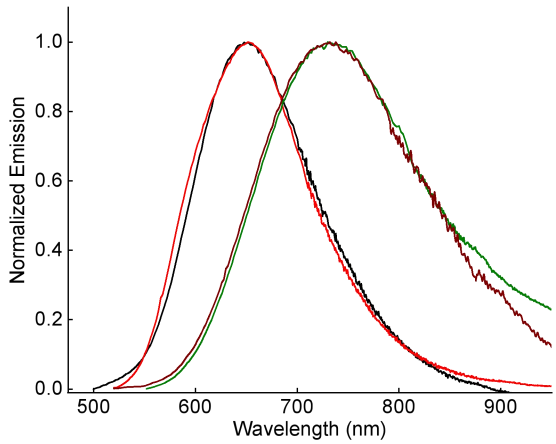

Figure 4.11. Normalized emission spectra of **2** in ethyl acetate (black), chloroform (red), acetone (green), and acetonitrile (wine)

.

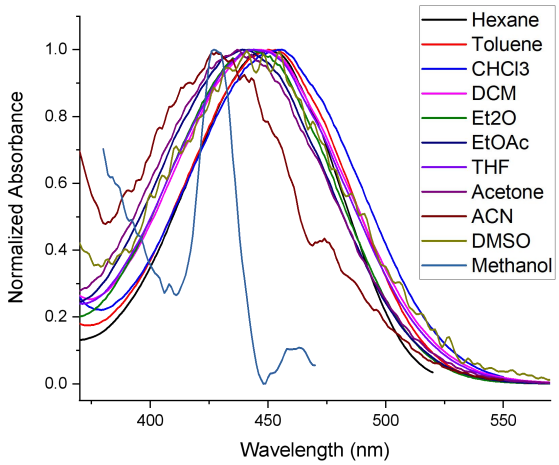

Figure 4.12. Normalized excitation spectra of **3** in various solvents monitored at the most red shifted emission.

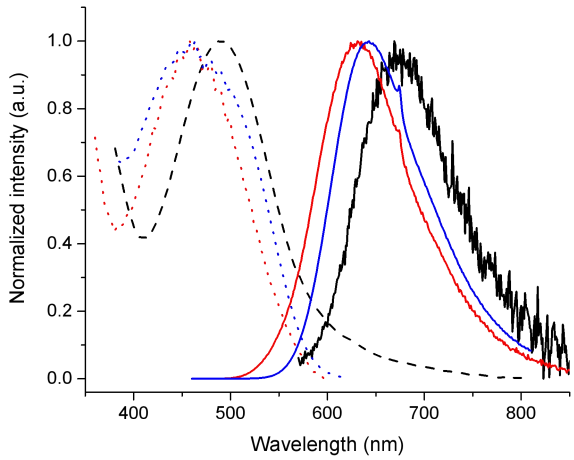

Figure 4.13. Normalized absorption (dotted line) and emission (solid line) spectra of **3** (blue) as a thin film on glass cover slips.

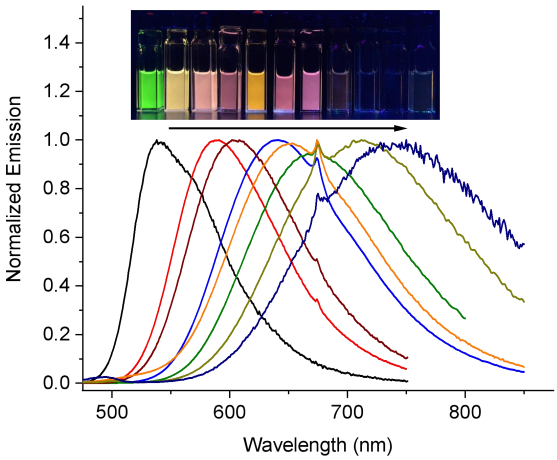

Figure 4.14. Normalized emission spectra of **3** in hexane (black), toluene, (red), chloroform (blue), dichloromethane (olive), diethyl ether (wine), THF (orange), acetone (light green), and acetonitrile (navy blue) irradiated at the most red shifted absorbance. Inset: photograph of cuvettes of **1** irradiated with a handheld UV lamp in hexane, toluene, chloroform, dichloromethane, diethyl ether, ethyl acetate, THF, acetone, acetonitrile, methanol, and DMSO (left to right).

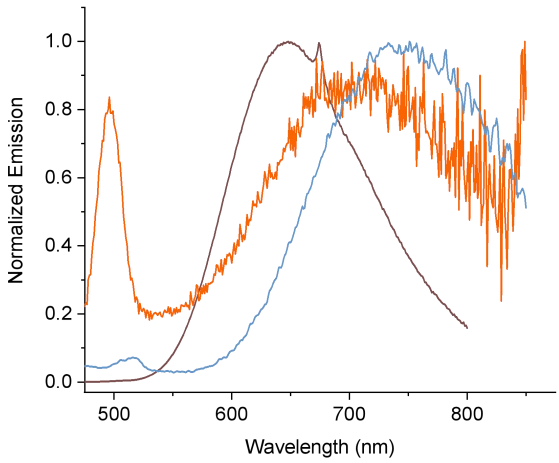

Figure 4.15. Normalized emission spectra of **3** in ethyl acetate (brown), methanol, (orange), DMSO (blue) irradiated at the most red-shifted absorbance.

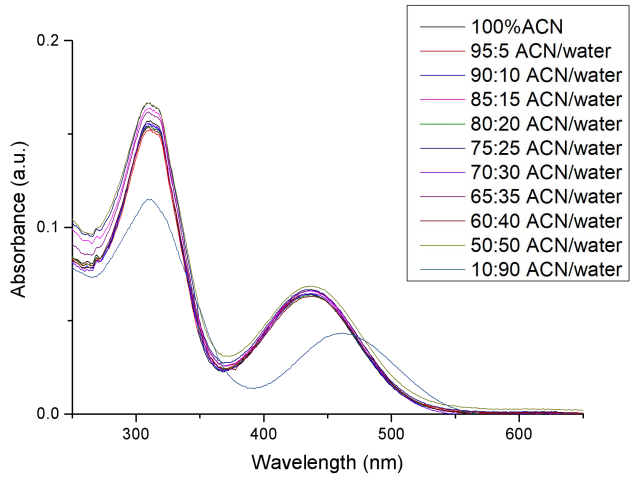

Figure 4.16. Absorbance of **3** in various acetonitrile/water volume % mixtures.

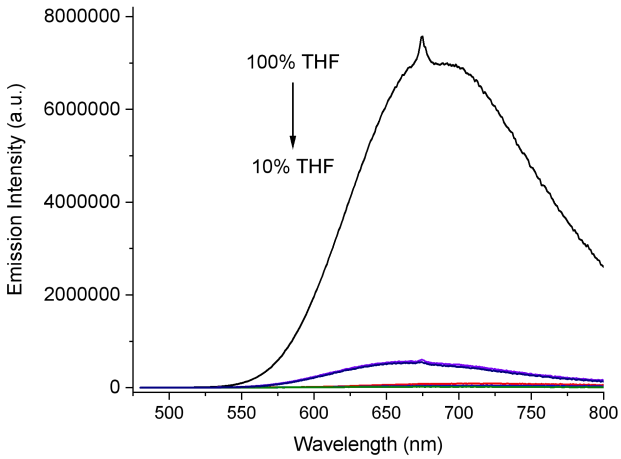

Figure 4.17. Change in emission of **1** with various vol% water in THF: 100, 80, 60, 40, 20, 10% THF.

Table S9. Emission and emission yield contingent on water content **1** in degassed THF.

THF concentration (%)	Φ_{fl} (%)	Emission (nm)
100	42	685
80	0.5	715
60	0.4	720
40	0.1	690
20	4.5	665
10	5.0	665

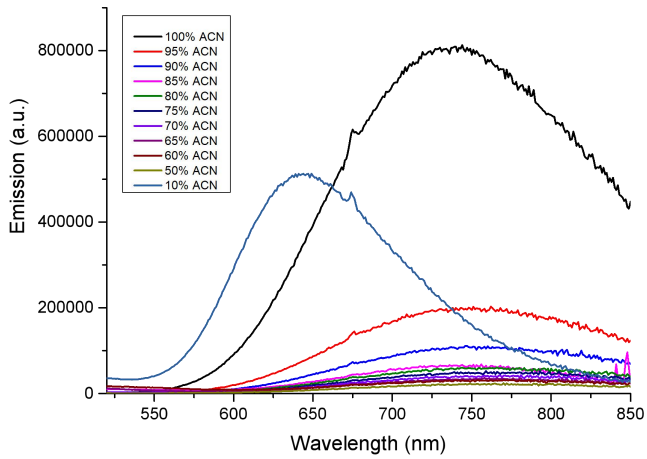

Figure 4.18. Emission of **3** in various volume % of acetonitrile/water mixtures.

Table S10. various volume % of acetonitrile/water mixtures.

Solvent	**Φ_{Fl} (%)**
100% ACN	4.2
95:5 ACN/H_2O	1.2
90:10 ACN/H_2O	0.5
85:15 ACN/H_2O	0.6
80:20 ACN/H_2O	0.3
75:25 ACN/H_2O	0.2
70:30 ACN/H_2O	0.3
65:35 ACN/H_2O	0.3
60:40 ACN/H_2O	0.4
50:50 ACN/H_2O	0.7
10:90 ACN/H_2O	2.6

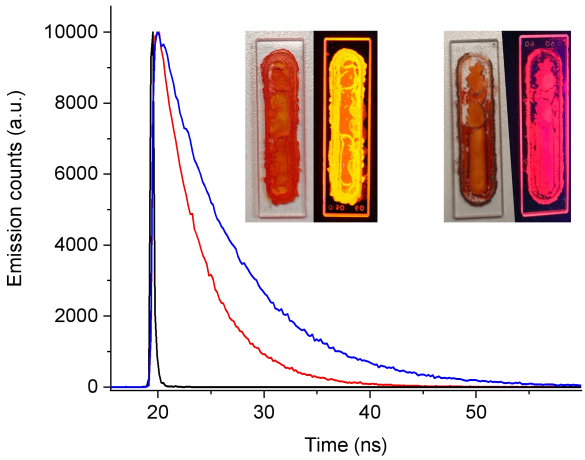

Figure 4.19. Excited state kinetics of **2** (blue), **1** (red), and IRF (black) measured in anhydrous and degassed THF excited at 405 nm with a ps-LED. Inset: photograph of **2** (left series) and **1** (right series) deposited on a 60 µL well slide under ambient light (left) and irradiated with a handheld UV lamp (right).

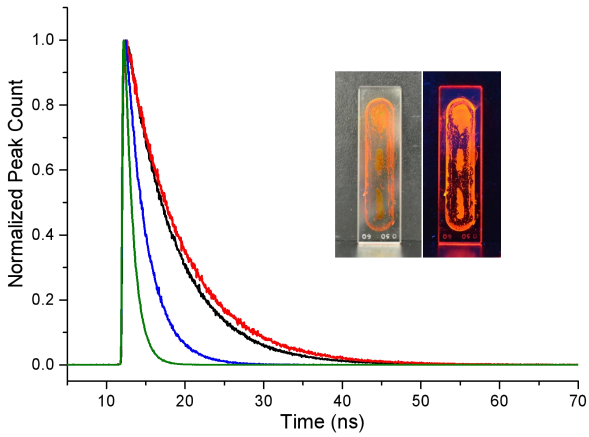

Figure 4.20. Excited lifetime kinetics of **3** in toluene (black; 6.15 ns), THF (red; 7.02 ns), acetone (blue; 2.71 ns), and acetonitrile (olive; 1.29 ns) excited with a 405 nm ps-LED. Inset: photograph of **3** deposited on a 60 L well slide under ambient light (left) and irradiated with a handheld UV lamp (right).

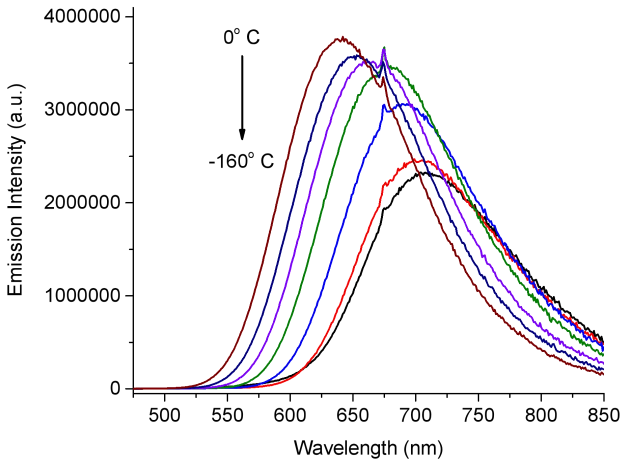

Figure 4.21. Temperature dependent emission of **2** measured in degassed 2-methyltetrahydrofuran and excited at 445 nm.

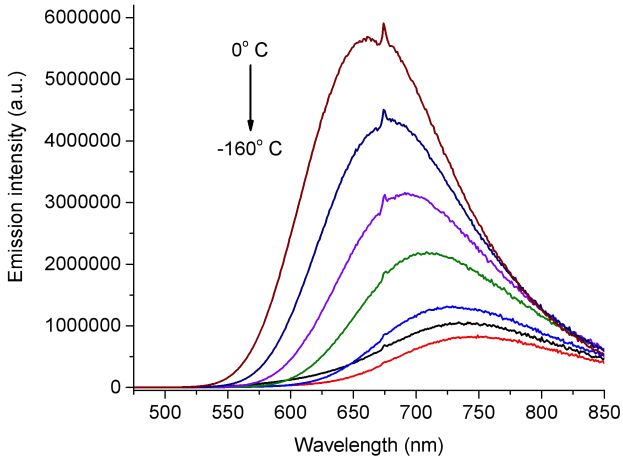

Figure 4.22. Temperature dependent emission of **1** measured in degassed 2-methyltetrahydrofuran and excited at 450 nm.

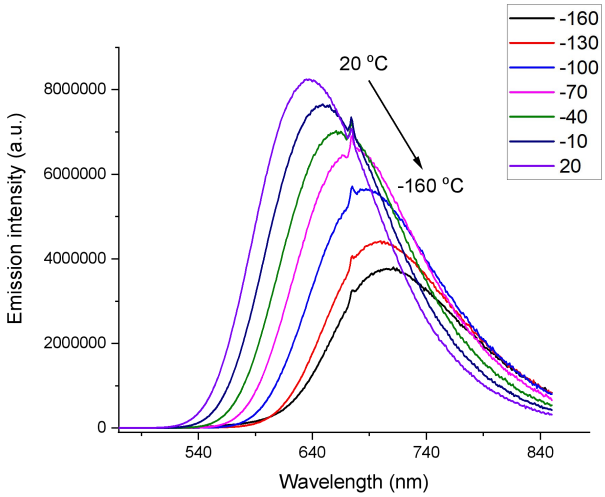

Figure 4.23. Temperature dependent emission of **3** in degassed 2-methyltetrahydrofuran.

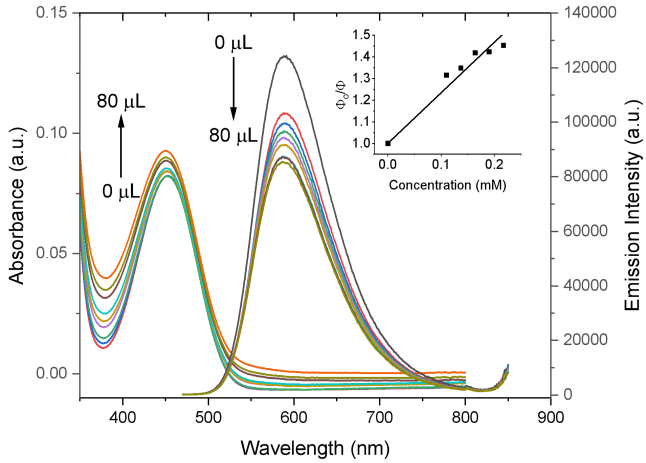

Figure 4.24. Change in absorption (left) and emission (right) spectra of **3** in toluene with the addition of various amounts of aniline. Inset: Stern-Volmer plot of **3** with aniline in toluene.

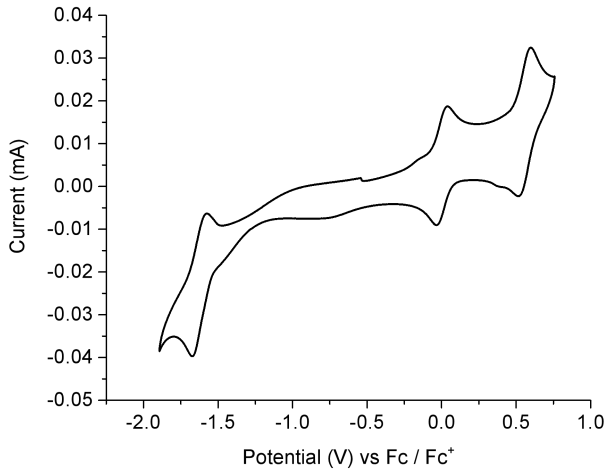

Figure 4.25. Cyclic voltammetry of **3** (1 mM) in $TBAPF_6$ (0.2 M) in propylene carbonate with ferrocene as internal reference measured at 100 mV/s.

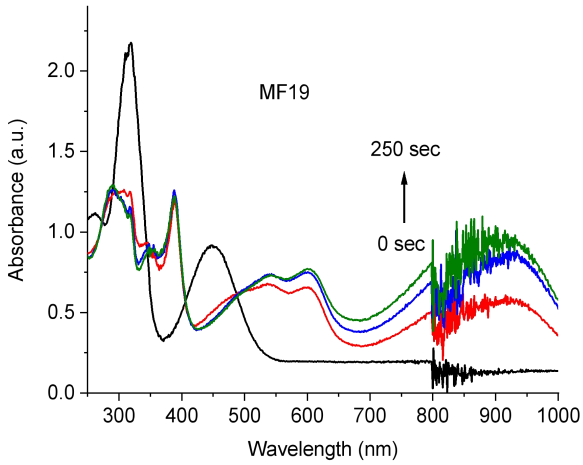

Figure 4.26. Change in absorption of **2** with an applied at potential of +1.5 V in 0.1 M $TBAPF_6$ and degassed dichloromethane measured at 30 sec. intervals.

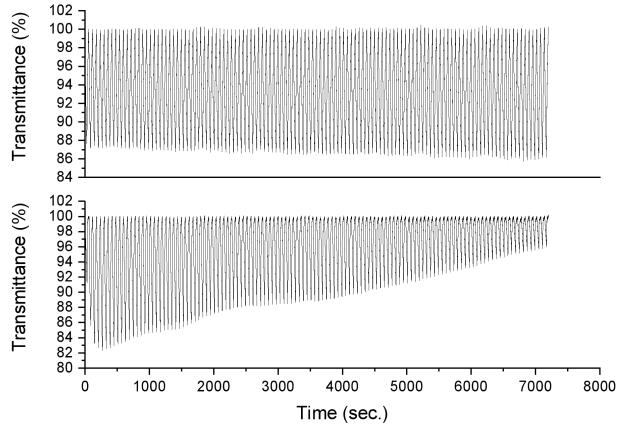

Figure 4.27. Change in transmittance intensity of **2** (top) and **1** (bottom) monitored at 917 nm. in 0.1 M $TBAPF_6$ and degassed dichloromethane with pplied potentials of + 0.9 V and -0 V for 30s for **2**; + 1.35 V and 0 V for 30s for **1**.

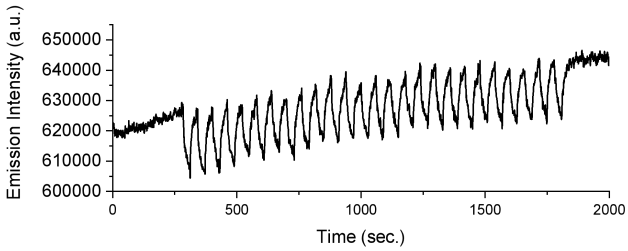

Figure 4.28. Change in fluorescence intensity of **2** excited at 450 nm and monitored at 670 nm in 0.1 M $TBAPF_6$ and degassed dichloromethane with applied potentials of + 1.1 V and -0 V for 30 s.

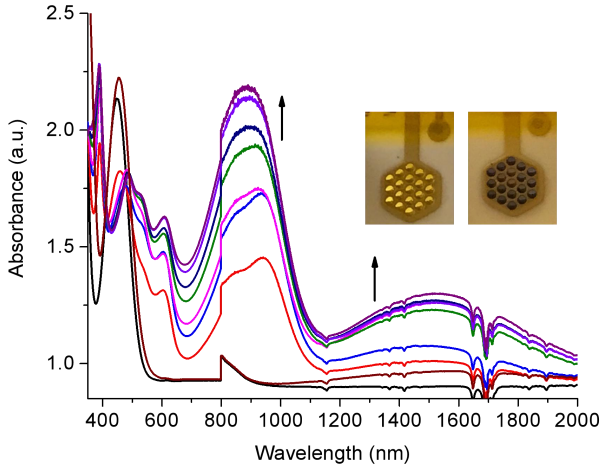

Figure 4.29. Spectroelectrochemistry of 3 (0.5 mM) in $TBAPF_6$ (0.1 M) anhydrous and degassed dichloromethane with applied potential of +1.3 V from 0 (black line) to 210 sec measured at 30 sec intervals and a final potential of -0.1 V after 300 sec (maroon line).

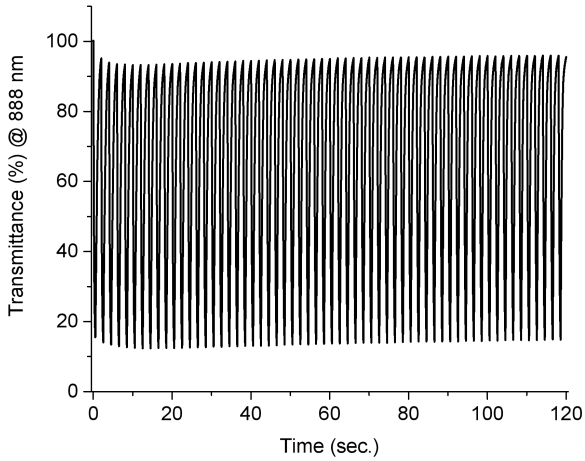

Figure 4.30. Change in transmittance of 3 (0.5 mM) in $TBAPF_6$ (0.1 M) anhydrous and degassed dichloromethane monitored at 888 nm switching with applied potentials of +1.3 and -0.1 V at 90 sec intervals.

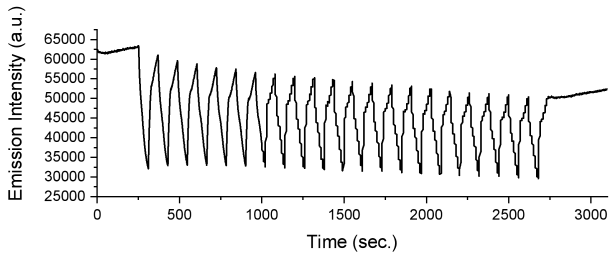

Figure 4.31. Change in fluorescence intensity of **3**. Excited at 445 nm and monitored on 690 nm in 0.1 M $TBAPF_6$ and degassed dichloromethane with applied potentials of + 1.1 V and -0.1 V to reach the second oxidation state for 30 s.

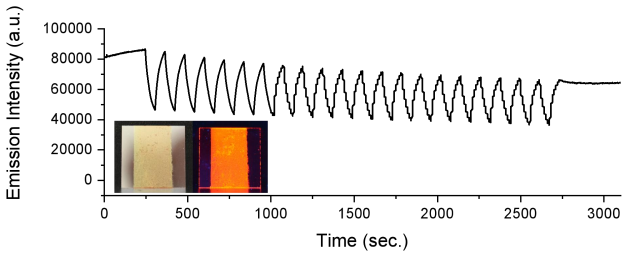

Figure 4.32. Change in fluorescence intensity of **3**. Excited at 445 nm and monitored on 690 nm in 0.1 M $TBAPF_6$ and degassed dichloromethane with applied potentials of + 0.8 V and -0.1 V for 30 s. Inset: photographs of **3** deposited on a glass slide and irradiated under ambient light (left) and a handheld UV lamp (right).

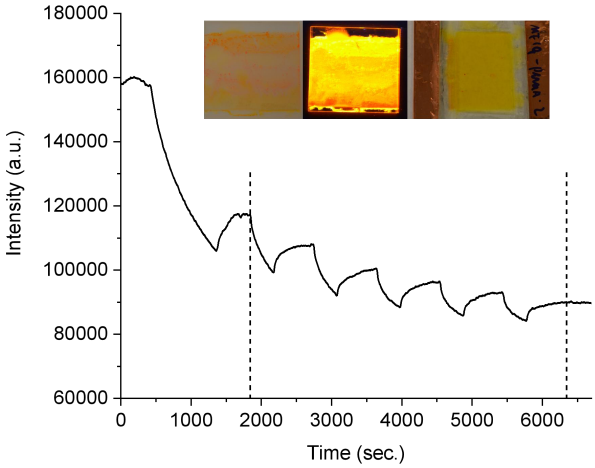

Figure 4.33. Change in emission intensity of the operating electrofluorochromic device prepared with **2** as the active layer with applied potential switching between + 1.5 V for 5 min and -0.3 V for 9 min. in the region delimited by the dashed lines. Excited at 470 nm and monitored at 645 nm. Inset: photographs of the **2** spray coated on a glass slide under ambient light (left) and irradiated with UV handheld lamp (middle). Fully assembled electrofluorochromic device prepared with **2** (right).

A)

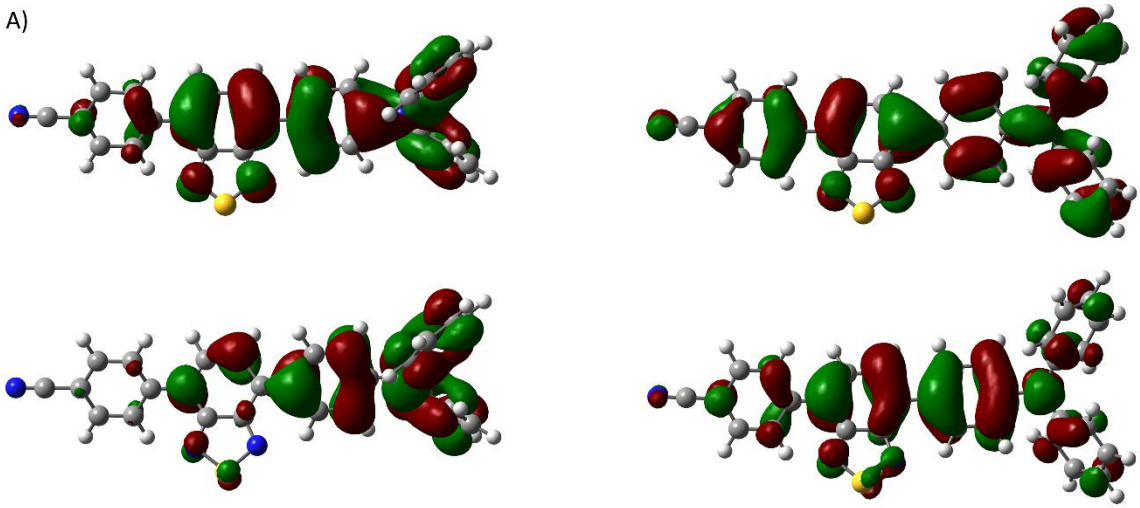

B)

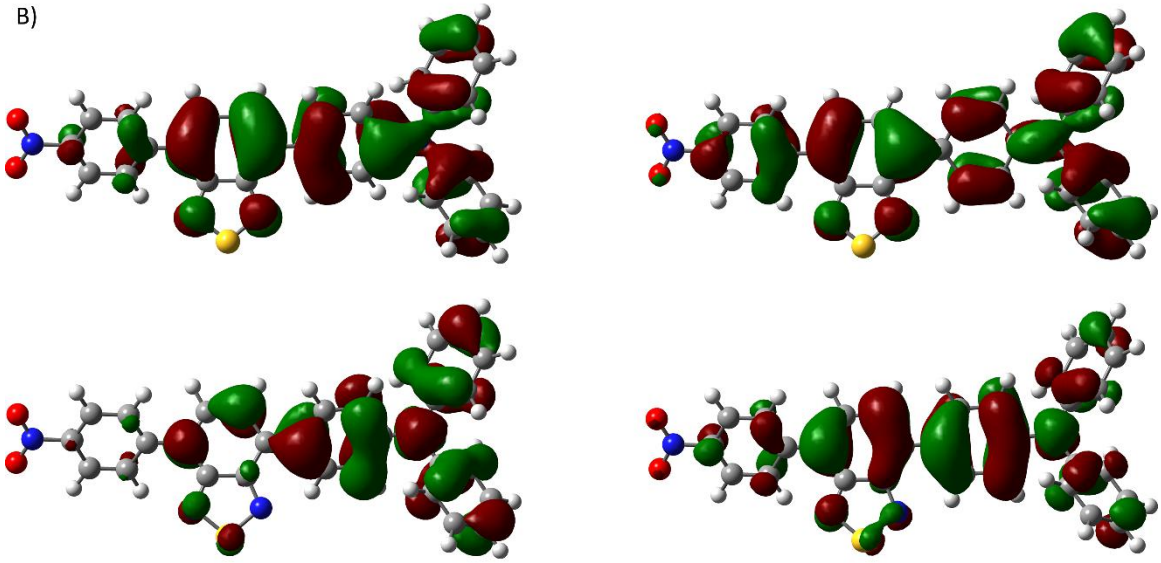

C)

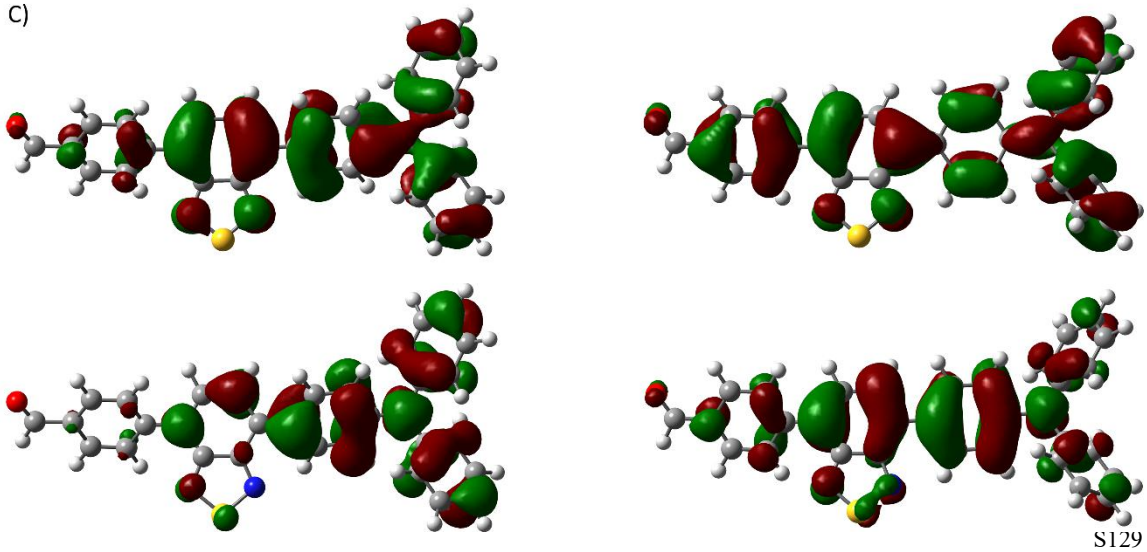

Figure 4.34. Frontier orbtials calculated with the Natural Transition Orbitals by CAM-DFT with the 6-311g+(d,p) basis set of the HOMO (top) and LUMO (bottom) of the radical cation (left) and dication (right) of **2** (A), **1** (B), and **3** (C).

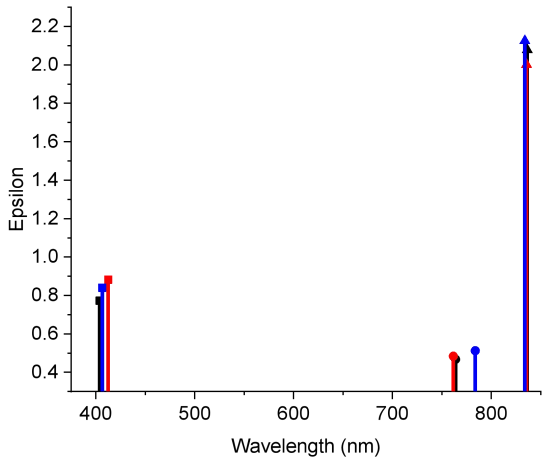

Figure 4.35. Calculated epsilon values by CAM-DFT/TD-DFT with the 6-311g+(d,p) basis set for the **2** (black), **1** (red), and **3** (blue) for the neutral state (square), radical cation (circle), and dication (triangle).

Table S11.

D—H···*A*	*D*—H	H···*A*	*D*···*A*	*D*—H···*A*
C17—H17···O1^{i}	0.95	2.45	3.186 (2)	134.3

Symmetry code: (i) −*x*+1/2, *y*+1/2, −*z*+1/2.Table S12.

atom	x	y	z
N	4.55494	0.08944	-0.19809
C	5.28358	1.26451	0.12199
C	4.91386	2.05291	1.21159
C	6.38476	1.64137	-0.6463
C	5.62785	3.20202	1.51768
H	4.06443	1.76254	1.8172
C	7.10459	2.7829	-0.32475
H	6.67587	1.03503	-1.49498
C	6.72879	3.57234	0.75498
H	5.32816	3.80409	2.36733
H	7.95816	3.06218	-0.93106
H	7.28866	4.4664	1.00032
C	3.1447	0.10202	-0.18864
C	2.42177	-1.00578	0.25998
C	2.43649	1.22405	-0.62301

C	1.03845	-0.99129	0.27021
H	2.94965	-1.88572	0.60428
C	1.05275	1.23298	-0.60461
H	2.97367	2.09712	-0.97025
C	0.32291	0.12658	-0.16502
H	0.50713	-1.86313	0.62671
H	0.5311	2.12371	-0.93382
C	-1.15393	0.14264	-0.20029
C	-1.84739	0.70848	-1.2339
C	-1.95415	-0.42334	0.84801
C	-3.26807	0.74184	-1.29445
H	-1.29959	1.132	-2.06648
C	-3.39613	-0.3956	0.78373
C	-4.0712	0.20515	-0.32829
H	-3.72271	1.19032	-2.16941
N	-1.50059	-0.98221	1.96597
N	-3.97158	-0.93593	1.85346
C	5.25831	-1.09947	-0.5227
C	4.85992	-1.88569	-1.60379
C	6.36308	-1.49287	0.23209
C	5.54918	-3.04852	-1.91471
H	4.00747	-1.58291	-2.19897
C	7.05807	-2.64827	-0.09441
H	6.6763	-0.88873	1.07441
C	6.65373	-3.43529	-1.16555
H	5.22716	-3.64873	-2.75749
H	7.91458	-2.94033	0.50165
H	7.1942	-4.3402	-1.41457
S	-2.78671	-1.43346	2.84408
C	-5.5458	0.24741	-0.43
C	-6.18012	1.39425	-0.91479
C	-6.3302	-0.85371	-0.07585
C	-7.55496	1.44285	-1.055
H	-5.59193	2.2667	-1.16922
C	-7.70511	-0.81782	-0.21493
H	-5.85885	-1.7486	0.30468
C	-8.32346	0.33278	-0.70571
H	-8.03462	2.33923	-1.42593
H	-8.30207	-1.67979	0.0534
C	-9.74683	0.37533	-0.84799
N	-10.8902	0.4095	-0.96371

Table S13.

atom	x	y	z
N	4.52798	0.10963	-0.18631
C	5.25998	1.26868	0.1598
C	4.84986	2.04952	1.24486
C	6.39402	1.61633	-0.58038
C	5.57655	3.17672	1.58114
H	3.9907	1.75262	1.8317
C	7.10407	2.7515	-0.23729
H	6.69231	1.01434	-1.42839
C	6.69988	3.53172	0.84173
H	5.2725	3.77449	2.4306
H	7.97259	3.03425	-0.81789
H	7.26375	4.4167	1.10845
C	3.13708	0.12669	-0.17508
C	2.41654	-1.02356	0.19107
C	2.44122	1.29711	-0.52541
C	1.04233	-0.99392	0.21814
H	2.94497	-1.91887	0.48834
C	1.06689	1.30283	-0.51525
H	2.98633	2.1794	-0.83112
C	0.33538	0.1637	-0.1439
H	0.50209	-1.87594	0.52796
H	0.54636	2.21092	-0.78908
C	-1.1357	0.19132	-0.16392
C	-1.82597	0.89847	-1.11225
C	-1.93279	-0.51861	0.79471
C	-3.24394	0.93036	-1.17871
H	-1.27951	1.43444	-1.87779
C	-3.37215	-0.47993	0.72917
C	-4.04533	0.2621	-0.2955
H	-3.69691	1.48918	-1.98784
N	-1.48324	-1.22381	1.82752
N	-3.95144	-1.15815	1.71466
C	5.22708	-1.06695	-0.54039
C	4.78103	-1.84259	-1.61489
C	6.36501	-1.43783	0.18242
C	5.47592	-2.98759	-1.95814
H	3.91889	-1.52864	-2.18827
C	7.04307	-2.59034	-0.16734

H	6.69065	-0.8397	1.02305
C	6.60308	-3.36542	-1.23595
H	5.14403	-3.582	-2.79949
H	7.91419	-2.89071	0.40036
H	7.14179	-4.26435	-1.50795
S	-2.774	-1.78763	2.63179
C	-5.51972	0.30684	-0.39524
C	-6.16136	1.50737	-0.70878
C	-6.29226	-0.84207	-0.20841
C	-7.5367	1.56419	-0.84113
H	-5.58085	2.41261	-0.83244
C	-7.66724	-0.79783	-0.34466
H	-5.8138	-1.77947	0.0367
C	-8.29443	0.40758	-0.6607
H	-8.02404	2.50115	-1.07702
H	-8.25708	-1.69471	-0.20801
C	-9.71868	0.45733	-0.79724
N	-10.8621	0.49723	-0.90808

Table S14.

atom	x	y	z
N	4.47004	0.19469	-0.09548
C	5.22101	1.39634	0.10426
C	4.91939	2.21646	1.19085
C	6.2639	1.69937	-0.76937
C	5.66454	3.36572	1.38945
H	4.1421	1.93581	1.89027
C	6.98907	2.85828	-0.56431
H	6.48369	1.04821	-1.60515
C	6.69207	3.68948	0.51199
H	5.45148	4.00103	2.23905
H	7.78911	3.11575	-1.24584
H	7.27225	4.58936	0.67221
C	3.1418	0.19276	-0.07536
C	2.40616	-1.01966	0.18188
C	2.39672	1.40447	-0.31067
C	1.0603	-1.00771	0.23263
H	2.94754	-1.92641	0.40909
C	1.05181	1.38853	-0.31179
H	2.92832	2.31144	-0.55793
C	0.29739	0.18938	-0.025

H	0.53458	-1.91298	0.48822
H	0.54543	2.31259	-0.53933
C	-1.10916	0.19498	-0.00026
C	-1.83684	1.34178	-0.41224
C	-1.94021	-0.92454	0.41652
C	-3.21285	1.4175	-0.46175
H	-1.30197	2.21403	-0.75319
C	-3.37515	-0.82786	0.36367
C	-4.04085	0.35393	-0.09812
H	-3.65578	2.32657	-0.84229
N	-1.53542	-2.07827	0.91519
N	-3.98556	-1.90993	0.83079
C	5.21736	-1.00543	-0.31686
C	4.88859	-1.82475	-1.39604
C	6.28267	-1.30784	0.52957
C	5.63008	-2.97282	-1.6149
H	4.09303	-1.54456	-2.07486
C	7.00389	-2.46542	0.30465
H	6.52207	-0.65749	1.36064
C	6.68041	-3.29585	-0.76469
H	5.39583	-3.6078	-2.45913
H	7.82128	-2.72289	0.96527
H	7.25755	-4.19473	-0.94067
S	-2.85163	-2.96042	1.28151
C	-5.49184	0.46549	-0.18359
C	-6.10185	1.71003	0.03764
C	-6.29336	-0.6403	-0.50313
C	-7.47182	1.8456	-0.04127
H	-5.50726	2.57066	0.31278
C	-7.66268	-0.50297	-0.60888
H	-5.84259	-1.60265	-0.69047
C	-8.25394	0.73771	-0.37057
H	-7.93775	2.80233	0.15151
H	-8.27619	-1.35355	-0.87345
C	-9.67665	0.87672	-0.46471
N	-10.8171	0.98859	-0.54029

Table S15.

atom	x	y	z
N	4.92949	-0.23581	0.03348
C	5.66515	0.97821	0.03781

C	5.31329	2.02388	-0.81543
C	6.75661	1.13564	0.89133
C	6.03548	3.20804	-0.80468
H	4.47126	1.90611	-1.48601
C	7.4847	2.31649	0.8854
H	7.03351	0.32831	1.55782
C	7.12682	3.36073	0.04182
H	5.74978	4.01156	-1.47318
H	8.33053	2.42359	1.55417
H	7.693	4.284	0.04335
C	3.52083	-0.21615	0.01278
C	2.80782	0.7683	0.70137
C	2.80184	-1.17828	-0.70018
C	1.42516	0.79379	0.66929
H	3.34305	1.51881	1.26852
C	1.4187	-1.15802	-0.71051
H	3.33119	-1.94075	-1.25668
C	0.69877	-0.17435	-0.02827
H	0.90222	1.56675	1.21554
H	0.88935	-1.90552	-1.28935
C	-0.77737	-0.19621	-0.02535
C	-1.48353	-1.36532	0.04759
C	-1.56524	1.00086	-0.10823
C	-2.90443	-1.41946	0.04894
H	-0.94577	-2.3008	0.13716
C	-3.00765	0.94703	-0.09626
C	-3.69532	-0.30692	-0.01147
H	-3.36926	-2.39402	0.13595
N	-1.09921	2.23977	-0.23381
N	-3.57114	2.14566	-0.21011
C	5.62888	-1.4711	0.04348
C	6.7311	-1.66263	-0.78888
C	5.22927	-2.50449	0.89061
C	7.42265	-2.86514	-0.76823
H	7.0451	-0.86479	-1.45033
C	5.91509	-3.71011	0.89467
H	4.37915	-2.35943	1.5455
C	7.01712	-3.89693	0.06908
H	8.2775	-2.99881	-1.42055
H	5.59291	-4.5036	1.55857
H	7.55507	-4.83688	0.07915

S	-2.3748	3.2365	-0.3198
C	-5.17027	-0.39887	0.00975
C	-5.81677	-1.41392	-0.70177
C	-5.94189	0.49904	0.75376
C	-7.19321	-1.54285	-0.66852
H	-5.23727	-2.10092	-1.30456
C	-7.31853	0.38113	0.79987
H	-5.45991	1.29199	1.30709
C	-7.92454	-0.64039	0.08584
H	-7.69665	-2.32174	-1.22258
H	-7.91887	1.0659	1.38112
N	-9.38394	-0.76741	0.12668
O	-9.90038	-1.66886	-0.51042
O	-10.012	0.03371	0.7965

Table S16.

atom	x	y	z
N	4.89902	-0.23445	0.02548
C	5.63861	0.97148	0.05483
C	5.26269	2.0373	-0.76797
C	6.74778	1.07939	0.89874
C	5.99828	3.20792	-0.73876
H	4.42276	1.93149	-1.44161
C	7.46709	2.25953	0.92333
H	7.02031	0.25391	1.5429
C	7.09681	3.32329	0.1063
H	5.72048	4.02957	-1.38609
H	8.31628	2.35365	1.58769
H	7.66784	4.24293	0.12633
C	3.51207	-0.21255	-0.01316
C	2.7996	0.82751	0.61201
C	2.80419	-1.23168	-0.67739
C	1.42633	0.8404	0.57516
H	3.3334	1.59105	1.16056
C	1.43138	-1.20187	-0.70839
H	3.34301	-2.00788	-1.20293
C	0.70876	-0.17464	-0.07883
H	0.89354	1.63159	1.08123
H	0.90455	-1.96743	-1.26228
C	-0.761	-0.19259	-0.08626
C	-1.46278	-1.36761	-0.02247

C	-1.54599	1.00663	-0.14768
C	-2.88095	-1.42429	0.00353
H	-0.92488	-2.30429	0.04987
C	-2.98547	0.947	-0.12384
C	-3.6702	-0.30862	-0.03777
H	-3.34412	-2.39896	0.09099
N	-1.08402	2.24671	-0.26874
N	-3.55319	2.14443	-0.22555
C	5.59574	-1.4667	0.04503
C	6.74394	-1.62307	-0.73621
C	5.13728	-2.50916	0.85544
C	7.41909	-2.82923	-0.71246
H	7.08155	-0.81432	-1.37069
C	5.82932	-3.70634	0.8757
H	4.26768	-2.36467	1.48295
C	6.96617	-3.8705	0.09173
H	8.29882	-2.96121	-1.32891
H	5.48738	-4.51054	1.51423
H	7.5028	-4.81069	0.1097
S	-2.36477	3.23955	-0.3369
C	-5.1449	-0.39899	0.00319
C	-5.80055	-1.4013	-0.71666
C	-5.90145	0.48725	0.77482
C	-7.17689	-1.52786	-0.66613
H	-5.23075	-2.07899	-1.33893
C	-7.27761	0.36923	0.83971
H	-5.41027	1.26899	1.33599
C	-7.89401	-0.63819	0.11575
H	-7.69015	-2.29604	-1.226
H	-7.86874	1.04354	1.44214
N	-9.35494	-0.76523	0.17729
O	-9.88024	-1.65523	-0.46719
O	-9.97014	0.02584	0.8692

Table S17.

atom	x	y	z
N	4.83622	-0.24594	0.01538
C	5.61614	0.94898	0.02539
C	5.36247	1.93731	-0.9267
C	6.63678	1.08739	0.96646
C	6.13385	3.08562	-0.92072

H	4.60301	1.78429	-1.68277
C	7.38744	2.24706	0.96704
H	6.81479	0.30994	1.69786
C	7.13921	3.24302	0.02583
H	5.95958	3.85134	-1.66502
H	8.16847	2.37817	1.70428
H	7.74052	4.14326	0.02652
C	3.50864	-0.20721	-0.06326
C	2.77948	0.97137	0.32936
C	2.76555	-1.3476	-0.53541
C	1.43353	0.99623	0.26546
H	3.31749	1.80334	0.76043
C	1.42176	-1.30478	-0.60146
H	3.30231	-2.20455	-0.91582
C	0.67749	-0.13717	-0.19951
H	0.90354	1.8662	0.61827
H	0.90936	-2.14737	-1.03913
C	-0.7319	-0.11923	-0.24558
C	-1.46494	-1.3224	-0.35165
C	-1.5389	1.08006	-0.14072
C	-2.84645	-1.39504	-0.29702
H	-0.93493	-2.26083	-0.41945
C	-2.97242	0.9904	-0.09254
C	-3.65067	-0.26906	-0.14879
H	-3.30483	-2.37349	-0.32435
N	-1.10931	2.32959	-0.1347
N	-3.56475	2.17831	-0.05127
C	5.53898	-1.48547	0.09903
C	6.6576	-1.69066	-0.7092
C	5.11137	-2.45193	1.01053
C	7.33004	-2.89422	-0.62124
H	6.97217	-0.92934	-1.41075
C	5.80526	-3.64562	1.09538
H	4.27671	-2.24988	1.66972
C	6.907	-3.86932	0.27836
H	8.18639	-3.07586	-1.25717
H	5.49478	-4.39549	1.81088
H	7.44655	-4.80532	0.348
S	-2.41083	3.30261	-0.06194
C	-5.10642	-0.3843	-0.06161
C	-5.7661	-1.37706	-0.79873

C	-5.84997	0.46339	0.76957
C	-7.13764	-1.51739	-0.71893
H	-5.2117	-2.02392	-1.46521
C	-7.22006	0.31465	0.873
H	-5.35588	1.22447	1.35407
C	-7.83788	-0.6698	0.12228
H	-7.6591	-2.26741	-1.29516
H	-7.80363	0.94959	1.52329
N	-9.30167	-0.82435	0.22396
O	-9.82601	-1.69702	-0.43994
O	-9.90039	-0.07117	0.96635

Table S18.

atom	x	y	z
N	4.62288	-0.23552	0.01954
C	5.32261	-1.47032	0.02423
C	6.42172	-1.66007	-0.81281
C	4.92625	-2.50599	0.87023
C	7.11328	-2.86264	-0.79771
H	6.73328	-0.86079	-1.47367
C	5.612	-3.71166	0.86863
H	4.0785	-2.36274	1.52856
C	6.71095	-3.89657	0.03852
H	7.96556	-2.9947	-1.45372
H	5.29212	-4.5068	1.53169
H	7.24882	-4.8366	0.04415
C	5.35688	0.97926	0.01726
C	6.45653	1.13804	0.86008
C	4.99476	2.02521	-0.8314
C	7.18246	2.32016	0.84792
H	6.74146	0.33071	1.52316
C	5.71492	3.21065	-0.82674
H	4.14619	1.90665	-1.49354
C	6.8144	3.36459	0.00893
H	8.03466	2.42817	1.50843
H	5.42105	4.01427	-1.49158
H	7.37892	4.28886	0.00569
C	3.21348	-0.21675	0.00969
C	2.48985	-1.17425	-0.70437
C	2.50541	0.7624	0.71045
C	1.10649	-1.15479	-0.70402

H	3.01556	-1.93262	-1.26996
C	1.12239	0.78722	0.68914
H	3.04474	1.50941	1.27842
C	0.39121	-0.17647	-0.00943
H	0.57298	-1.89863	-1.28377
H	0.60302	1.55626	1.24432
C	-1.08521	-0.19914	0.00467
C	-1.8745	0.9975	-0.06804
C	-1.7903	-1.36851	0.07849
C	-3.31734	0.94229	-0.04693
C	-3.21147	-1.42367	0.09056
H	-1.25125	-2.30413	0.15993
C	-4.00474	-0.31234	0.03935
H	-3.67496	-2.39889	0.17699
N	-1.40971	2.23697	-0.19248
N	-3.88172	2.14126	-0.15372
S	-2.68689	3.2332	-0.2676
C	-5.48012	-0.4069	0.06973
C	-6.24867	0.48254	0.82359
C	-6.12939	-1.42183	-0.64547
C	-7.62622	0.35045	0.87097
H	-5.76471	1.27359	1.37876
C	-7.50344	-1.55118	-0.6015
H	-5.54678	-2.1014	-1.25482
C	-8.26334	-0.66399	0.16069
H	-8.21444	1.03999	1.46667
H	-8.0035	-2.33233	-1.16045
C	-9.72983	-0.77866	0.2254
H	-10.2295	-0.02269	0.8589
O	-10.3835	-1.61917	-0.35208

Table S19.

atom	x	y	z
N	4.59092	-0.23446	0.0099
C	5.28773	-1.46787	0.02257
C	6.42651	-1.62521	-0.77148
C	4.83888	-2.50878	0.83972
C	7.10207	-2.83142	-0.75384
H	6.75754	-0.81689	-1.40999
C	5.53095	-3.70628	0.85353
H	3.97631	-2.36355	1.47675

C	6.6585	-3.87167	0.05675
H	7.97488	-2.96399	-1.37996
H	5.19613	-4.50956	1.49698
H	7.19538	-4.8118	0.06986
C	5.33375	0.97085	0.03608
C	6.44307	1.07834	0.87911
C	4.9604	2.0345	-0.7899
C	7.16549	2.25688	0.89988
H	6.71444	0.25363	1.52478
C	5.69876	3.20377	-0.76442
H	4.11983	1.92867	-1.46277
C	6.79764	3.31913	0.07992
H	8.01541	2.35065	1.5634
H	5.42256	4.02408	-1.41417
H	7.37103	4.23737	0.09692
C	3.2058	-0.21074	-0.01933
C	2.49082	-1.23486	-0.67
C	2.49777	0.83581	0.60194
C	1.11851	-1.20428	-0.69036
H	3.02484	-2.01506	-1.19446
C	1.1248	0.84925	0.57589
H	3.0361	1.60347	1.14023
C	0.40028	-0.17144	-0.06312
H	0.58736	-1.97345	-1.23493
H	0.59662	1.64504	1.07938
C	-1.06836	-0.18987	-0.05768
C	-1.85631	1.00825	-0.10689
C	-1.76917	-1.36617	0.00767
C	-3.29599	0.94575	-0.071
C	-3.18628	-1.42518	0.04717
H	-1.22982	-2.30268	0.07148
C	-3.97947	-0.31116	0.01734
H	-3.64687	-2.40096	0.13513
N	-1.39731	2.2493	-0.22844
N	-3.86596	2.1428	-0.16508
S	-2.68063	3.24026	-0.28348
C	-5.45352	-0.40623	0.06998
C	-6.20797	0.47574	0.84573
C	-6.11117	-1.41486	-0.64556
C	-7.58462	0.34147	0.91416
H	-5.71563	1.26034	1.40259

C	-7.48447	-1.54373	-0.5822
H	-5.53809	-2.08835	-1.27047
C	-8.23104	-0.66514	0.20217
H	-8.16372	1.02329	1.52714
H	-7.9939	-2.31846	-1.14142
C	-9.69824	-0.78331	0.28832
H	-10.1904	-0.03491	0.93599
O	-10.3555	-1.62047	-0.28804

Table S20.

atom	x	y	z
N	4.52716	-0.2452	0.00088
C	5.23198	-1.48789	0.08509
C	6.33049	-1.70554	-0.74456
C	4.82611	-2.43923	1.01985
C	7.00692	-2.90762	-0.65282
H	6.63085	-0.9535	-1.46227
C	5.52251	-3.63225	1.10771
H	4.00299	-2.22979	1.69117
C	6.60592	-3.8688	0.27073
H	7.84988	-3.0974	-1.30423
H	5.22684	-4.37147	1.84049
H	7.14772	-4.8033	0.34312
C	5.3125	0.95059	0.0038
C	6.31961	1.10093	0.95529
C	5.07726	1.92185	-0.96825
C	7.07708	2.25722	0.94572
H	6.48656	0.33383	1.70022
C	5.85364	3.06785	-0.97161
H	4.32499	1.76104	-1.73012
C	6.84675	3.23804	-0.01499
H	7.84989	2.39617	1.69028
H	5.69129	3.82165	-1.73077
H	7.45209	4.13557	-0.02167
C	3.20159	-0.20461	-0.07385
C	2.4529	-1.35039	-0.52647
C	2.47451	0.98233	0.30026
C	1.11029	-1.30563	-0.59122
H	2.98643	-2.21609	-0.89084
C	1.12944	1.00795	0.24437
H	3.01592	1.82303	0.70929

C	0.36472	-0.13145	-0.20049
H	0.59805	-2.15513	-1.01498
H	0.60393	1.88516	0.58538
C	-1.03847	-0.11297	-0.23714
C	-1.8509	1.08272	-0.10077
C	-1.77777	-1.31767	-0.36913
C	-3.28391	0.98862	-0.03714
C	-3.15241	-1.39365	-0.30587
H	-1.24845	-2.2537	-0.46561
C	-3.96452	-0.27174	-0.11128
H	-3.60788	-2.3723	-0.35389
N	-1.42499	2.33217	-0.0782
N	-3.87743	2.17391	0.02962
S	-2.72741	3.3024	0.02498
C	-5.40975	-0.39806	0.00215
C	-6.15231	0.46201	0.82449
C	-6.07507	-1.41904	-0.70211
C	-7.51942	0.29411	0.94413
H	-5.65684	1.23856	1.38681
C	-7.44068	-1.56236	-0.59894
H	-5.52278	-2.07382	-1.36271
C	-8.1679	-0.70889	0.2309
H	-8.08757	0.94702	1.59634
H	-7.9605	-2.33152	-1.15518
C	-9.63813	-0.86254	0.36425
H	-10.1288	-0.14163	1.041
O	-10.2784	-1.70628	-0.21375

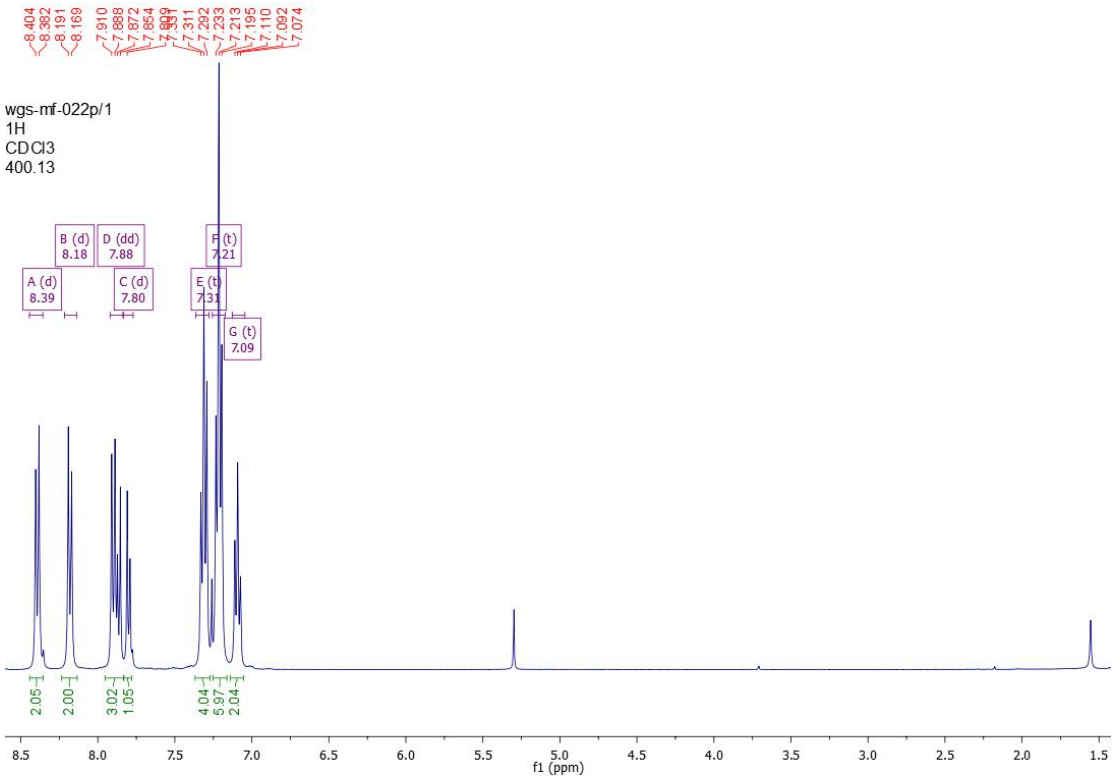

Figure 4.36. ^{1}H NMR spectra of **1** measured in $CDCl_3$.

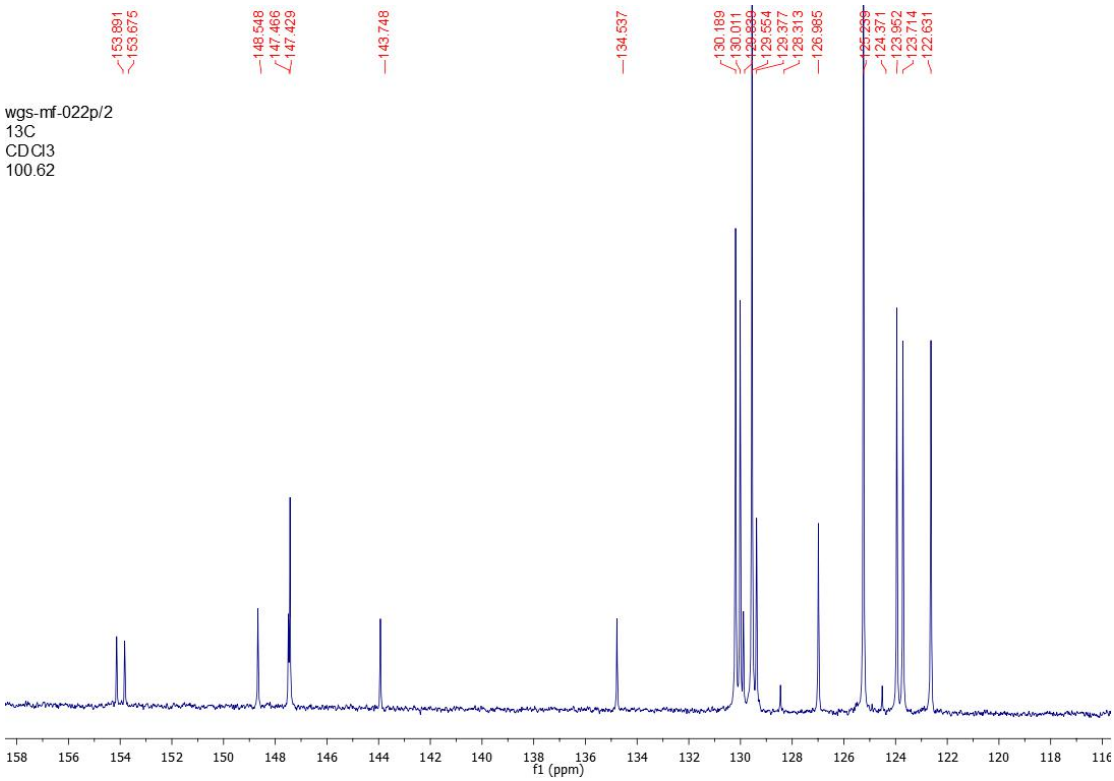

Figure 4.37. ^{13}C NMR spectra of **1** measured in $CDCl_3$.

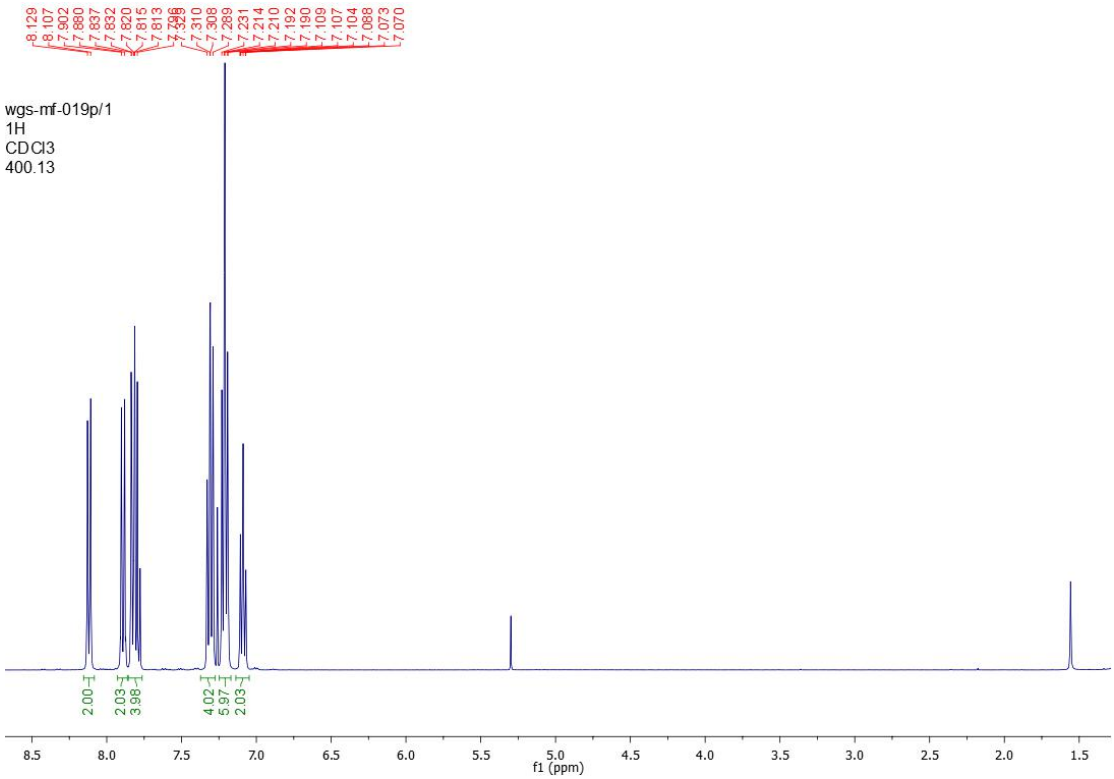

Figure 4.38. ^{1}H NMR spectra of **2** measured in $CDCl_3$.

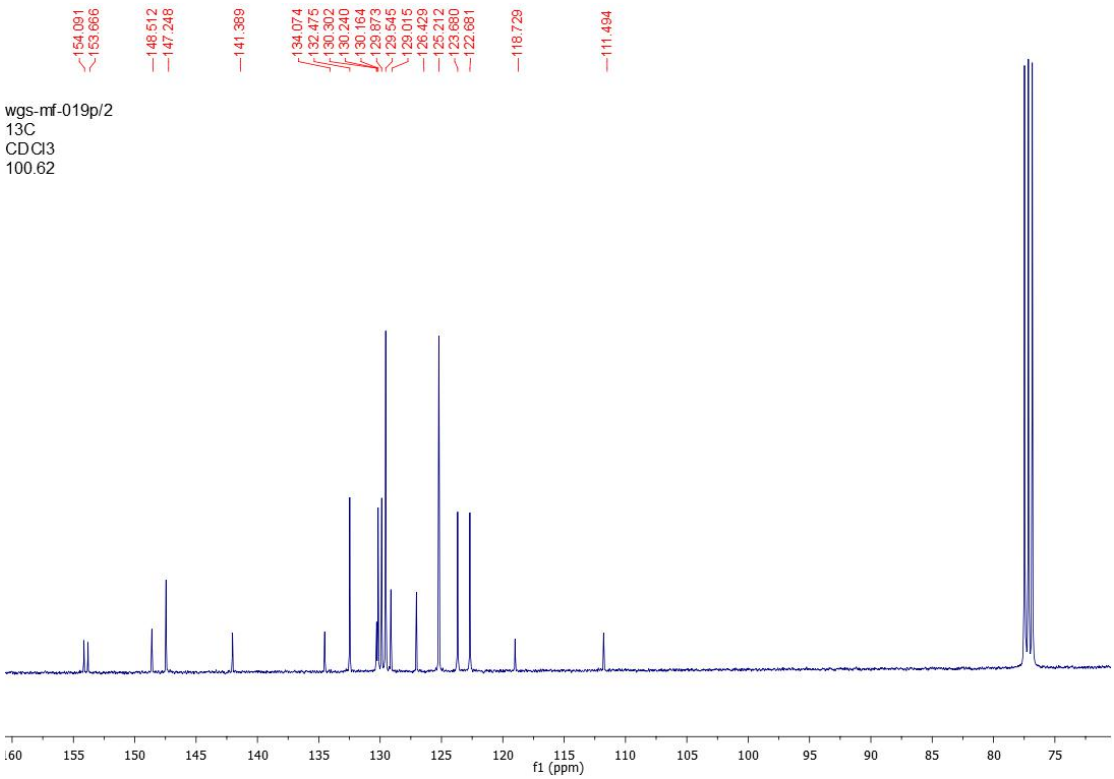

Figure 4.39. ^{13}C NMR spectra of **2** measured in $CDCl_3$.

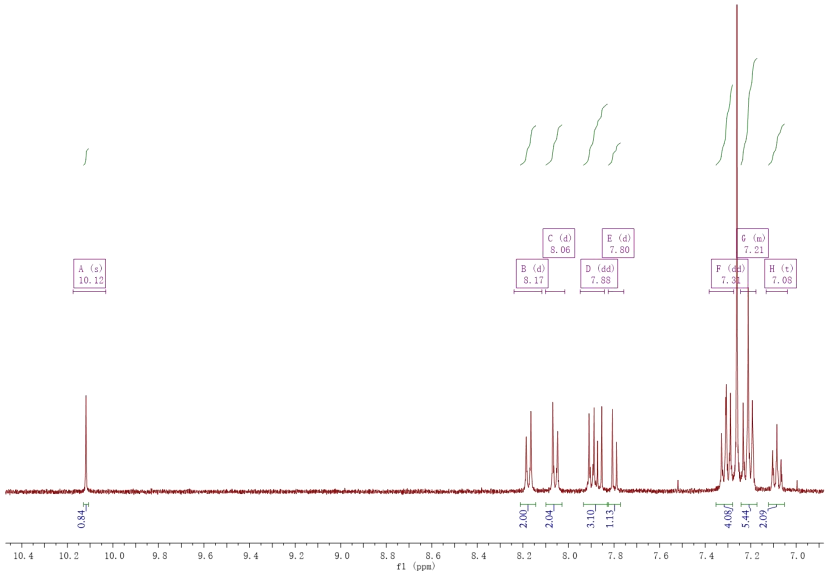

Figure 4.40. ^{1}H NMR spectra of **3** measured in $CDCl_3$.

5. Study of anthraquinone based derivatives: attempt for reduction layer

5.1. Introduction

In this chapter, an electrochromic material that can be electrochemically reduced was prepared. Its electrochemical reversibility makes it a suitable cathodic material for use in an electrochromic device. Such materials are of interest for use as active layers in working electrochromic devices. The use of complementary anodic and cathodic layers at opposite electrodes gives the devices charge storage capacities. The color of the devices can be switched with an applied potential in the usual way. However, the electrochemically induced color change is maintained even after the potential is no longer applied. This passive device requires less energy to operate, providing the redox properties of the two layer are well matched. While most electrochromic materials are anodic, few molecules are cathodic. Antraquinone is a potential cathodic molecule for use in a passive device. It has the potential to be electrochemically reduced twice. To date, it has mostly been used in super capacitors.[1]

As mentioned in the chapter 1, the small organic molecule prepared from TPA and anthraquinone resulted in highly solvatochromic fluorescence.[2] More examples of anthraquinone derivatives have found uses in electrochromic applications. Anthraquinone imides were synthesized by Wan's group having electrochromic properties in the near-infrared region.[3] This was the first example to explore anthraquinone derivatives and tune the electrochromic properties. By careful design of the molecule, they synthesized a new type of anthraquinone imide bearing functional groups at the 6-position on the anthraquinone moiety. Although the reaction yields were less than 50%, it was however comparatively high for anthraquinone related reactions. The four compounds prepared showed reversible reductions with applied negative potentials. Beside these two processes on the anthraquinone core, the introduction of another functional group ($-NO_2$) gave rise to a third reversible process. The spectroelectrochemical studies further demonstrated that the new anthraquinone imides were redox active with electrochromic absorption in a range of 700-1600 nm, making them useful as an NIR tag.

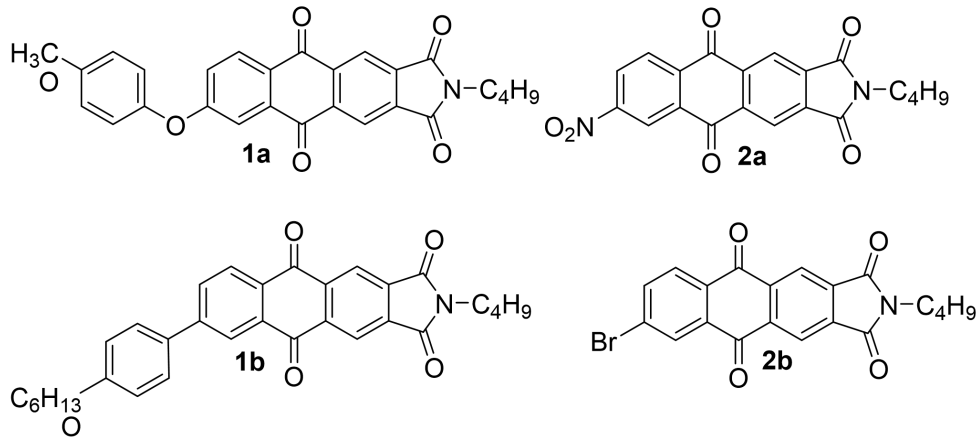

Figure 5.1. Structure of anthraquinone derivatives investigated by Wan's group.

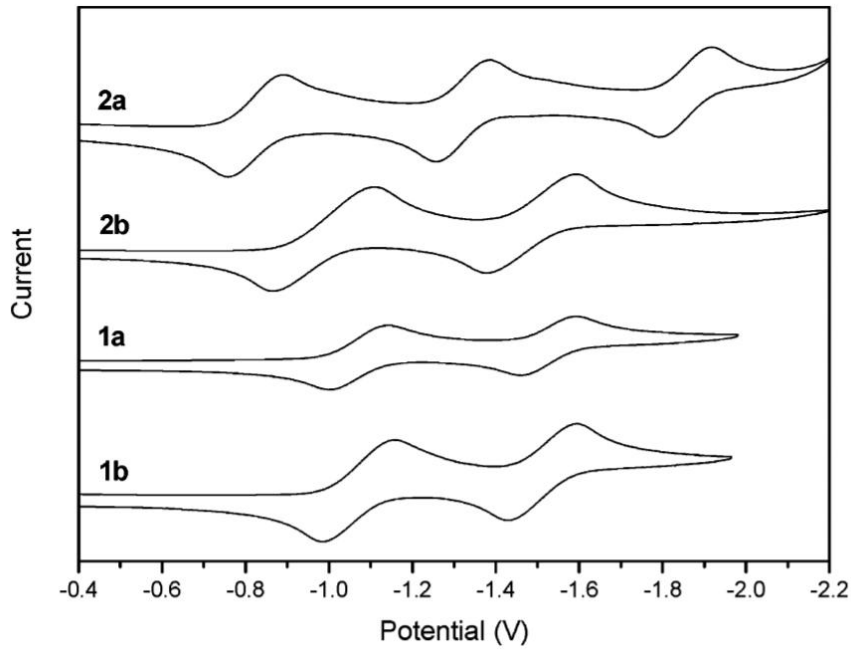

Figure 5.2. Cyclic voltammograms of anthraquinone derivatives. Reprinted with permission from [3]. Copyright (2008) American Chemical Society.

Small molecules often suffer from self-bleaching. They also easily diffuse into the electrolyte layer. These have negative effects on the coloration efficiency and the material's capacity to regenerate their resting transmittance (%) after multiple redox cycles. These limitations can be addressed by immobilizing the molecule on the electrodes. This remains a major challenge for anthraquinone derivatives. Liou's group took advantage of anthraquinone and TPA by combining them with polyimides.[4] The resulting AQ-PIs and OAQ-PIs were made by one-step polymerization, with applications in memory devices, electrochromics and gas separation. Unfortunately, the electrochromic properties were governed by the TPA moiety, rather than the anthraquinone core. However, the memory property was ascribed to the anthraquinone moieties. The device was switched to the on state by holding a negative voltage and subsequently resetting to the off state by removing the applied potentials without any color loss. The device could be turned on again with a second negative sweep. This indicated that the anthraquinone improved the color memory properties of these polymers.

We therefore pursued anthraquinone derivatives as charge memory layers in a dual-role device. The goal was to prepare anthraquinone monomers with the fewest synthetic steps possible and to use processes that are practical for large scale production. The target monomer was to be immobilized on the device electrodes using known polymerization methods, such as oxetanes to form a cross-linked network. In the meantime, the reversible reduction process of the polymer was expected to be preserved.

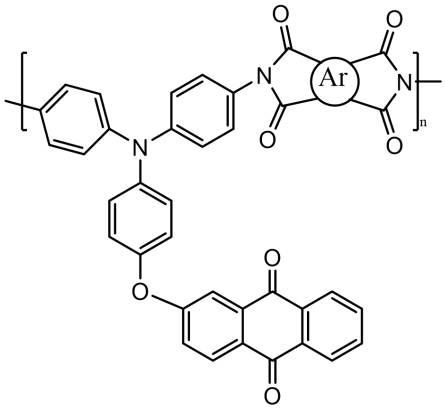

AQ-ArPI

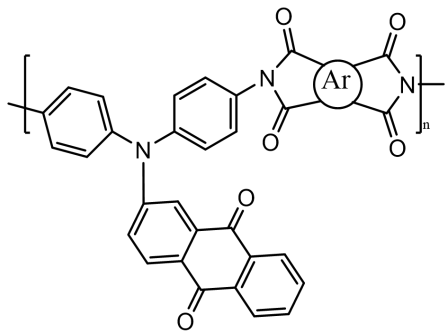

QAQ-ArPI

Figure 5.3. Structures of polyimides investigated by Liou's group.

5.2. Results and discussion

We coupled the core (**3**) with (**4**) to anthraquinone (**Figure 5.9**) to improve its solubility in organic solvents. The flexible side chains were expected to increase the polymer layer's stability and durability. Meanwhile, the PEG chain was expected to favor ion mobility across the polymer film. We further functionalized the end hydroxy group with an acryloyl group to immobilize the derivative on the ITO surface.

Electrochemistry of **1**

The compound exhibited a fully reversible reduction as shown in cyclic voltammogram in **Figure 5.4** (vs Fc/Fc^{+}). The reversible reduction peaks occurred at - 780 mV and - 1200 mV. Surprisingly, unlike other anthraquinone derivatives, there was no second reversible reduction peak. To further study this and to ensure the second reduction was not masked by the first oxdiation, square wave voltammetry was also done. As shown below, with a pulse technique of pulse height 15 mV, pulse width 25 ms, step height - 5 mV, no second reduction occurred. The peaks in the cyclic voltammogram were consistent with the peaks shown in square wave voltammogram.

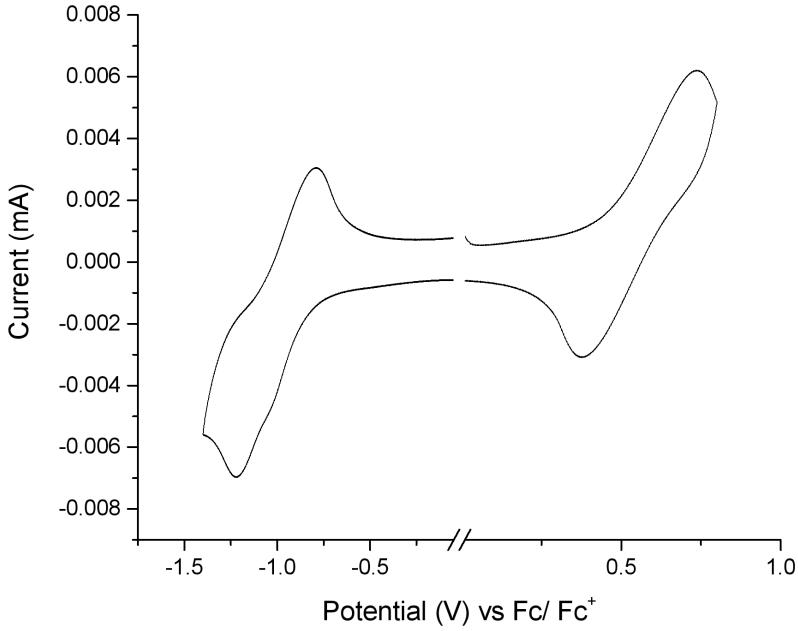

Figure 5.4. Cyclic voltammogram of **1** in anhydrous dichloromethane with 0.1 M $TBAPF_6$ measure at 100 mV/s calibrated versus the reversible ferrocene/ferrocenium couple.

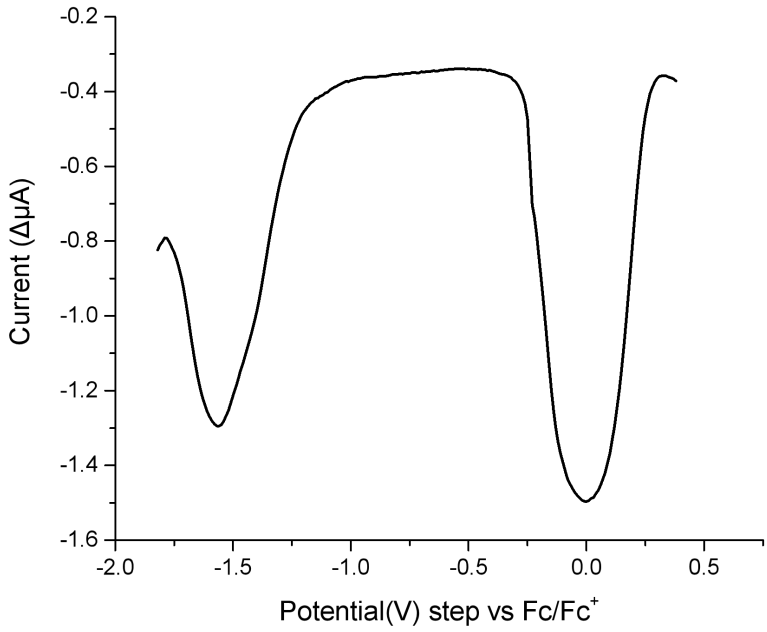

Figure 5.5. Square wave voltammogram of **1** in anhydrous dichloromethane with 0.1 M $TBAPF_6$ calibrated versus the reversible ferrocene/ferrocenium couple.

Spectroelectrochemistry of **1**

Given **1** met a key requirement for electrochromic use, reversible electrochemistry, its spectroelectrochemistry was investigated. The change in the absorption spectrum was continuously monitored while an external potential of -1.2 V was applied for certain intervals. As shown in the **Figure 5.7**, the original peak at 380 nm decreased and it shifted to 430 nm. Two new peaks appeared at 301 nm and 545 nm. This illustrates its potential use as an electrochromic material. After being electrochemically reduced, a potential of + 0.1 V was applied to oxidize the reduced state and the resulting change in absorption showed the full reversibility of **1**.

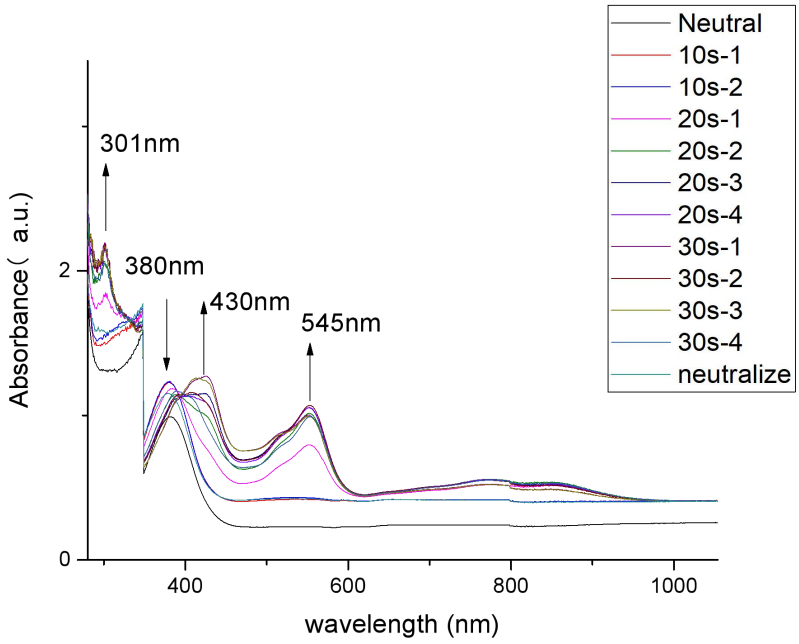

Figure 5.6. Spectroelectrochemistry of **1** in dichloromethane with 0.1 M $TBAPF_6$.

From the above spectroelectrochemical study, two new peaks were found at 301 nm and 545 nm. The change in transmittance when switching the applied potentials was monitored at a single wavelength. The change in transmittance (%) was monitored continuously for two hours to investigate its suitability as an electrochromic material. A potential of -1.2 V was chosen as the reduction potential and +0.1 V was chosen as the neutralization potential. Each potential was applied for every 30 seconds alternatively for 120 cycles. The compound showed stable switching both at 545 nm and 301 nm with 40 % difference in transmittance.

From Equation (**2.2**) in chapter 2, we can calculate the coloration efficiency (CE) from the switching study. The CE at 301 nm was 202 $cm^2 \cdot C^{-1}$ and 219 $cm^2 \cdot C^{-1}$ at 545nm. The values are among the highest from reported values for anthraquinone polymers.[5, 6]

$$\eta = \frac{\Delta OD}{Q}, \text{ where } \Delta OD = \log\left[\frac{T_{ox}}{T_{red}}\right].$$

A)

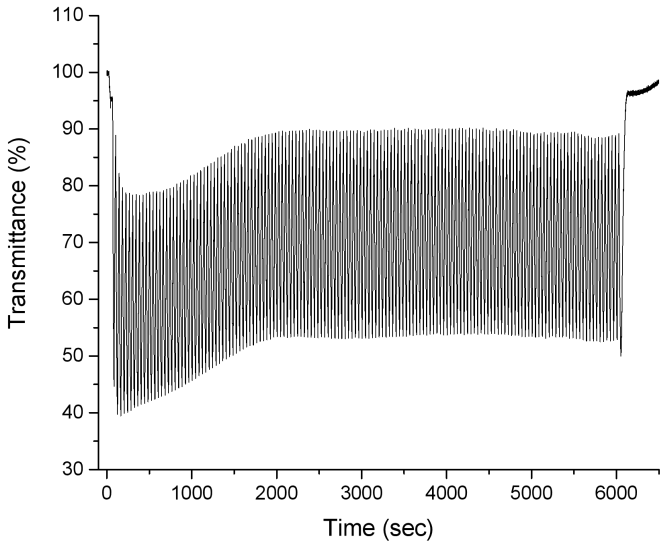

B)

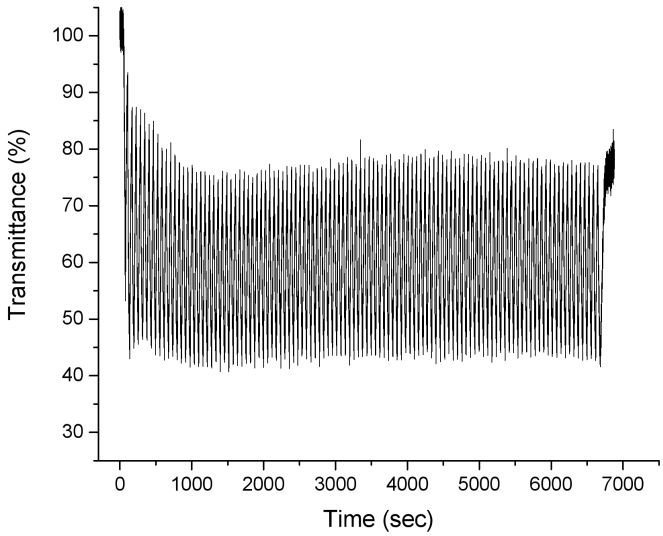

Figure 5.7. Change in transmittance (%) of **1** monitored at 545 nm (A) and 301 nm (B). Applied potential switch between -1.2 V and +0.1V at 30 seconds intervals.

Immobilization of **1**

The immobilization of **1** on the working electrode was done to assess its switching performance. As the antraquinone core is sensitive to light, photochemical and 'click' chemistry were not pursued. Moreover, methods that were scale for immobilization, notably copolymerization was investigated. Inspired from environmentally 'green' ring opening process,[7] triglycidyl isocyanurate was chosen for immobilization by copolymerization. A thin film of the monomer to be polymerized from a mixture of **1** and triglycidyl isocyanurate in a given solvent was spray coated on an ITO plate. The substrate was then heated at 160 ℃ for 2 h in a glovebox to afford a pale yellowish thin film. To ensure its electrochemical properties were preserved, cyclic voltammetry was done. As shown in **Figure 5.8**, the peaks height continuously decreases with 5 complete cycles. Also, the electrolyte solution become greenish. These indicate that delamination of the copolymer from the ITO surface occcured. Surprisingly, the original pale yellow color of the polymer on the ITO plate switched to violet with electrochemical reduction.

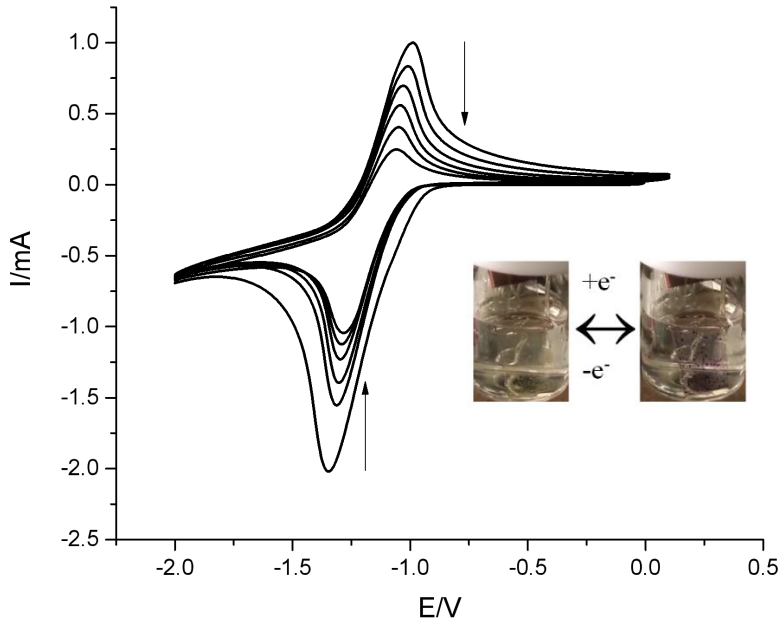

Figure 5.8. Cyclic voltammogram of the co-polymer of **1** and cross-linker in acetonitrile with 0.1 M $TBAPF_6$. Insert: electrochemically mediated color change on the ITO coated surface.

Immobilization of **2**

Due to the delamination of the copolymer of **1**, its functionalization with acryloyl was pursued. This was in part because the polymerization of acryloyl can be done at low temperatures.[8] Thermal-polymerization of **2** on the ITO surface was done by heating the plate at 60 ℃for 1 h.

The resulting polymer was done easily dissolved in either dichloromethane and acetonitrile.

Experimental section

Synthesis of **1** and **2**.

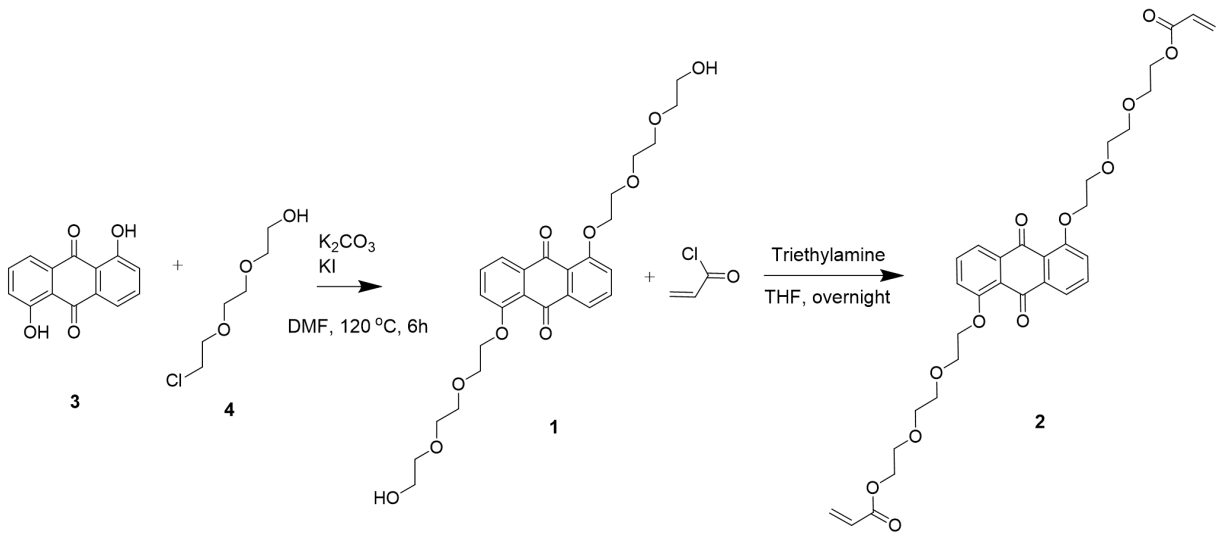

Figure 5.9. Synthesis route of targets **1** and **2**.

1,5-Di-2-[2-(2-ethoxy)ethoxy]ethanol-antraquinone (**1**). 1,5-Dihydroxy-anthraquinone (500 mg, 1 eq) was dissolved in anhydrous DMF followed by dissolving K_2CO_3 (1.44 g, 5eq), KI (17.3 mg, 0.05eq), 2-[2-(2-chloroethoxy)ethoxy]ethanol (750 μmL, 2.5 eq) was then slowly added into the mixture. The mixture was heated at 120℃ for 6 h. After cooling, the DMF was removed by rotavapor. The crude product then purified by a silica column with hexane: acetone = 30:70. The pure product was obtained as a yellow powder (48%). ^{1}H NMR (300 MHz, $CDCl_3$) δ= 7.90 (dd, *J* = 7.8, 1.0 Hz, 1H), 7.72 – 7.64 (t, 1H), 7.29 (d, *J* = 8.5 Hz, 1H), 4.37 – 4.30 (t, 2H), 4.07 – 4.02 (t, 2H), 3.92 – 3.87 (t, 2H), 3.79 – 3.72 (m, 5H), 3.67 – 3.64 (m, 2H). MS (m/z) calculated from $C_{26}H_{32}O_{10}$: 504.2, found: 549.2

1,5-Di-2-[2-(2-ethoxy)ethoxy]aryloyl-antraquinone(**2**). **1** (300 mg,1 eq) was dissolved in anhydrous THF (30 mL), followed by triethylamine (290 μL, 3.5 eq) and degassing with N_2 for 20 minutes. The mixture was covered with an ice bath, and acryloyl chloride (150 μL, 3 eq) was slowly added. The mixture was stirred in the ice bath for 40 minutes and then warmed to 45 ℃. After removing the solvent, the crude product was purified by silica column with acetone:hexane=40:60. The target compound was obtained as a greenish powder with (48%). ^{1}H NMR (300 MHz, $CDCl_3$) δ=7.88 (dd, *J* = 7.7, 1.0 Hz, 1H), 7.66 (t, *J* = 8.1 Hz, 1H), 7.28 (dd, *J* = 8.4, 0.9 Hz, 1H), 6.42 (dd, *J* = 17.3, 5.2, 1.5 Hz, 1H), 6.21 – 6.04 (m, 1H), 5.89 – 5.74 (m, 1H),

4.31 (t, J = 5.1, 1.9 Hz, 4H), 4.02 (t, 2H), 3.92 – 3.82 (m, 2H), 3.81 – 3.69 (m, 4H). MS (m/z) calculated from $C_{32}H_{36}O_{12}$: 612.6, found: 613.2.

5.3. Conclusion

In summary, two anthraquinone monomers were successfully synthesized. The concept of making reduction layers from anthraquinone derivatives was proven. This idea took advantage of a straightforward synthesis, making it useful for future device applications such as 'smart windows', OLED or other organic electronics. **1** was spectroscopically characterized along with cyclic voltammetry. It provided a new pathway to design a reduction layer for use in electrochromic passive devices. The compound showed an electrochromic behavior in the visible region. Unfortunately, the monomers could not be immobilized as designed.

5.4. Supporting information

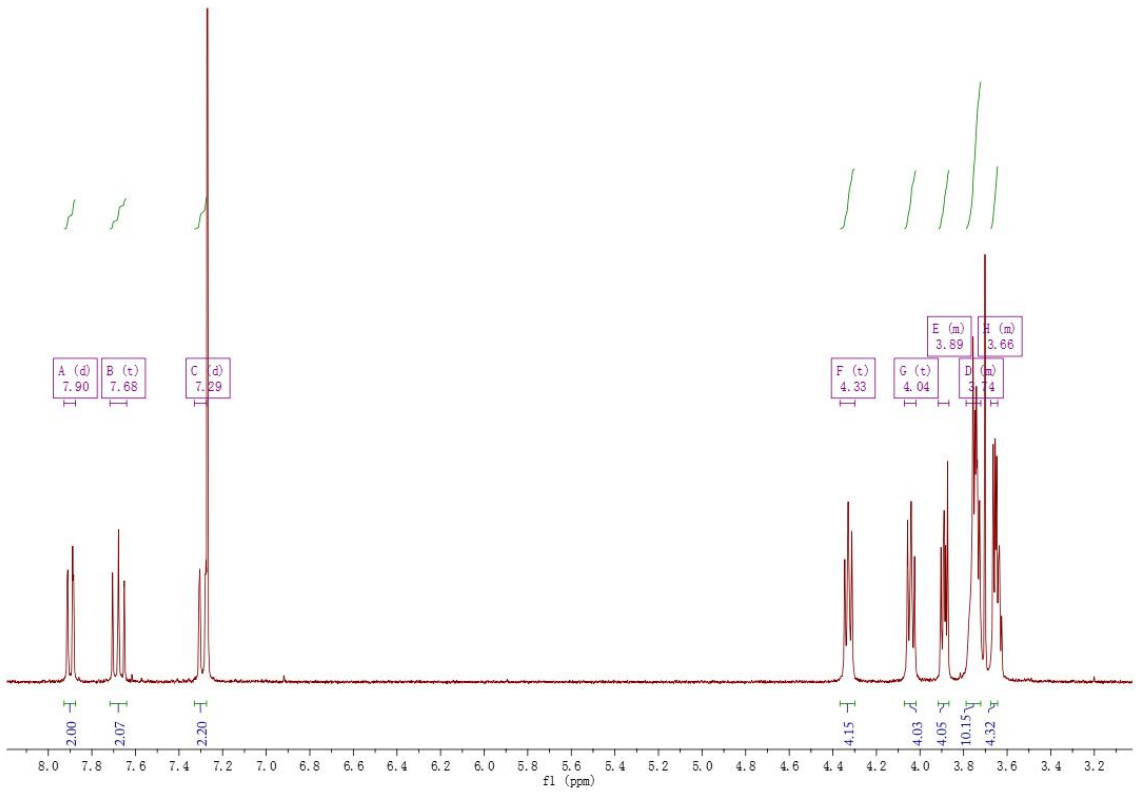

Figure 5.10. ^{1}H NMR of compound **1**.

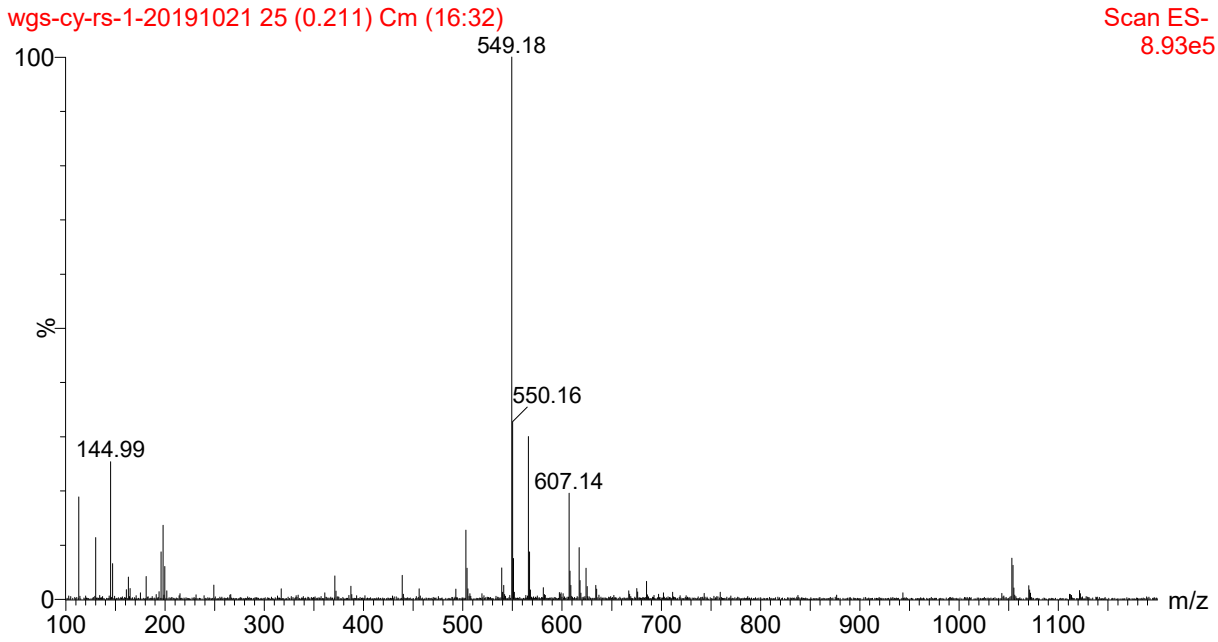

Figure 5.11. Mass spectrum of compound **1.**

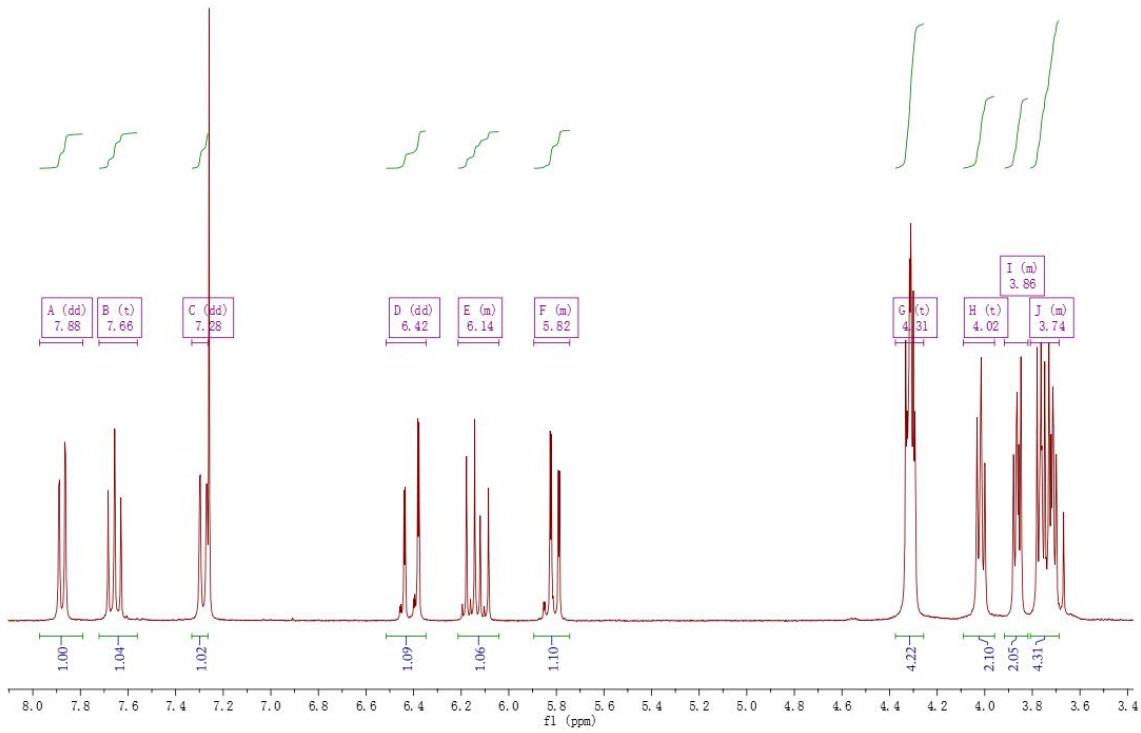

Figure 5.12. ^{1}H NMR of compound **2**.

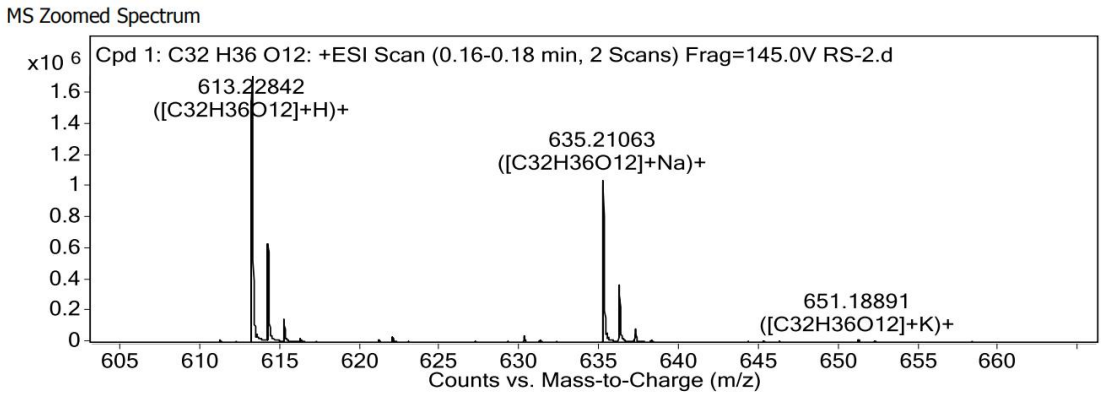

MS Spectrum Peak List

Ion	Formula	Abund	*Expe. m/z*	*Calc. m/z*	Diff(ppm)
(M+H)+	C32H36O12	1707916.5	613.22842	613.22795	-0.77
(M+Na)+	C32H36O12	1057556.03	635.21063	635.2099	-1.15

Figure 5.13. Mass spectrum of compound **2**.

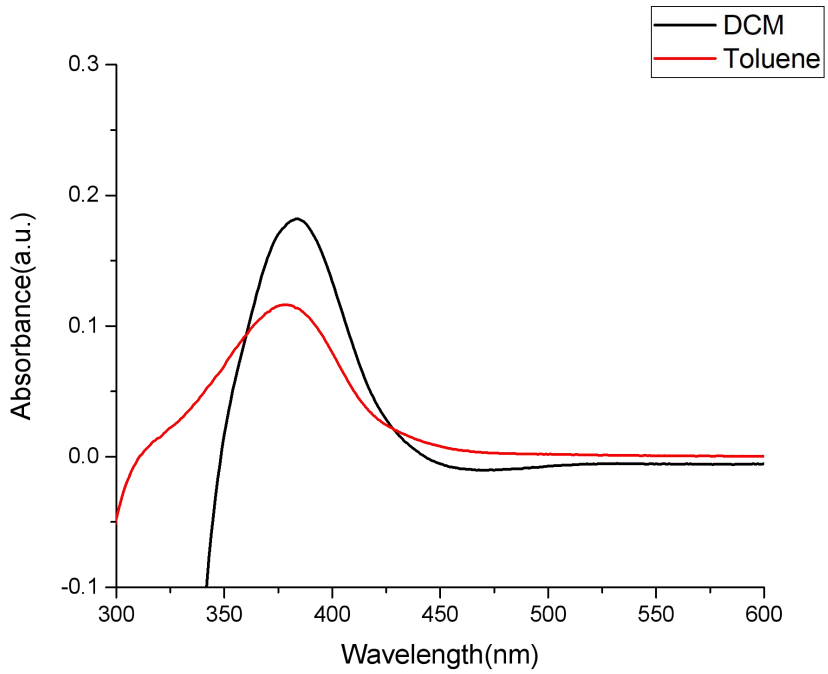

Figure 5.14. Absorption spectra of **1** in DCM (black) and toluene (red).

References

1. Gusmão, R.; Sofer, Z. k.; Pumera, M., Functional protection of exfoliated black phosphorus by noncovalent modification with anthraquinone. *ACS nano* **2018,** *12* (6), 5666-5673.
2. Li, Y.; Tan, T.; Wang, S.; Xiao, Y.; Li, X., Highly solvatochromic fluorescence of anthraquinone dyes based on triphenylamines. *Dyes and Pigments* **2017,** *144*, 262-270.
3. Qiao, W.; Zheng, J.; Wang, Y.; Zheng, Y.; Song, N.; Wan, X.; Wang, Z. Y., Efficient synthesis and properties of novel near-infrared electrochromic anthraquinone imides. *Organic letters* **2008,** *10* (4), 641-644.
4. Hu, Y.-C.; Chen, C.-J.; Yen, H.-J.; Lin, K.-Y.; Yeh, J.-M.; Chen, W.-C.; Liou, G.-S., Novel triphenylamine-containing ambipolar polyimides with pendant anthraquinone moiety for polymeric memory device, electrochromic and gas separation applications. *Journal of Materials Chemistry* **2012,** *22* (38), 20394-20402.
5. Wang, G.; Fu, X.; Huang, J.; Wu, L.; Du, Q., Synthesis and spectroelectrochemical properties of two new dithienylpyrroles bearing anthraquinone units and their polymer films. *Electrochimica Acta* **2010,** *55* (23), 6933-6940.
6. Hsiao, S. H.; Lin, J. Y., Electrosynthesis of ambipolar electrochromic polymer films from anthraquinone–triarylamine hybrids. *Journal of Polymer Science Part A: Polymer Chemistry* **2016,** *54* (5), 644-655.
7. Leal-Duaso, A.; Pérez, P.; Mayoral, J. A.; García, J. I.; Pires, E., Glycerol-Derived Solvents: Synthesis and Properties of Symmetric Glyceryl Diethers. *ACS Sustainable Chemistry & Engineering* **2019,** *7* (15), 13004-13014.
8. Aguilar, M. R.; San Román, J., *Smart polymers and their applications*. Woodhead Publishing: 2019.

6. Conclusion

Organic electrochromic materials have a great potential for use in applications such as smart windows, OLEDs, and biosensors. By taking advantage of small organic molecules, the electrochromic materials can be readily synthesized, allowing for their straightforward preparation and good control of both purity and morphology. These electrochromic layers also have the advantages of fast electrochemical responsive, significant color change and full spectrum tunability. This is possible by incorporating various electronic groups into benzothiadiazole chromophores. On the other hand, polymers are more advantageous because of their long term stability and durability towards repeated applied potential cycles. However, most polymers that are used in electrochromic applications switch colors in the visible region and they are not electroluminochromic, especially in the solid state. This is because of their intermolecular packing that quenched the emission. Compared to polymers, electronic groups can be easily incorporated into small molecules. The strategy of combining electroactive groups with conjugated fluorophores has the advantage of tuning the emission in the solid state along with desired high emission yield in the thin films. Aggregation-induced-emission (AIE) is another promising way of increasing the solid state emission for electronic applications. Although small molecules that can be functionalized and are less stable than functional polymers, they can nevertheless be play a dual role in devices. They can undergo color changes and reversible fluorescence quenching. Moreover, they can be combined with conductive polymers as an electron storage layer to give ‘color memory’ devices. The advantage of these passive devices is their color change can maintained even after the potential is no longer applied. As such passive devices are more energy efficient than active devices.

In chapter 2, a small organic molecule capable of playing a dual role in both electrochromism and electrofluorochromism was evaluated. The compound was characterized for its photophysical and electrochemical properties. A working device was also fabricated. The studies proved that a compound having targeted properties can be rationally designed. To solve the problem of remain high emission yield in the sold state, we used AIE effect to help with. To remain the electrochromic property in solid state, we coupled an electrochomic group on the core. Indeed, the solid state emission with moderate emission yield is possible by conjugating an electronic group with a benzothiadiazole fluorophore. In this case, the TPA group was chosen for its electroactivity, notably its reversible oxidation property. Benzothiadiazole was chosen for its intrinsic fluorescence, which is maintained either when aggregated or in the solid state. Further extend these compound into different region such as deep red/NIR region, we tried to coupled different end groups with different electronic propertie. A strong electron donating end group (*N’N*-dimethylamine) was chosen for visible electrochromism. Combining the electroactive TPA

and the BZT fluorophore resulted in a dual role material that was capable of color switching in the visible region and reversible florescence quenching in both solution and working devices. Dual electrochromic/electrofluorochromic devices are therefore possible with small molecules and the color can be tuned by varying the electronic groups. The result compound can remain a long term durability and high coloration efficiency in solution state which among the top efficiency of the reported cases. Moreover, we made the compound into an operating active device which proved the idea of the remaining electrochromic and electrofluorochromic properties in solid states as well.

In chapter 3, a series of small organic molecules were investigated. Different from the chapter 2, end groups of varying electron withdrawing capacities were studied. Since the electron withdrawing groups will create the '*push-pull*' effect, we coupled these end groups in order to extend the conjugated system as well as emission spectrum while not break the remaining high emission yield in the solid state. The nitro, cyano, and aldehyde electron withdrawing groups were conjugated with a TPA-BZT core. Not surprisingly, these chromophores remained electroactive, while their electrochromic properties were contingent on the electron accepting group. By tuning the electronic strength of the end group, the color and emission wavelength could be modulated with solvent polarity. Of interest was their solid state emission. The desired emission in the solid state was possible by adjusting the electronic groups. High quantum yields in the solid state (upwards of 50%) were possible. This is the one as a state of art value for solid state emission yield. They are suitable for use as emitting materials in OLEDs, organic light-emitting-cells (OLECs) and electrofluorochromic devices. Indeed, the fluorophores could be used in an operating electrofluorochromic device.

Finally in chapter 4, an anthraquinone derivative was investigated as cathodic layer in passive devices. Although chapter 2 showed the dual role of the fluorophore, it suffered from self-bleaching similar to conventional fluorophores. To make the passive device in order for energy saving considerations, a reduction layer that can store the electrons has to be designed and put into the 'sandwich' style device. The anthraquinone was successfully prepared for its charge storage property and it was found to be a promising electrochromic material in the visible region. By immobilizing the cathodic layer on electroactive substrates, a fully redox device capable of both electrochromic oxidation and reduction would be possible. The anthraquinone derivatives showed a large transmittance change (over 40%) and it showed a long-term switching stability. The remaining problem that must be resolved is how to immobilize the layer robustly, while preserving its reversible electroactivity. By functionalizing anthraquinone with other pre-polymerization groups such as oxetanes, oxiranes or diazides, it could potentially be thermal-polymerized on electrodes.

In this master thesis, the two important layers in a 'smart window' device were investigated. By combining the TPA and BZT moieties, dual role materials capable of electrochromism and electrofluorochromism were achieved. By using anthraquinone as reduction layer, ion storage

can potentially be realized. Combining a layer of small molecules that are both electrochromic and electrofluorochromic with a cathodic layer opens the possibility of preparing passive electrochromic devices. These are expected to be more performant than active devices by being more stable and durable towards multiple electrochemical switching. By introducing long alkoxy chains into the polymeric system, it is also possible to make the layer flexible and ultimately stretchable as for future use in wearable device.